A CHEMOSENSORY ROLE FOR THE ZEBRAFISH LATERAL LINE SYSTEM

by

ANIRBAN MAJUMDER

(Under the Direction of James D. Lauderdale)

ABSTRACT

An important function of the vertebrate nervous system is chemosensation, and the ability to detect and distinguish between harmful and useful compounds and react appropriately. However, the neural mechanisms underlying chemosensory responses in vertebrates are poorly understood. Studies addressing chemosensory mechanisms would be greatly facilitated by using a vertebrate model that is easy to stimulate, has a simple well-characterized nervous system, and in which neural activity can be easily detected. Here, I present evidence for the first time demonstrating that the zebrafish lateral line can act as a chemosensory system. The lateral line is a hydrodynamic sensory system found in fish and amphibians. It is comprised of superficial sensory structures called neuromasts that are innervated by afferent and efferent nuclei in the brain. Using *c-fos* induction as a marker for neural activity I show that neuromasts, as well as neurons deep in the brain, respond to specific pungent natural compounds normally associated with nociception, or the sensation of pain. We take advantage of the optical transparency of the zebrafish larvae to functionally image the response using an optical imaging approach that we have developed. Using this approach we can detect neural activity in higher order components of the lateral line system in response to noxious stimuli. Our results assign an additional sensory role for the lateral line system in zebrafish and demonstrate the potential of this system for studying neural mechanisms associated with nociception in vertebrates, including humans.

.

INDEX WORDS: chemosensation, lateral line, zebrafish, calcium imaging, cameleon, FRET, SOARS

A CHEMOSENSORY ROLE FOR THE ZEBRAFISH LATERAL LINE SYSTEM

by

ANIRBAN MAJUMDER

B.Sc., Visva Bharati University, India, 1996

M.Sc., Visva Bharati University, India, 1998

A Dissertation Submitted to the Graduate Faculty of The University of Georgia in Partial Fulfillment of the Requirements for the Degree

DOCTOR OF PHILOSOPHY

ATHENS, GEORGIA

2006

A CHEMOSENSORY ROLE FOR THE ZEBRAFISH LATERAL LINE SYSTEM

by

ANIRBAN MAJUMDER

Major Professor: James D. Lauderdale

Committee: Marcus Fechheimer
Gaylen Edwards
Scott T. Dougan
Charles H. Keith
Andrew T. Sornborger

Electronic Version Approved:

Maureen Grasso
Dean of the Graduate School
The University of Georgia
December 2006

DEDICATION

উৎসর্গ
মা ও বাবা

(To Maa and Baba)

ACKNOWLEDGEMENTS

None of what I have achieved would be possible without the constant guidance and support from Dr. James Lauderdale and members of my graduate advisory committee, Dr. Charles H. Keith, Dr. Scott T. Dougan, Dr. Marcus Fechheimer, Dr. Gaylen Edwards and Dr. Andrew T. Sornborger. I thank them all for their advice and support. I would also like to thank Dr. Marcus Fechheimer for being a wonderful graduate coordinator and for being there whenever needed. I also thank my colleagues Jiha Kim and Jorn Lakowski for their support and their wonderful company for five years in the lab. I would also like to thank Dr Sujoy K. Dhara for his constant support and encouragement.

TABLE OF CONTENTS

Page

LIST OF CHARTS

Page

LIST OF FIGURES

Page

Chapter 1

Introduction and Literature Review

Vertebrates rely on inputs from different sensory systems to respond appropriately to their environment. These include sensory systems tuned for vision, hearing, smell, taste, and touch. Each system has specialized receptors that detect a specific type of stimulus and transduce the information into electrical impulses that are transmitted to a primary sensory ganglion. Information about the modality, intensity, duration and location of the stimulus are then passed on from the peripheral nervous system to appropriate regions in the central nervous system for processing. The processing of these sensory inputs and the resultant behavioral response involve activity in complex circuits formed by numerous neurons, often spread across large regions of the nervous system. Moreover, behavioral responses often involve the integration of inputs from more than one sensory system (Purves 2004). Thus understanding stimulus specific neural activity underlying a behavioral response will require the ability to simultaneously detect neural activity in a large area of the nervous system. Here we approach this problem using the lateral line sensory system in zebrafish.

Overview of lateral line system

The lateral line is a mechanosensory system found in aquatic vertebrates like fish and amphibians. Mechanosensory function of the lateral line has been extensively studied in many species and it is believed that the lateral line plays a crucial role in detecting water movement and changes in pressure, enabling the animal to detect predator and prey, discern the two, find

mates, and avoid obstacles (Coombs 1989a). Its ability to act as a hydrodynamic sensor has made it a crucial sensory organ for aquatic life. The sensory structures of the lateral line system, called neuromasts, are present on the surface of the animal in a stereotypic pattern. Individual neuromasts are composed of hair cells surrounded at their base by support cells. Each hair cell has a kinocilium protruding out and surrounded at its base by shorter stereocilia. The protruding cilia are encapsulated by a gelatinous capula, secreted by the neuromast cells (Purves 2004). The number and complexity of the neuromast pattern varies from species to species and changes with development (Coombs 1989b; Webb and Shirey 2003). Two types of neuromasts, surface neuromasts and canal neuromasts are present in most species. Surface neuromasts are more likely to detect water movements along the surface of the body, and are likely to be important in rheotaxis, or tendency to face and swim against the current (Montgomery 1997; Montgomery et al. 2000; Montgomery et al. 2002; Montgomery et al. 2003). On the other hand canal neuromasts are responsible for detecting waves generated by objects (Coombs 1989b).

Neuromasts receive both afferent and efferent innervation. Neuromasts of the head region receive afferent connections from the anterior lateral line ganglion, situated posterior to the eye and anterior to the ear, while those of the trunk and tail region are innervated by afferent projections from the posterior lateral line ganglion, situated posterior to the ear (Metcalfe et al. 1985).

Efferent connections, both excitatory and inhibitory, originate from several nuclei in the brain. Axon tracing revealed three types of efferent nuclei in the zebrafish: the ROLE (rhombencephalic octavo-lateral efferent) and the RELL (rhombencephalic efferent of the lateral line) in the hindbrain, and the DELL (diencephalic efferent of the lateral line) in the forebrain (Metcalfe et al. 1985; Bricaud et al. 2001). All three clusters innervate both the anterior and

posterior lateral line system. While different neurons within each hindbrain cluster are thought to innervate the anterior and posterior lateral line system, it is not known if the same is true for the diencephalic nuclei (Bricaud et al. 2001).

Neurons of the efferent nuclei in the hindbrain are cholinergic (Meredith et al. 1987) while the identified forebrain efferent neurons are immunoreactive to antibodies against tyrosine hydroxylase (TH), an enzyme required for catecholamine synthesis (Bricaud et al. 2001). This suggests that the DELL neurons are catecholaminergic. Although not demonstrated directly, it has been suggested that the DELL neurons are dopaminergic based on the observation that dopaminergics are found in the fore and midbrain while noradrenergic neurons are restricted to the hindbrain (Guo et al. 1999). Tyrosine hydroxilase immunoreactivity is also seen in the network of dopaminergic terminals that surround the neuromast hair cells. It has also been argued that the DELL neurons are excitatory as they express tyrosine hydroxylase (Bricaud et al. 2001). Neurons of identified hindbrain nuclei, which express choline acetyltransferase, may represent a cholinergic inhibitory component of the lateral line system (Flock and Russell 1973; Brantley and Bass 1988; Danielson et al. 1988).

Similarities between the lateral line system and auditory system

Developmental, structural and functional similarities between the lateral line system of fish and amphibians, and auditory system of vertebrates in general, including mammals, make it a potential model system for studying several aspects of hearing in mammals. The lateral line is part of the octavolateralis (alternately termed acousticolateralis) system of aquatic vertebrates, which also includes the internal ear (Dijkgraaf 1989; Lopez-Schier and Hudspeth 2005). The lateral line system and the ear are closely related in terms of their origin from closely apposed

ectodermal placodes, presence of similar secondary sensory cells and support cells, positions of the cranial sensory ganglia, and their projections in the hindbrain (Bricaud et al. 2001). It has been suggested that while the fish ear serves to detect sound in the far field, neuromasts of the lateral line do the same in the near field. Though the evidence is not conclusive, it has been speculated that the vertebrate inner ear has evolved originally from the lateral line system (Jorgensen 1989) and that the lateral line, present in ancestral vertebrates, was lost in vertebrates that adapted to terrestrial life (Jorgensen 1989; Raible and Kruse 2000).

Fate mapping experiments suggest that neuromasts and the lateral line ganglia that innervate them, and the inner ear develop from contiguous and possibly overlapping ectodermal placodes (Whitfield et al. 1996; Kozlowski et al. 1997; Dambly-Chaudiere et al. 2003). Structurally, the neuromasts resemble the sensory patches of the inner ear in fish (Whitfield et al. 1996). The lateral line system and auditory system are also similar in terms of receptor morphology and function. Both systems detect stimulus through secondary sensory hair cells. Arrangement of kinocilia and stereocilia in the neuromst hair cells resemble the sensory hair cells found in the inner ear of other vertebrates, including mammals. The neuromast hair cells and those found in the inner ear both respond to mechanical stimuli and sense movement by deflection of the similarly arranged stereocilia and stereovilli (Kroese 1989; Raible and Kruse 2000). This opens up ion channels to allow entry of K^+. The resultant change in membrane potential leads to opening of calcium channels and subsequent release of neurotransmitters.

Molecular mechanisms for neuromast sensory function

There is no published study that directly addresses the molecular mechanism of neuromast function. However, the lateral line hair cells of fish are thought to be equivalent to the

mammalian inner ear hair cells (Coombs 1989b). Studies that addressed molecular mechanisms of mechanosensation in the inner ear hair cells of mouse suggest the involvement of mechanically gated ion channels. In mammals, inner ear hair cells have been shown to express the mechanically gated transient receptor potential (TRP) channel TRPA1 (Corey et al. 2004). Loss of function experiments suggest that these channels are responsible for hearing and are gated by the flexing of hair cell cilia. In zebrafish, two such channels, called zfTRPA1 and zfTRPA2, which are believed to be paralogs, were identified and knocked down using a morpholino antisense approach (Corey et al. 2004). These channel proteins were knocked down individually as well as simultaneously. This resulted in a reduction in uptake of FM1-43, a dye known to be taken up specifically by neuromast hair cells, in only the zfTRPA1 or double knockdown embryos suggesting that zfTRPA1 channels are present and functional in the neuromasts. Interestingly, in mammals TRPA1 channels are also implicated in chemosensation (Bandell et al. 2004; Kwan et al. 2006).

Cell culture based assays show that mammalian TRPA1 channels are activated by various natural compounds (Sidi et al. 2003; Story et al. 2003; Bandell et al. 2004; Kwan et al. 2006), and by changes in temperature demonstrating that in mammals, TRPA1 channels have multiple roles, and function in both mechanosensation and chemoception. TRPA belongs to a superfamily of ion channels called TRP channel superfamily. Many other channels of this superfamily are demonstrated to be chemoreceptors (Clapham et al. 2001; Voets et al. 2005). In mammals TRPA1 (also ANKTM1) has been shown to be expressed in a subset of nociceptive sensory neurons where it is co-expressed with another TRP superfamily member, TRPV1 but not with a third member of the same family, TRPM8 (Story et al. 2003). Mouse and human TRPA1 channels are activated by pungent natural compounds cinnamon oil (cinnamaldehyde),

wintergreen oil (methyl salicylate), clove oil (eugenol), mustard oil (allyl isothiocyanate), and ginger oil (gingerol), all compounds that evoke a burning sensation in humans (Dedov et al. 2002; Bandell et al. 2004; Jordt et al. 2004; Bautista et al. 2005). Similarly, TRPV1 responds to capsaicin, the substance that makes pepper hot, and gingerol, the major constituent of ginger oil, while TRPM8 is sensitive to menthol (Story et al. 2003). Both receptors are associated with detection of noxious stimuli and in the sense of pain or nociception in mammals. These observations led us to hypothesize that in zebrafish, the neuromast hair cells may be involved in chemosensation as well as mechanosensation. Whether neuromasts respond to these organic compounds has never been tested. Previous studies do, however, provide electrophysiological evidence that neuromasts can sense salt solutions and metal ions (Katsuki et al. 1971).

Electrophysiological studies showed that lateral line responds to salt solutions

While it is known that teleosts respond to chemical stimuli in the mouth and gill cavity, behavioral studies in several species suggest that they also respond to chemical stimuli over their entire body. This phenomenon was referred to as the "common chemical sense" and was attributed to special receptors and to free nerve endings in the epidermis (Withear 1952). These receptors were referred to as the terminal buds. Because the terminal buds were structurally similar to the pit organ of sharks, a type of lateral line organ, it was thought that the pit organs could function as organs of taste (Budker 1938), a type of chemosensation. Electrophysiolocal studies conducted on sharks and teleosts (Katsuki et al. 1969; Katsuki et al. 1971) suggested that the lateral line can sense salt solutions. For these studies the lateral line nerve was exposed and the distal cut end was separated into bundles containing single or a few fibers and neural discharges were recorded. Most experiments were performed on the lateral line nerve Ramus

lateralis. The ramus mandibularis externus, whose branches innervate the lateral line canal and the row of pit organs in the mandibular region were also used. Branches of this system also innervate the Lorenzini's ampullary organ, comprised of pressure or temperature receptors, present on the snout of sharks. The organs were exposed to salt solutions and neural discharges were compared. A comparison of responses from the three, the lateral line canal, mandibular row of pit organs, and the Lorenzini's organ, suggested that while all three responded to mechanical stimulation and Lorenzini's organ had the greatest sensitivity to electrical stimulation. The pit organ had the greatest sensitivity to chemical stimulation while the canal organ showed almost no response to chemicals. Potassium salts produced stronger excitatory effects than sodium salt solutions. The effects were reversible up to a certain concentration. Various monovalent cations were also tested and K^+, Rb^+, Na^+, Cs^+, Li^+ were effective in that order. Presence of divalent calcium ions, however, suppressed the effects of the monovalent cations and anions had no significant effect.

In order to test if the response was different from those involved in gustation in higher animals, acid, sweet (sugar) and bitter (quinine) substances were tested. These had either no effect or a suppressive effect on the discharge rate of these nerves, and it was concluded that the response was not similar to mammalian taste buds (Katsuki 1982). Also these studies demonstrated that the discharges were not a response to osmotic changes and were specific to the salts. Similar results suggesting chemoreception were obtained from mullets (*Mugil cephalus*), catfish (*Ictalurus punctatus*) and carp (*Cyprinus carpio*) (Katsuki et al. 1971).

Studies on lateral line of the amphibian *Xenopus* produced similar results. They were found to be exceptionally sensitive to NH_4Cl, in agreement with the general belief that aquatic predators are more sensitive to NH_4Cl. In fish, divalent cations reduce spontaneous activity as

well as responses to monovalent cations. In the *Xenopus* lateral line the discharge rate was doubled by $CaCl_2$ and $MgCl_2$. Liver extracts also stimulated the lateral line organ in *Xenopus,* suggesting that these animals may be able to detect certain substances present in food using their lateral line organ. *Xenopus* embryos do not have a tongue but are still capable of responding to food extracts. During metamorphosis, the lateral line degenerates, and a tongue develops. This suggests a role for the lateral line in the sense of taste (Katsuki 1982). To confirm the involvement of the neuromast hair cells, membrane potentials were also recorded from the receptor hair cells. Membrane potential was recorded in the mudpuppy (*Necturus maculosus*), known for large hair cells in their lateral line organ and potential changes induced by chemical stimuli were observed (Yanagisawa et al. 1974).

For the current study described in chapter 2, the response of zebrafish neuromasts to various pungent compounds were tested. The responding neuromasts were detected using expression of *c-fos,* an established marker for neural activation.

C-fos as a marker for neural activation

To test our idea that neuromasts are activated by chemicals, we needed a method to detect activated neuromast hair cells in the zebrafish embryo. *C-fos* is an immediate-early gene that is rapidly induced when neurons, including sensory neurons are activated and it is a well established marker for neural activity (Herdegen and Leah 1998). However, c-fos expression in activated non-neuronal sensory cells has not been documented. *C-fos*, a member of activator protein-1 (AP-1) family of transcription factors, forms a heterodimer with *Jun* to bind to DNA and regulates transcription of downstream genes (Curran and Franza 1988; Barth et al. 2004). Several extracellular signals and signal transduction pathways control AP-1 activation by

modulating *c-fos*. These include Ca^{2+} (Morgan and Curran 1986), cAMP (Kruijer et al. 1985) and MAPK (mitogen-activated protein kinase) (Bernstein et al. 1994). *C-fos* can be induced by a wide range of stimuli, including odorants, touch and pain (Naranjo et al. 1991a; Mack and Mack 1992; Guthrie et al. 1993). In response to application of peripheral noxious stimuli, specific neurons express *c-fos* in rat CNS (Hunt et al. 1987). Many other studies have confirmed the expression of *c-fos* in activated neurons (Hunt et al. 1987; Draisci and Iadarola 1989; Harris 1998; Herdegen and Leah 1998; Hua et al. 2004). In mammals, noxious stimulation by compounds similar to those used in this study, led to increased *c-fos* mRNA within 30 minutes of application of stimulus (Draisci and Iadarola 1989; Naranjo et al. 1991b). In zebrafish, *c-fos* has been used as a marker for neural activation in the CNS (Baraban et al. 2005).

Functional imaging of neural activity in the lateral line system

To analyze the neural activity underlying a sensory response, it is essential to detect neural activity in a large area of the nervous system in live animals. To identify and functionally analyze the contributions of individual neurons to the process, such system scale detection methods will have to have cellular resolution. The detection scheme also has to be adequately non-invasive since behavior will likely be modified by techniques that disrupt the circuitry. All of these requirements are hard to meet in mammalian models using currently available techniques. Optical detection techniques that will measure activity induced changes within neurons have the potential to provide the required resolution. However mammalian models are optically opaque, restricting the usefulness of optical techniques to studying only superficial layers of their brains. This usually requires a craniotomy to expose the brain tissue, making the

process highly invasive. Also the large size of the nervous system implies that only a small region can be analyzed at a time using such methods.

Many of these problems, like lack of transparency, large size of the brain, and presence of an opaque cranium, can be overcome by using the zebrafish embryo as a model system to study vertebrate sensory responses. Many neurobiological features of zebrafish are conserved with other vertebrates including mammals and the zebrafish is being employed extensively as a model to study functional and developmental aspects of sensory systems like vision, olfaction and hearing in vertebrates. The zebrafish embryo is ideal for analyzing sensory function by optical techniques because they are optically transparent, and all components of its nervous system can be accessed non-invasively by optical techniques that use confocal or two-photon microscopy. Moreover, the small size of the nervous system in these embryos implies the potential to analyze large parts of the nervous system simultaneously.

To utilize the above features of the zebrafish embryo we developed an optical technique to visualize neural activity globally in the nervous system of a live animal, at cellular resolution, such that activation of individual neurons can also be monitored. The technique was applied to detect responses in the lateral line system in the live zebrafish embryo. The lateral line system of the zebrafish is ideal starting point for analyzing sensory responses using our optical method. The lateral line offers the following advantages. It is anatomically simple and well characterized. It features discrete sense organs arranged in a defined pattern, such that each organ can be individually recognized. The sensory structures are easy to visualize and their innervations are easy to label. Anatomy of the major sensory projections of the system are simple and well documented and thus are easy to relate to results from functional studies (Metcalfe et al. 1985; Raible and Kruse 2000; Dambly-Chaudiere et al. 2003). We also show that the lateral line

system can respond to defined chemicals, making it easy to stimulate them in a controlled fashion under optical imaging conditions. Thus the lateral line, with its well characterized morphology, easy accessibility, and chemosensory function, offered the scope to detect stimulus induced activity simultaneously in multiple neurons i.e. in a complete circuit, in a non-invasive manner in a live organism. This ability is crucial to linking behavior to neural activity. Traditional electrophysiological methods do not allow simultaneous recording at the systems level and are not adequately non-invasive. Currently available methods that detect activity at the systems scale each have their strengths and weaknesses and are introduced in the following section.

Available methods for intrinsic imaging of neural activity

Most methods for imaging neural activity *in vivo* do not directly measure voltage changes in neurons (Grinvald et al. 1986; Frostig et al. 1990; Ogawa et al. 1990; Blasdel 1992b; Blasdel 1992a; Bonhoeffer et al. 1995; Everson et al. 1998). Instead, they measure proxies for neuronal activity. Three commonly used approaches to detect such proxies are magnetic resonance imaging (MRI), positron emission tomography (PET) and optical methods. The optical methods were ideal for our study because the zebrafish embryos are transparent and optical techniques could be employed non-invasively. The optical imaging methods fall under two broad categories: those that rely on metabolic changes that arise due to increased metabolic demands, as a proxy for neural activity, and those that use physiological changes. Examples of metabolic changes are changes in blood oxygenation level (BOLD) in capillary networks surrounding nerve tissue. Changes in NADH/Flavoprotein fluorescence is another potential indicator of neural activity.

Physiological changes include changes in intracellular calcium or membrane potential that can be measured using extrinsic or genetically encoded indicators.

Metabolic indicators:

Blood oxygen level as proxy for neural activity

Measurement of the Blood Oxygenation Level Dependent (BOLD) signal either by optical methods or by functional Magnetic Resonance Imaging (fMRI) methods (Ogawa et al. 1990) estimates relative oxy- or deoxyhemoglobin concentrations in the vasculature of neural tissue (Grinvald et al. 1986; Frostig et al. 1990; Blasdel 1992a; Blasdel 1992b; Bonhoeffer et al. 1995; Everson et al. 1998). Techniques using blood oxygenation as a proxy for measuring neuronal activity have limited spatial and temporal resolution. Moreover the amplitude of blood related signals is not linearly related to the metabolic load (Norris 2006). These techniques are limited to animals with the requisite blood-carrying capillary network. Moreover, they cannot be used to measure neuronal activity in developing mammalian embryos or other vertebrates, such as zebrafish, which lack suitable blood flow. While zebrafish embryos lack adequate blood flow to allow BOLD based approaches, their optical transparency make all neural structures readily accessible to fluorimetric confocal and laser scanning microscopy.

NADH and FP fluorescence as potential proxies for neural activity

Autofluorescence of nicotinamide dinucleotide (NADH) and flavoproteins such as lipoamide dehydrogenase (LipDH) and electron transfer flavoprotein (ETF) can be used to monitor neural activation since mitochondrial metabolism and neural activity are closely coupled (Duchen 1992; Mironov and Richter 2001; Schuchmann et al. 2001). Depolarization of neurons

(Duchen 1992; Mironov and Richter 2001; Schuchmann et al. 2001). Depolarization of neurons opens Ca^{2+} channels, leading to an increase of Ca^{2+} ions in the cytoplasm. Some of this Ca^{2+} is taken up by the mitochondria (Budd and Nicholls 1996). The uptake of Ca^{2+} induces calcium cycling in the mitochondria, reducing the proton gradient in the inner mitochondrial membrane. This leads to a transient increase in oxidation of NADH and flavoproteins in the mitochondria (Figure 1.1) (Reinert et al. 2004). Flavoproteins fluoresce when oxidized but not when they are reduced. On the other hand, NADH does not fluoresce when oxidized, but fluoresce when reduced. Thus they produce anti-correlated fluorescent signals when a neuron is activated (Reinert et al. 2004). Measuring these two anti-correlated signals should potentially provide a method for monitoring neural activity. There is evidence that the NADH/FP signal is linearly proportional to spiking activity (Jobsis and Duffield 1967a; Jobsis and Duffield 1967b; Reinert et al. 2004) and that the signal is linearly proportional to stimulation amplitude and stimulation frequency in electrically stimulated cerebellar cortex (Dora et al. 1986). Fluorimetric methods that directly measure the metabolic load of neural tissue can alleviate some of the disadvantages of measuring blood related signals discussed above (Chance and Williams 1955; Chance and Williams 1956; Chance and Baltscheffsky 1958; Shibuki et al. 2003).

Changes in NADH and FP fluorescence, however, are small, making detection and analysis problematic. The potential for applying our new statistical analysis tool described in chapter 3 in analyzing ratiometric NADH/FP signals, and its advantages, are discussed later.

Physiological changes as proxies for neural activity

Changes in intracellular calcium

Calcium plays a central role in cellular physiology. Changes in intracellular calcium levels resulting from the influx of calcium through voltage-gated calcium channels are used extensively as a proxy for the electrical activity of cells. Many fluorescent calcium indicator dyes are available for measuring changes in intracellular calcium. These indicators show a shift in their excitation or emission spectra when they bind to calcium and can be ratiometric (dual emission or dual excitation) or non-ratiometric. Non-ratiometric indicators include small molecule dyes like fluo-2,3,4, Oregon green BAPTA, and rhod-2. However ratiometric indicator dyes, were used in experiments described in the following chapters because they present certain advantages over non-ratiometric ones. These are discussed in more detail in the following sections.

Advantages of a ratiometric approach

Ratiometric fluorescent indicators are used extensively in biological imaging to measure changes in Ca^{2+} concentrations. Their usefulness stems from a number of reasons. Artifacts such as those introduced by variability in illumination and photobleaching of the dye are eliminated by taking the ratio of signals at two different wavelengths. Ratiometry also allows quantitative estimates of physiological variables of interest (Truong et al. 2001). A large number of ratiometric calcium and voltage indicator dyes are available and some of these are genetically encoded fluorescent resonant energy transfer (FRET) based indicators that get rid of invasive dye loading procedures and problems due to differential distribution associated with extrinsic dyes.

With ratiometric techniques, fluorescence is measured either via excitation (Grynkiewicz et al. 1985) or emission (Takahashi et al. 1999) at two different wavelengths. With these

techniques, an anti-correlated signal occurs when, in one channel, fluorescence increases when the variable of interest increases but in the other channel, fluorescence decreases when the variable of interest increases. Because the two measurements are made simultaneously or quasi-simultaneously, photon path length and volume factors are eliminated from the ratio (Grynkiewicz et al. 1985; Bright et al. 1987; Takahashi et al. 1999).

Ratiometric indicators

A large number of extrinsic dyes such as the calcium indicators Fura-2,3,4F and Indo-1,5F (Jackson et al. 1987) and voltage indicators Di-4,8-Anepps (Molecular Probes) as well as genetically encoded calcium (Miyawaki et al. 1997) and voltage indicators (Gonzalez and Tsien 1995; Gonzalez and Tsien 1997; Siegel and Isacoff 1997; Siegel and Isacoff 2000) based on fluorescent resonant energy transfer (FRET) are ratiometric. Genetically encoded FRET indicators are seeing increased application (Higashijima et al. 2003; Li et al. 2005) since they can may be non-invasively introduced and accurately targeted to specific brain region. They are usually non-toxic in stable lines as any adverse effects become apparent while establishing the transgenic line (Xiang et al. 2006, submitted).

Ratiometric calcium indicator dyes

The measurement of intracellular calcium levels in living cells can be accomplished through the use of calcium indicator dyes. Fluorescence from these dyes can be measured either by widefield fluorescence imaging or by confocal or multiphoton microscopy. Particularly with confocal or multiphoton techniques, it is easiest to excite with a single laser, making emission ratiometry the method of choice.

The majority of ratiometric dyes, however, are suitable for excitation ratiometry (fura-2, bis-fura-2; (Takahashi et al. 1999). Indo-1 is an emission ratiometric dye, and can be used to do emission ratiometry in confocal microscopes (Isshiki et al. 1998). Unfortunately, indo-1 bleaches extremely rapidly. A solution to these problems is to mix non-ratiometric dyes to form a ratiometric one. For example, one may simultaneously load cells with fluo-3 or fluo-4 and Fura-red. Fluo-3 and fluo-4 are calcium indicators whose fluorescence increases with increasing $[Ca^{2+}]$, and Fura-red's fluorescence decreases with increasing $[Ca^{2+}]$ (Lipp and Niggli 1993; Bischofberger and Schild 1995; Gomez et al. 2001).

Such dyes, (fura-2, fluo-3, fluo-4) can be introduced into cells by bulk loading techniques such as ester loading or cell permeabilization, or by techniques such as microinjection (Takahashi et al. 1999). Although these dyes are extremely valuable in measuring changes in intracellular calcium, most calcium indicators act as chelators and can affect the function of the loaded neurons (Takahashi et al. 1999). Moreover loading techniques can damage cells and it is usually difficult to specifically load particular types of cells in a tissue. A problem with ratiometric approach using a mix of dyes is that differential bleaching, compartmentalization, or clearance of the two dyes may give rise to ratiometric signals that are partially independent of changes in $[Ca^{2+}]_i$ (Lipp and Niggli 1993).

The extent of dye compartmentalization, clearance, and bleaching can be evaluated by examining and quantifying the fluorescent images at the two component wavelengths before the formation of the ratiometric image. Several schemes are available to inhibit dye compartmentalization and clearance, including loading at low temperature (Keith et al. 1985; Roe et al. 1990) and the use of anion transport inhibitors such as probenecid (Merritt et al. 1990) and the use of dextran-conjugated indicators (Schlatterer et al. 1992). In the case of differential

bleaching, the options are more limited: the medium can be made hypoxic (Takahashi et al. 1999) or illumination can be minimized. Since many cells will suffer under long term hypoxia, minimizing exposure is often the only practical option. Minimizing exposure is made more difficult because the quantum efficiency of Fura-Red is quite low (0.013 in the Ca^{2+} free form (Kao 1994), so the red image can be quite dim unless high concentrations of dye are used (which can exacerbate compartmentalization and buffering of $[Ca^{2+}]i$). The use of dual dye ratiometric analysis for time course studies therefore constrains the investigator to work with very low light level images.

To circumvent these problems, genetically encoded calcium biosensors have been generated using variants of *Aequorea* Green Fluorescent Protein (GFP) (Zhang et al. 2002; Miyawaki et al. 2003; Miesenböck 2004; Miesenböck and Kevrekidis 2005; Miyawaki 2005). Because genetically encoded biosensors can be selectively expressed, in principle they should be able to dissect the activity of neural circuits in an intact animal more efficiently than synthetic calcium indicator dyes. Moreover, when these dyes are expressed in an animal, animal viability and/or behavior offers an assay of whether they affect cell function (Higashijima et al. 2003). One such genetically encoded dye, used in experiments described in later chapters, is cameleon.

Cameleon as a genetically encoded calcium indicator

Cameleons are genetically encoded Ca^{2+} indicators (GECI's) (Miyawaki et al. 1997; Tsien 1998). They are chimeric proteins built of a short-wavelength variant of GFP which serves as a fluorescence resonance energy transfer (FRET) donor, the CaM-binding peptide of myosin light-chain kinase (M13), and a long-wavelength variant of GFP which serves as a FRET acceptor. Binding of Ca^{2+} to the CaM moiety causes a change in conformation as the CaM and

M13 domains interact, causing a change in conformation. This brings the modified GFP domains close enough to allow FRET from the shorter to the longer-wavelength variant of GFP (Patterson et al. 2000; Habuchi et al. 2002). FRET signals from cameleon allows emission ratiometry, eliminating artifacts due to bleaching, variable illumination, and reducing the effects of movement or changes in focus that are seen with single-wavelength monitoring. Emission ratioing is an ideal readout for fast imaging by laser-scanning confocal microscopy (Higashijima et al. 2003; Miyawaki 2005).

There are several different cameleons (Truong et al. 2001; Nagai et al. 2004; Miyawaki 2005). YCs are classified into several groups based on the composition of their Ca^{2+} binding domain (Miyawaki 2003). For experiments described here, we used the yellow cameleon 2.1 (YC2.1). YC2.1 has cyan and yellow fluorescent proteins (CFP and YFP) as the FRET donor and acceptor, respectively. In zebrafish, YC2.1 was used to study Ca^{2+} dynamics in sensory and spinal cord neurons (Higashijima et al. 2003).

Cameleons were expected to be superior to synthetic dyes for investigating activity of neural circuits in living animals. While YCs display robust Ca^{2+} responses *in vitro* and in transiently transfected cell samples, their dynamic range is significantly reduced in the nervous systems of transgenic vertebrates (Miyawaki et al. 1999; Truong et al. 2001; Miyawaki et al. 2003; Nagai et al. 2004; Miyawaki 2005). Most YCs, including YC2.1, exhibit at most a 120% change in the ratio of YFP/CFP upon Ca^{2+} binding in solution. This dynamic range appears to be attenuated in cells that have a large amount of CaM and CaM-associated proteins (Hasan et al. 2004; Heim and Griesbeck 2004; Palmer et al. 2004). Because cameleon YC2.1 signals are weak, measuring stimulus-dependent responses in the Rohan-Beard neurons of transgenic zebrafish required extensive spatial averaging of fluorescence signals before ratiometric analysis

(Higashijima et al. 2003). To visualize changes in FRET signal from cameleon at high spatio-temporal resolution, a new statistical optimization technique, that takes advantage of correlated information in the entire image, was necessary.

Statistical approaches for analyzing weak ratiometric signals

Cameleon is highly suited in terms of expression and ratiometric nature, and because its genetically encoded. But the fluorescence changes involved are extremely small. Low signal from cameleons, or the use of low light level images for ratiometry using mixed dyes, however, presents a set of problems. A ratio formed with low pixel intensities may be wildly inaccurate largely due to fluctuations in the ratio when the denominator is close to zero. As a consequence, ratiometric analyses of low-intensity data have necessitated subjective thresholding and extensive data averaging. This is typically done either in space where a region of interest (ROI) is typically chosen, e.g. (Higashijima et al. 2003), or in time where pixel timecourses are averaged (Russ 1998).

With user-defined ROIs, particularly with noisy data, active regions may go undetected by eye. The eye can typically only detect contrast differences at the 2% level or above. Thus, to utilize cameleon FRET signals or low light fluorescent data, a new statistical method was necessary. The method, described in chapter 3, determines the anti-correlated subspace in a user-independent (objective) way by finding weighted masks (eigenimages resulting from an optimization problem) that indicate where anti-correlated activity is occurring in the dataset. This is preferable to the subjective or user defined ROI which leaves room for error when fluorescence changes are very small.

excitable neuron-like cell and have been extensively used in calcium imaging studies. When these cells are exposed to nerve growth factor (NGF), they differentiate into cells that morphologically and physiologically resemble neurons: they extend long processes, and become electrically excitable (Tischler et al. 1983). During differentiation into a neuron-like cell expression of voltage-gated sodium channels are upregulated (Bouron et al. 1999) and the cell becomes electrically excitable (Tischler et al. 1983). Additionally, they increase their expression of voltage gated calcium channels. The differentiated PC12 cells exhibit repetitive calcium waves in response to appropriate neurotransmitters (Black et al. 2003). These cells also exhibit changes in calcium in response to depolarizing solutions such as potassium-containing solutions.

To demonstrate the suitability of our technique for detecting Cameleon FRET signals, dissociated neuronal cultures from the spinal cord of cameleon-expressing transgenic zebrafish were used. For system level imaging, we used whole embryos of the same transgenic line at day 4 of development.

References

Bandell, M., Story, G.M., Hwang, S.W., Viswanath, V., Eid, S.R., Petrus, M.J., Earley, T.J., and Patapoutian, A. 2004. Noxious cold ion channel TRPA1 is activated by pungent compounds and bradykinin. *Neuron* **41**(6): 849-857.

Baraban, S.C., Taylor, M.R., Castro, P.A., and Baier, H. 2005. Pentylenetetrazole induced changes in zebrafish behavior, neural activity and c-fos expression. *Neuroscience* **131**(3): 759-768.

Barth, A.L., Gerkin, R.C., and Dean, K.L. 2004. Alteration of neuronal firing properties after in vivo experience in a FosGFP transgenic mouse. *J Neurosci* **24**(29): 6466-6475.

Bautista, D.M., Movahed, P., Hinman, A., Axelsson, H.E., Sterner, O., Hogestatt, E.D., Julius, D., Jordt, S.E., and Zygmunt, P.M. 2005. Pungent products from garlic activate the sensory ion channel TRPA1. *Proc Natl Acad Sci U S A* **102**(34): 12248-12252.

Bernstein, L.R., Ferris, D.K., Colburn, N.H., and Sobel, M.E. 1994. A family of mitogen-activated protein kinase-related proteins interacts in vivo with activator protein-1 transcription factor. *J Biol Chem* **269**(13): 9401-9404.

Bautista, D.M., Movahed, P., Hinman, A., Axelsson, H.E., Sterner, O., Hogestatt, E.D., Julius, D., Jordt, S.E., and Zygmunt, P.M. 2005. Pungent products from garlic activate the sensory ion channel TRPA1. *Proc Natl Acad Sci U S A* **102**(34): 12248-12252.

Bernstein, L.R., Ferris, D.K., Colburn, N.H., and Sobel, M.E. 1994. A family of mitogen-activated protein kinase-related proteins interacts in vivo with activator protein-1 transcription factor. *J Biol Chem* **269**(13): 9401-9404.

Bischofberger, J. and Schild, D. 1995. Different spatial patterns of [Ca2+] increase caused by N- and L-type Ca2+ channel activation in frog olfactory bulb neurones. *J Physiol* **487 (Pt 2)**: 305-317.

Black, M.J., Woo, Y., and Rane, S.G. 2003. Calcium channel upregulation in response to activation of neurotrophin and surrogate neurotrophin receptor tyrosine kinases. *J Neurosci Res* **74**(1): 23-36.

Blasdel, G.G. 1992a. Differential imaging of ocular dominance and orientation selectivity in monkey striate cortex. *J Neurosci* **12**(8): 3115-3138.

-. 1992b. Orientation selectivity, preference, and continuity in monkey striate cortex. *J Neurosci* **12**(8): 3139-3161.

Bonhoeffer, T., Kim, D.S., Malonek, D., Shoham, D., and Grinvald, A. 1995. Optical imaging of the layout of functional domains in area 17 and across the area 17/18 border in cat visual cortex. *Eur J Neurosci* **7**(9): 1973-1988.

Bouron, A., Becker, C., and Porzig, H. 1999. Functional expression of voltage-gated Na+ and Ca2+ channels during neuronal differentiation of PC12 cells with nerve growth factor or forskolin. *Naunyn Schmiedebergs Arch Pharmacol* **359**(5): 370-377.

Brantley, R.K. and Bass, A.H. 1988. Cholinergic neurons in the brain of a teleost fish (Porichthys notatus) located with a monoclonal antibody to choline acetyltransferase. *J Comp Neurol* **275**(1): 87-105.

Bricaud, O., Chaar, V., Dambly-Chaudiere, C., and Ghysen, A. 2001. Early efferent innervation of the zebrafish lateral line. *J Comp Neurol* **434**(3): 253-261.

Bright, G.R., Fisher, G.W., Rogowska, J., and Taylor, D.L. 1987. Fluorescence ratio imaging microscopy: temporal and spatial measurements of cytoplasmic pH. *J Cell Biol* **104**(4): 1019-1033.

Budd, S.L. and Nicholls, D.G. 1996. A reevaluation of the role of mitochondria in neuronal Ca2+ homeostasis. *J Neurochem* **66**(1): 403-411.

Budker, P. 1938. Les cryptes sensorielles et les denticules cutanes des plagiostomes. *Annales de L'institut Oceanographique, Paris* **18**: 207-288.

Chance, B. and Baltscheffsky, H. 1958. Respiratory enzymes in oxidative phosphorylation. VII. Binding of intramitochondrial reduced pyridine nucleotide. *J Biol Chem* **233**(3): 736-739.

Chance, B. and Williams, G.R. 1955. Respiratory enzymes in oxidative phosphorylation. II. Difference spectra. *J Biol Chem* **217**(1): 395-407.

-. 1956. The respiratory chain and oxidative phosphorylation. *Adv Enzymol Relat Subj Biochem* **17**: 65-134.

Clapham, D.E., Runnels, L.W., and Strubing, C. 2001. The TRP ion channel family. *Nat Rev Neurosci* **2**(6): 387-396.

Coombs, S., Gorner, P., Munz, H. 1989a. A brief overview of the mechanosensory lateral line system. in *The mechanosensory lateral line* (ed. S. Coombs, Gorner, P., Munz, H.). Springer-Verlag.

-. 1989b. *The mechanosensory lateral line neurobiology and evolution*. Springer-verlag.

Corey, D.P., Garcia-Anoveros, J., Holt, J.R., Kwan, K.Y., Lin, S.Y., Vollrath, M.A., Amalfitano, A., Cheung, E.L., Derfler, B.H., Duggan, A., Geleoc, G.S., Gray, P.A., Hoffman, M.P., Rehm, H.L., Tamasauskas, D., and Zhang, D.S. 2004. TRPA1 is a candidate for the mechanosensitive transduction channel of vertebrate hair cells. *Nature* **432**(7018): 723-730.

Curran, T. and Franza, B.R., Jr. 1988. Fos and Jun: the AP-1 connection. *Cell* **55**(3): 395-397.

Dambly-Chaudiere, C., Sapede, D., Soubiran, F., Decorde, K., Gompel, N., and Ghysen, A. 2003. The lateral line of zebrafish: a model system for the analysis of morphogenesis and neural development in vertebrates. *Biol Cell* **95**(9): 579-587.

Danielson, P.D., Zottoli, S.J., Corrodi, J.G., Rhodes, K.J., and Mufson, E.J. 1988. Localization of choline acetyltransferase to somata of posterior lateral line efferents in the goldfish. *Brain Res* **448**(1): 158-161.

Dedov, V.N., Tran, V.H., Duke, C.C., Connor, M., Christie, M.J., Mandadi, S., and Roufogalis, B.D. 2002. Gingerols: a novel class of vanilloid receptor (VR1) agonists. *Br J Pharmacol* **137**(6): 793-798.

Dijkgraaf, S. 1989. in *The Mechanosensory Lateral Line: Neurobiology and Evolution* (ed. S. Coombs, Gorner, P., Munz, H.). Sringer-verlag.

Dora, E., Tanaka, K., Greenberg, J.H., Gonatas, N.H., and Reivich, M. 1986. Kinetics of microcirculatory, NAD/NADH, and electrocorticographic changes in cat brain cortex during ischemia and recirculation. *Ann Neurol* **19**(6): 536-544.

Draisci, G. and Iadarola, M.J. 1989. Temporal analysis of increases in c-fos, preprodynorphin and preproenkephalin mRNAs in rat spinal cord. *Brain Res Mol Brain Res* **6**(1): 31-37.

Duchen, M.R. 1992. Ca(2+)-dependent changes in the mitochondrial energetics in single dissociated mouse sensory neurons. *Biochem J* **283 (Pt 1)**: 41-50.

Everson, R.M., Prashanth, A.K., Gabbay, M., Knight, B.W., Sirovich, L., and Kaplan, E. 1998. Representation of spatial frequency and orientation in the visual cortex. *Proc Natl Acad Sci U S A* **95**(14): 8334-8338.

Flock, A. and Russell, I.J. 1973. The post-synaptic action of efferent fibres in the lateral line organ of the burbot Lota lota. *J Physiol* **235**(3): 591-605.

Frostig, R.D., Lieke, E.E., Ts'o, D.Y., and Grinvald, A. 1990. Cortical functional architecture and local coupling between neuronal activity and the microcirculation revealed by in vivo high-resolution optical imaging of intrinsic signals. *Proc Natl Acad Sci U S A* **87**(16): 6082-6086.

Gomez, T.M., Robles, E., Poo, M., and Spitzer, N.C. 2001. Filopodial calcium transients promote substrate-dependent growth cone turning. *Science* **291**(5510): 1983-1987.

Gonzalez, J.E. and Tsien, R.Y. 1995. Voltage sensing by fluorescence resonance energy transfer in single cells. *Biophys J* **69**(4): 1272-1280.

-. 1997. Improved indicators of cell membrane potential that use fluorescence resonance energy transfer. *Chem Biol* **4**(4): 269-277.

Grinvald, A., Lieke, E., Frostig, R.D., Gilbert, C.D., and Wiesel, T.N. 1986. Functional architecture of cortex revealed by optical imaging of intrinsic signals. *Nature* **324**(6095): 361-364.

Grynkiewicz, G., Poenie, M., and Tsien, R.Y. 1985. A new generation of Ca2+ indicators with greatly improved fluorescence properties. *J Biol Chem* **260**(6): 3440-3450.

Guo, S., Brush, J., Teraoka, H., Goddard, A., Wilson, S.W., Mullins, M.C., and Rosenthal, A. 1999. Development of noradrenergic neurons in the zebrafish hindbrain requires BMP, FGF8, and the homeodomain protein soulless/Phox2a. *Neuron* **24**(3): 555-566.

Guthrie, K.M., Anderson, A.J., Leon, M., and Gall, C. 1993. Odor-induced increases in c-fos mRNA expression reveal an anatomical "unit" for odor processing in olfactory bulb. *Proc Natl Acad Sci U S A* **90**(8): 3329-3333.

Habuchi, S., Cotlet, M., Hofkens, J., Dirix, G., Michiels, J., Vanderleyden, J., Subramaniam, V., and De Schryver, F.C. 2002. Resonance energy transfer in a calcium concentration-dependent cameleon protein. *Biophys J* **83**(6): 3499-3506.

Harris, J.A. 1998. Using c-fos as a neural marker of pain. *Brain Res Bull* **45**(1): 1-8.

Hasan, M.T., Friedrich, R.W., Euler, T., Larkum, M.E., Giese, G., Both, M., Duebel, J., Waters, J., Bujard, H., Griesbeck, O., Tsien, R.Y., Nagai, T., Miyawaki, A., and Denk, W. 2004. Functional fluorescent Ca2+ indicator proteins in transgenic mice under TET control. *PLoS Biol* **2**(6): e163.

Heim, N. and Griesbeck, O. 2004. Genetically encoded indicators of cellular calcium dynamics based on troponin C and green fluorescent protein. *J Biol Chem* **279**(14): 14280-14286.

Herdegen, T. and Leah, J.D. 1998. Inducible and constitutive transcription factors in the mammalian nervous system: control of gene expression by Jun, Fos and Krox, and CREB/ATF proteins. *Brain Res Brain Res Rev* **28**(3): 370-490.

Higashijima, S., Masino, M.A., Mandel, G., and Fetcho, J.R. 2003. Imaging neuronal activity during zebrafish behavior with a genetically encoded calcium indicator. *J Neurophysiol* **90**(6): 3986-3997.

Hua, F., Harrison, T., Qin, C., Reifsteck, A., Ricketts, B., Carnel, C., and Williams, C.A. 2004. c-Fos expression in rat brain stem and spinal cord in response to activation of cardiac ischemia-sensitive afferent neurons and electrostimulatory modulation. *Am J Physiol Heart Circ Physiol* **287**(6): H2728-2738.

Hunt, S.P., Pini, A., and Evan, G. 1987. Induction of c-fos-like protein in spinal cord neurons following sensory stimulation. *Nature* **328**(6131): 632-634.

Isshiki, M., Ando, J., Korenaga, R., Kogo, H., Fujimoto, T., Fujita, T., and Kamiya, A. 1998. Endothelial Ca2+ waves preferentially originate at specific loci in caveolin-rich cell edges. *Proc Natl Acad Sci U S A* **95**(9): 5009-5014.

Jackson, A.P., Timmerman, M.P., Bagshaw, C.R., and Ashley, C.C. 1987. The kinetics of calcium binding to fura-2 and indo-1. *FEBS Lett* **216**(1): 35-39.

Jobsis, F.F. and Duffield, J.C. 1967a. Force, shortening, and work in muscular contraction: relative contributions to overall energy utilization. *Science* **156**(780): 1388-1392.

-. 1967b. Oxidative and glycolytic recovery metabolism in muscle. *J Gen Physiol* **50**(4): 1009-1047.

Jordt, S.E., Bautista, D.M., Chuang, H.H., McKemy, D.D., Zygmunt, P.M., Hogestatt, E.D., Meng, I.D., and Julius, D. 2004. Mustard oils and cannabinoids excite sensory nerve fibres through the TRP channel ANKTM1. *Nature* **427**(6971): 260-265.

Jorgensen, J.M. 1989. Evolution of octavolateralis sensory cells. in *The mechanosensory lateral line neurobiology and evolution* (ed. S. Coombs, Gorner, P., Munz, H.). Springer-verlag.

Kao, J.P. 1994. Practical aspects of measuring [Ca2+] with fluorescent indicators. *Methods Cell Biol* **40**: 155-181.

Katsuki, Y., Hashimoto, T., and Kendall, J.I. 1971. The chemoreception in the lateral-line organs of teleosts. *Jpn J Physiol* **21**(1): 99-118.

Katsuki, Y., Yanagisawa, K., Tester, A.L., and Kendall, J.I. 1969. Shark pit organs: response to chemicals. *Science* **163**(865): 405-407.

Katsuki, Y., Yanagisawa, K. 1982. Chemoreception in the lateral line organ. in *Chemoreception in fishes* (ed. T.J. Hara), pp. 227-257. Elsevier Scientific publishing Company.

Keith, C.H., Ratan, R., Maxfield, F.R., Bajer, A., and Shelanski, M.L. 1985. Local cytoplasmic calcium gradients in living mitotic cells. *Nature* **316**(6031): 848-850.

Kozlowski, D.J., Murakami, T., Ho, R.K., and Weinberg, E.S. 1997. Regional cell movement and tissue patterning in the zebrafish embryo revealed by fate mapping with caged fluorescein. *Biochem Cell Biol* **75**(5): 551-562.

Kroese, A.B.A., VanNetten, S. M. 1989. Sensory Transduction in lateral line hair cells. in *The mechanosensory lateral line* (ed. S. Coombs, Gorner, P., Munz, H.). Springer-Verlag.

Kruijer, W., Schubert, D., and Verma, I.M. 1985. Induction of the proto-oncogene fos by nerve growth factor. *Proc Natl Acad Sci U S A* **82**(21): 7330-7334.

Kwan, K.Y., Allchorne, A.J., Vollrath, M.A., Christensen, A.P., Zhang, D.S., Woolf, C.J., and Corey, D.P. 2006. TRPA1 contributes to cold, mechanical, and chemical nociception but is not essential for hair-cell transduction. *Neuron* **50**(2): 277-289.

Li, J., Mack, J.A., Souren, M., Yaksi, E., Higashijima, S., Mione, M., Fetcho, J.R., and Friedrich, R.W. 2005. Early development of functional spatial maps in the zebrafish olfactory bulb. *J Neurosci* **25**(24): 5784-5795.

Lipp, P. and Niggli, E. 1993. Ratiometric confocal Ca(2+)-measurements with visible wavelength indicators in isolated cardiac myocytes. *Cell Calcium* **14**(5): 359-372.

Lopez-Schier, H. and Hudspeth, A.J. 2005. Supernumerary neuromasts in the posterior lateral line of zebrafish lacking peripheral glia. *Proc Natl Acad Sci U S A* **102**(5): 1496-1501.

Mack, K.J. and Mack, P.A. 1992. Induction of transcription factors in somatosensory cortex after tactile stimulation. *Brain Res Mol Brain Res* **12**(1-3): 141-147.

Meredith, G.E., Roberts, B.L., and Maslam, S. 1987. Distribution of afferent fibers in the brainstem from end organs in the ear and lateral line in the European eel. *J Comp Neurol* **265**(4): 507-520.

Merritt, J.E., McCarthy, S.A., Davies, M.P., and Moores, K.E. 1990. Use of fluo-3 to measure cytosolic Ca2+ in platelets and neutrophils. Loading cells with the dye, calibration of traces, measurements in the presence of plasma, and buffering of cytosolic Ca2+. *Biochem J* **269**(2): 513-519.

Metcalfe, W.K., Kimmel, C.B., and Schabtach, E. 1985. Anatomy of the posterior lateral line system in young larvae of the zebrafish. *J Comp Neurol* **233**(3): 377-389.

Miesenböck, G. 2004. Genetic methods for illuminating the function of neural circuits. *Curr Opin Neurobiol* **14**(3): 395-402.

Miesenböck, G. and Kevrekidis, I.G. 2005. Optical imaging and control of genetically designated neurons in functioning circuits. *Annu Rev Neurosci* **28**: 533-563.

Mironov, S.L. and Richter, D.W. 2001. Oscillations and hypoxic changes of mitochondrial variables in neurons of the brainstem respiratory centre of mice. *J Physiol* **533**(Pt 1): 227-236.

Miyawaki, A. 2003. Visualization of the spatial and temporal dynamics of intracellular signaling. *Dev Cell* **4**(3): 295-305.

-. 2005. Innovations in the imaging of brain functions using fluorescent proteins. *Neuron* **48**(2): 189-199.

Miyawaki, A., Griesbeck, O., Heim, R., and Tsien, R.Y. 1999. Dynamic and quantitative Ca2+ measurements using improved cameleons. *Proc Natl Acad Sci U S A* **96**(5): 2135-2140.

Miyawaki, A., Llopis, J., Heim, R., McCaffery, J.M., Adams, J.A., Ikura, M., and Tsien, R.Y. 1997. Fluorescent indicators for Ca2+ based on green fluorescent proteins and calmodulin. *Nature* **388**(6645): 882-887.

Miyawaki, A., Mizuno, H., Nagai, T., and Sawano, A. 2003. Development of genetically encoded fluorescent indicators for calcium. *Methods Enzymol* **360**: 202-225.

Montgomery, J. 1997. The lateral line can mediate rheotaxis in fish. *Nature* **389**: 960-963.

Montgomery, J., Carton, G., Voigt, R., Baker, C., and Diebel, C. 2000. Sensory processing of water currents by fishes. *Philos Trans R Soc Lond B Biol Sci* **355**(1401): 1325-1327.

Montgomery, J.C., Macdonald, F., Baker, C.F., and Carton, A.G. 2002. Hydrodynamic contributions to multimodal guidance of prey capture behavior in fish. *Brain Behav Evol* **59**(4): 190-198.

Montgomery, J.C., McDonald, F., Baker, C.F., Carton, A.G., and Ling, N. 2003. Sensory integration in the hydrodynamic world of rainbow trout. *Proc Biol Sci* **270 Suppl 2**: S195-197.

Morgan, J.I. and Curran, T. 1986. Role of ion flux in the control of c-fos expression. *Nature* **322**(6079): 552-555.

Nagai, T., Yamada, S., Tominaga, T., Ichikawa, M., and Miyawaki, A. 2004. Expanded dynamic range of fluorescent indicators for Ca(2+) by circularly permuted yellow fluorescent proteins. *Proc Natl Acad Sci U S A* **101**(29): 10554-10559.

Naranjo, J.R., Mellstrom, B., Achaval, M., Lucas, J.J., Del Rio, J., and Sassone-Corsi, P. 1991a. Co-induction of jun B and c-fos in a subset of neurons in the spinal cord. *Oncogene* **6**(2): 223-227.

Naranjo, J.R., Mellstrom, B., Achaval, M., and Sassone-Corsi, P. 1991b. Molecular pathways of pain: Fos/Jun-mediated activation of a noncanonical AP-1 site in the prodynorphin gene. *Neuron* **6**(4): 607-617.

Norris, D.G. 2006. Principles of magnetic resonance assessment of brain function. *Journal of Magnetic Resonance Imaging* **23**(6): 794-807.

Ogawa, S., Lee, T.M., Kay, A.R., and Tank, D.W. 1990. Brain magnetic resonance imaging with contrast dependent on blood oxygenation. *Proc Natl Acad Sci U S A* **87**(24): 9868-9872.

Palmer, A.E., Jin, C., Reed, J.C., and Tsien, R.Y. 2004. Bcl-2-mediated alterations in endoplasmic reticulum Ca2+ analyzed with an improved genetically encoded fluorescent sensor. *Proc Natl Acad Sci U S A* **101**(50): 17404-17409.

Patterson, G.H., Piston, D.W., and Barisas, B.G. 2000. Forster distances between green fluorescent protein pairs. *Anal Biochem* **284**(2): 438-440.

Purves, D., Augustine, G.J., Fitzpatrick, D., Hall W. C., LaMantia, A., McNamara, J. O., Williams, S. M. 2004. *Neuroscience*. Sinauer Associates.

Raible, D.W. and Kruse, G.J. 2000. Organization of the lateral line system in embryonic zebrafish. *J Comp Neurol* **421**(2): 189-198.

Reinert, K.C., Dunbar, R.L., Gao, W., Chen, G., and Ebner, T.J. 2004. Flavoprotein autofluorescence imaging of neuronal activation in the cerebellar cortex in vivo. *J Neurophysiol* **92**(1): 199-211.

Roe, M.W., Lemasters, J.J., and Herman, B. 1990. Assessment of Fura-2 for measurements of cytosolic free calcium. *Cell Calcium* **11**(2-3): 63-73.

Russ, J.C. 1998. *The Image Processing Handbook*. CRC Press.

Schlatterer, C., Knoll, G., and Malchow, D. 1992. Intracellular calcium during chemotaxis of Dictyostelium discoideum: a new fura-2 derivative avoids sequestration of the indicator and allows long-term calcium measurements. *Eur J Cell Biol* **58**(1): 172-181.

Schuchmann, S., Kovacs, R., Kann, O., Heinemann, U., and Buchheim, K. 2001. Monitoring NAD(P)H autofluorescence to assess mitochondrial metabolic functions in rat hippocampal-entorhinal cortex slices. *Brain Res Brain Res Protoc* **7**(3): 267-276.

Shibuki, K., Hishida, R., Murakami, H., Kudoh, M., Kawaguchi, T., Watanabe, M., Watanabe, S., Kouuchi, T., and Tanaka, R. 2003. Dynamic imaging of somatosensory cortical activity in the rat visualized by flavoprotein autofluorescence. *J Physiol* **549**(Pt 3): 919-927.

Sidi, S., Friedrich, R.W., and Nicolson, T. 2003. NompC TRP channel required for vertebrate sensory hair cell mechanotransduction. *Science* **301**(5629): 96-99.

Siegel, M.S. and Isacoff, E.Y. 1997. A genetically encoded optical probe of membrane voltage. *Neuron* **19**(4): 735-741.

-. 2000. Green fluorescent protein-based sensors for detecting signal transduction and monitoring ion channel function. *Methods Enzymol* **327**: 249-259.

Story, G.M., Peier, A.M., Reeve, A.J., Eid, S.R., Mosbacher, J., Hricik, T.R., Earley, T.J., Hergarden, A.C., Andersson, D.A., Hwang, S.W., McIntyre, P., Jegla, T., Bevan, S., and Patapoutian, A. 2003. ANKTM1, a TRP-like channel expressed in nociceptive neurons, is activated by cold temperatures. *Cell* **112**(6): 819-829.

Takahashi, A., Camacho, P., Lechleiter, J.D., and Herman, B. 1999. Measurement of intracellular calcium. *Physiol Rev* **79**(4): 1089-1125.

Tischler, A.S., Greene, L.A., Kwan, P.W., and Slayton, V.W. 1983. Ultrastructural effects of nerve growth factor on PC 12 pheochromocytoma cells in spinner culture. *Cell Tissue Res* **228**(3): 641-648.

Truong, K., Sawano, A., Mizuno, H., Hama, H., Tong, K.I., Mal, T.K., Miyawaki, A., and Ikura, M. 2001. FRET-based in vivo Ca2+ imaging by a new calmodulin-GFP fusion molecule. *Nat Struct Biol* **8**(12): 1069-1073.

Tsien, R.Y. 1998. The green fluorescent protein. *Annu Rev Biochem* **67**: 509-544.

Voets, T., Talavera, K., Owsianik, G., and Nilius, B. 2005. Sensing with TRP channels. *Nat Chem Biol* **1**(2): 85-92.

Webb, J.F. and Shirey, J.E. 2003. Postembryonic development of the cranial lateral line canals and neuromasts in zebrafish. *Dev Dyn* **228**(3): 370-385.

Whitfield, T.T., Granato, M., van Eeden, F.J., Schach, U., Brand, M., Furutani-Seiki, M., Haffter, P., Hammerschmidt, M., Heisenberg, C.P., Jiang, Y.J., Kane, D.A., Kelsh, R.N., Mullins, M.C., Odenthal, J., and Nusslein-Volhard, C. 1996. Mutations affecting development of the zebrafish inner ear and lateral line. *Development* **123**: 241-254.

Withear, M. 1952. The innervation of the skin of teleost fishes. *Q J Microsc Sci* **93**: 289–305.

Yanagisawa, K., Asanuma, A., and Katsuki, Y. 1974. [Proceedings: Chemoreceptors of the lateral line organs in Necturus]. *Nippon Seirigaku Zasshi* **36**(8-9): 315.

Zhang, J., Campbell, R.E., Ting, A.Y., and Tsien, R.Y. 2002. Creating new fluorescent probes for cell biology. *Nat Rev Mol Cell Biol* **3**(12): 906-918.

Figure 1.1: Schematic diagram of the coupling of autofluorescence signal from NADH and flavoproteins with neuronal activation. (1): depolarization activates Na^{+} -K^{+} pump and voltage-gated Ca^{2+} channels. (2): entry of Ca^{2+} into the mitochondria and Ca^{2+} cycling. (3): ATP synthase. (4): NADH and pyruvates are provided by glycolysis and lactate dehydrogenase. (5): Ca^{2+} -activated pyruvate dehydrogenase complex converts pyruvate to provide energy for the tricarboxylic acid cycle. (6): Oxidation- reduction of FAD (flavin adenine dinucleotide) and FMN (flavin mononucleotide) in respiratory chain complexes produces changes in autofluorescence. Figure adapted from Reinart et al (Reinert et al. 2004).

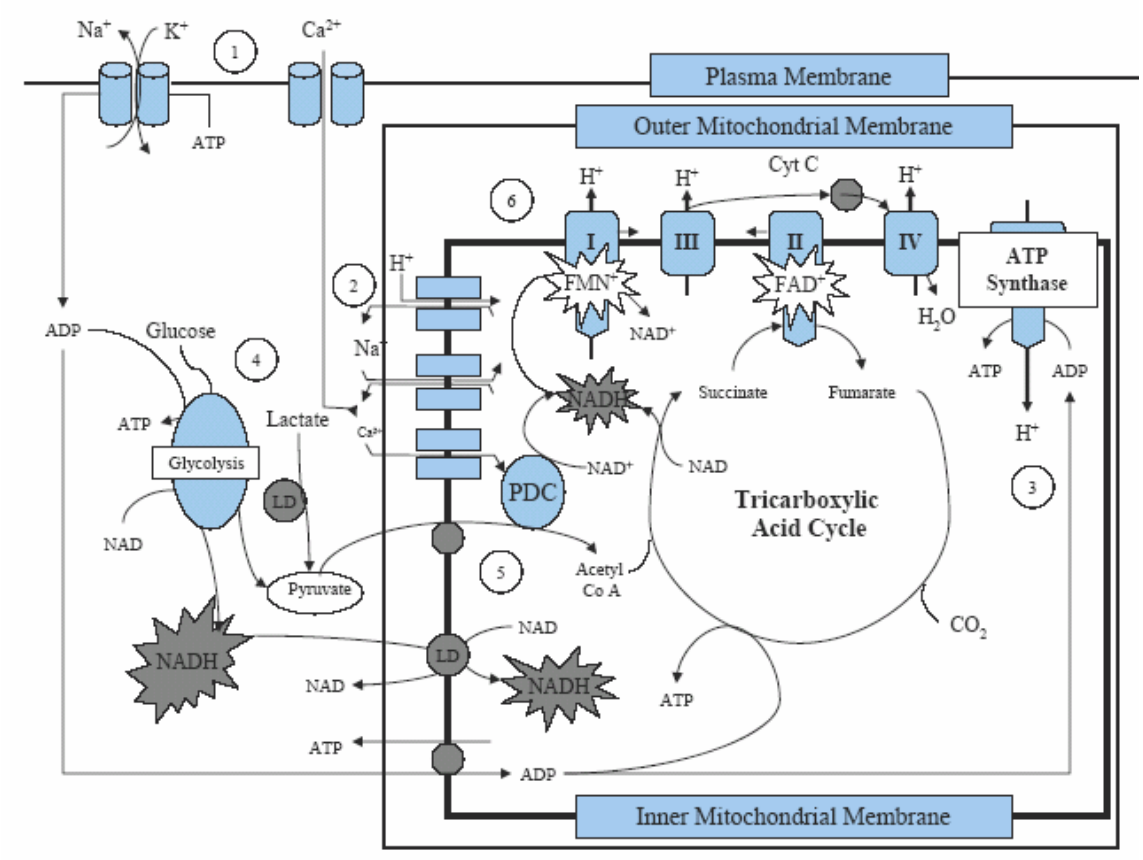
Na+
K+
Ca2+
1
ATP
Plasma Membrane
Outer Mitochondrial Membrane
Cyt C
H+
6
I
III
II
IV
ATP Synthase
FMN+
FAD+
NAD+
H2O
2
Na+
ADP
Glucose
4
ATP
Glycolysis
Lactate
Ca2+
NADH
Succinate
Fumarate
ATP
ADP
H+
NAD
LD
PDC
Tricarboxylic Acid Cycle
3
Pyruvate
5
Acetyl Co A
CO2
NADH
NAD
LD
NADH
ATP
ATP
ADP
Inner Mitochondrial Membrane

Chapter 2

Zebrafish neuromasts respond to chemical stimulation[1]

[1]Majumder A., Porter E., Sornborger A., Keith C., Lauderdale J.D.
To be submitted to Current Biology

Abstract

The lateral line system of fish and amphibians is a mechanosensory system that detects water currents and changes in water pressure. Here we show that the sensory organs of the system, called neuromasts, are also capable of responding to pungent chemical stimulants independently of mechanosensory stimuli. Exposure of embryos to specific chemicals induces expression of the neural activity marker *c-fos* in neuromasts and the number of neuromasts activated depends on the stimulant. Expression of *c-fos* in specific nuclei in the brain in response to such chemical stimulation suggests components of a functional circuit for processing lateral line signals. Based on the response profile, we discuss the possible involvement of transient receptor potential channels in triggering neuromast responses. We conclude that the lateral line system has the potential to act as a chemosensory organ in zebrafish, and possibly in other aquatic animals.

Introduction

The lateral line is a mechanosensory system present in fish and amphibians. It helps detect water currents, and is thought to be essential for prey detection, predator avoidance, schooling, and courtship (Pitcher et al. 1976; Partridge and Pitcher 1979; Montgomery 1997; Montgomery et al. 2000; Montgomery et al. 2002). The sensory organs for the system are neuromasts, which are groups of sensory hair cells surrounded by support cells. The sensory cells receive afferent projections from two cranial ganglia. The anterior lateral line ganglion innervates the neuromasts of the head region while those from the posterior lateral line ganglion innervate neuromasts on the trunk and tail of the fish (Metcalfe et al. 1985). Neuromasts also receive efferent innervations from the brain, where three groups of efferent neurons have been

identified based on dye filling experiments (Metcalfe et al. 1985; Bricaud et al. 2001). Mechanosensitivity of the sensory hair cells of neuromasts and the inner ear has been attributed to mechanically gated ion channels that open when stereocilia on the hair cells are positively deflected (Hudspeth and Corey 1977; Hudspeth 1982; Corey et al. 2004). Physiological evidence suggests that these are non-selective cation channels of the transient receptor potential (TRP) channel superfamily (Corey et al. 2004). In mouse, zebrafish and *Xenopus*, TRPA1, a member of the TRP family, has been shown to be a major contributor to mechanoception. Cell culture based assays show that mammalian TRPA1 channels are also activated by various natural compounds, and by changes in temperature (Story et al. 2003; Bandell et al. 2004; Jordt et al. 2004) demonstrating that TRPA1 channels have multiple roles, functioning in mechanosensation, thermoception and chemoception.

Based on the above information, we hypothesized that the sensory hair cells of the zebrafish neuromasts have a dual role and sense motion as well as chemicals. This implies that the lateral line may serve as a chemosensory system in the zebrafish. To test this idea we tested a series of pungent natural compounds for their ability to stimulate neuromasts. In vertebrates TRPA1 is often expressed in a subset of nociceptive sensory neurons where it is co-expressed with TRPV1 but not TRPM8, both members of the TRP superfamily. To investigate chemoception in the lateral line, we stimulated with compounds that are known agonists of one or more members of the TRP channel superfamily. In mouse and human, TRPA1 channels are activated by the pungent natural compounds cinnamon oil (cinnamaldehyde), wintergreen oil (methyl salicylate), clove oil (eugenol), mustard oil (allyl isothiocyanate), and ginger oil (gingerol), all compounds that evoke a burning sensation in humans (Bandell et al. 2004).

Similarly, TRPV1 responds to capsaicin and gingerol while TRPM8 is sensitive to menthol (Story et al. 2003).

We tested several of the above compounds for their ability to induce *C-fos* expression in zebrafish neuromasts. *C-fos* is an immediate early gene that is rapidly induced within neurons, including sensory neurons, upon stimulation (Herdegen and Leah 1998). *C-fos* expression has previously been used to study nociceptive responses in mammals (Harris 1998; Hua et al. 2004). In zebrafish, *C-fos* activation can be clearly observed using mRNA *in situ* hybridization in whole-embryos (Baraban et al. 2005). Our results show that neuromasts are activated when zebrafish embryos are exposed to certain chemical stimuli, as hypothesized. We also show *C-fos* expression in groups of neurons in the brain in response to chemical stimuli, and these groups may represent higher order components of a functional circuit feeding the lateral line system.

A chemosensory role of the lateral line, especially its sensitivity to noxious chemical stimulants opens up the possibility of developing it as a model for studying nociception, and perhaps gustation, and for high throughput screening of potential drugs/pain therapeutics. Moreover, given the easy accessibility of the lateral line system to optical imaging, it may also serve as a system of choice for imaging neural responses to chemicals.

Materials and methods

Zebrafish strains and maintenance

Wild-type ("outbred", AB, WIK or TL) embryos were obtained from zebrafish (Danio rerio) lines maintained following standard procedures (Westerfield 2000). "Outbred" lines were originally obtained from a Florida fish farm and have been maintained for several years in our

colony. AB, WIK, and Tubingen long fin were obtained from the Zebrafish International Resource Center (ZIRC).

Whole-mount mRNA *in situ* hybridization

Whole-mount mRNA *in situ* hybridization was performed as described (Hargrave and Koopman 2000) except that the blocking solution contained 1% BSA instead of 2% and the post-antibody washes contained 0.5% BSA instead of 0.1%. Sense and antisense digoxigenin-labeled RNA probes were synthesized as described (Jowett and Lettice 1994) from PCR-generated DNA templates in which the T7 and SP6 phage promoters were incorporated into the PCR product (Mullis et al. 1986; Mullis and Faloona 1987; Stoflet et al. 1988). *C-fos* transcription templates were generated by PCR amplification of the *C-fos* gene (Baraban et al. 2005) from zebrafish genomic DNA using the following primers:

T7-cfos (5'-TAATACGACTCACTATAGGGAGA**AACTGTCACGGCGATCTCTT**-3'); SP6-cfos (5'-ATTTAGGTGACACTATAGAAGAG**CTTGCAGATGGGTTTGTGTG**-3'); Phage promoter sequences are underlined; nucleotides in bold are homologous to zebrafish. T7 and SP6 polymerases were used to generate sense and anti-sense probes, respectively. PCR products were purified using the 'Qiaquick PCR purification kit' prior to probe synthesis. Hybridization and post-hybridization wash steps were performed at 65°C. Dig-labeled probes were detected using anti-digoxigenin-alkaline phosphatase (Roche) and NBT/BCIP substrate. After color development, larvae were post-fixed in 4% para-formaldehyde/PBS at 4°C and cleared in 70% glycerol/PBS.

Stimulation

All stimulation experiments were carried out at room temperature. 4 day old larvae were minimally anaesthetized using 0.02% MS-222 in egg water (60µg Instant Ocean Sea Salts per mL of RO water, (Westerfield 2000) and split into groups of 20 to 30. Egg water containing MS-222 was then replaced with egg water without anaesthetic, and left for at least 10 minutes for recovery from anaesthesia. Each group was then exposed to the compound being tested or its carrier for 30 seconds. The larvae were then transferred to egg water, twice, to minimize carry over of the potential stimulant. Larvae were fixed in 4% paraformaldehyde/PBS at 4°C exactly 30 minutes after the end of stimulation. Compounds used were acetic acid diluted in egg water, ginger oil (2.0%), peppermint oil (0.25%), allyl isothiocyanate (0.075%), clove oil (0.1%), cinnamon oil (0.15%), and wintergreen oil (0.075%), each dissolved in DMSO prior to dilution in egg water to yield a final DMSO concentration of 10%. 3 mL of each of the above solutions were used for stimulation. Ginger oil was stored in aliquots at -20C, all other compounds were stored at room temperature. For control experiments, larvae were handled identically except that they were not exposed to the test compound. For mechanical stimulation, larvae were placed in glass scintillation vials, and subjected to 1 minute of vortexing at lowest speed, and fixed after 30 minutes or were placed on a shaker for a full thirty minutes before the embryos were fixed.

Neuromast staining

Neuromasts were visualized by staining with the fluorescent dye 2-(4-(dimethylamino)styryl)-N-ethylpyridinium iodide (DASPEI, Molecular Probes). Larvae were first anesthetized with 0.2% MS-222, and then soaked in 0.001% DASPEI in egg water. After 10

minutes, larvae were rinsed three times in egg water and then observed under epifluorescent illumination.

Immunohistochemistry

Sections were labeled with anti-Tyrosine hydroxylase antibody (Chemicon AB152). After washing away gelatin sections were incubated for 1 hour in blocking solution (1% goat serum, 2mg/mL BSA, 1% dimethylsulfoxide [DMSO], 0.2% Triton X-100 in PBS) and then incubated for 24 hours at 4°C in primary anti-tyrosine hydroxylase antibody diluted 1:1000 in blocking solution (PBS1% goat serum, 2mg/mL BSA, 1% DMSO, 0.2% Triton X-100 in PBS), rinsed 6 times for 10 minutes in incubation buffer, and incubated 1hr at 4°C in Cy3 conjugated anti-rabbit IgG antibody diluted 1:200 in blocking solution. They were then rinsed 3 times for 10 minutes followed by 1 time for 20 minutes in PBS and mounted in 80% glycerol/PBS.

Results

Neuromast activation can be detected by assaying for *c-fos* expression

Since neuromasts are known mechanosensors, we stimulated 4 day old zebrafish embryos mechanically by placing them in glass vials and vortexing them lightly. The embryos were then tested for expression of *c-fos* mRNA by *in situ* hybridization. *c-fos* is an early marker for neural activation (Herdegen and Leah 1998). In zebrafish, as in other organisms, *c-fos* activation can be observed using mRNA *in situ* hybridization in whole-embryos (Baraban et al. 2005). The *c-fos* expression pattern obtained (Figure 2.1B, 1B-inset) was compared to the stereotypic pattern of neuromasts on a similarly staged embryo vitally labeled with DASPEI (Figure 2.1A and insets), a vital dye specifically taken up by neuromasts upon short exposure. Our *C-fos* staining pattern

and DASPEI staining pattern are very similar and a high magnification view (Figure 2.1C) from another similarly stained sectioned embryo shows that the expression of *C-fos* is indeed in the neuromast cells. This suggests that *c-fos* can be used as a marker for activation of the neuromast hair cells in zebrafish.

Neuromasts are activated by specific chemical stimuli

To test if neuromasts can sense chemical stimuli, we chose compounds that are known agonists of one or more of 3 TRP channels, TRPA1, TRPV1 and TRPM8. The compounds tested were ginger oil, peppermint oil, acetic acid, allyl isothiocyanate, and cinnamon oil. We exposed 4 day old embryos to each compound and assayed for expression of *c-fos* mRNA in neuromasts by *in situ* hybridization. The average numbers of neuromasts expressing *c-fos* in response to different treatments are summarized in Chart 1.

Neuromasts expressing *c-fos* in the anterior and posterior lateral line system were counted separately. Mean and standard error of the number of anterior *c-fos* expressing neuromasts per fish was calculated based on the total number of embryos per stimulant (minimum of 40 embryos each) and a t-test was applied to determine if the estimated mean is significantly different from the mean of *c-fos* expressing neuromasts in DMSO (emulsifier for oils tested) treated embryos.

Ginger oil, acetic acid, peppermint, clove oil and wintergreen oil had statistically significant ($P \leq 0.05$) effects. 2% ginger oil had a strong effect and stimulated 14.08 out of a total of 36 anterior neuromasts at this developmental stage (Figure 2.2B, Chart 1). 0.5% Acetic acid had a similar effect and stimulated 14.31 anterior neuromasts per fish (Figure 2.2C, Chart 1). Peppermint oil stimulated 13.73 neuromasts (Figure not shown, Chart 1). The number of anterior neuromasts activated by clove oil and wintergreen oil stimulation was significantly different

from that of DMSO control. However, both stimulated an average of less than 3 anterior neuromasts per embryo (Figure not shown, Chart 1). Allyl isothiocyanate (0.27 per embryo) (Figure 2.2D, Chart 1) and cinnamon oil (0.56 per embryo) (Figure not shown, Chart 1) did not induce *C-fos* expression compared to DMSO (Figure 2.2A, Chart 1). Similar trends were observed for the posterior neuromasts (Figures not shown).

To determine whether *c-fos* expression in neuromasts was proportional to stimulant concentration, we tested different concentrations of ginger oil, which was a strong activator, and assayed for *c-fos* expression in the neuromasts. At all three concentrations tested, the average number of neuromasts that expressed *c-fos* per embryo was significantly ($P \leq 0.05$) higher than in control embryos exposed similarly to DMSO. A 0.25% solution of ginger oil induced *c-fos* expression in an average of 7.9 neuromasts in the head region. 1.0% and 2.0% ginger oil induced *c-fos* expression in an average of 10.7 and 14.08 neuromasts, respectively. Exposure to different strengths of ginger therefore generates a gradient in the average number of neuromasts stimulated and is depicted as percent of total number of neuromasts in Chart 2.

Ginger oil, acetic acid, and peppermint were strong activators, while mustard oil and cinnamon oil did not activate neuromasts. Clove oil and wintergreen oil (data not shown) both activated more strongly than DMSO, but were not as effective as ginger oil, acetic acid or peppermint.

Exposure to ginger oil induces *c-fos* expression neurons in the brain

If chemical stimulation of neuromasts is relevant to zebrafish behavior, it must activate specific pathways in the CNS. Exposure to high concentrations of ginger oil solution induced *c-fos* expression in a very specific bilaterally symmetrical pattern in the brain, in what appear to be

clusters of neurons (Figure 2.3B). 2% ginger oil produced the maximum number of such clusters in the majority of exposed embryos. Two groups of *c-fos* expressing neurons (labeled by the arrows in Figure 2.3B) noted in majority of embryos were also found in few of control embryos exposed to DMSO (Figure 2.3A). The group labeled with a solid arrowhead (Figure 2.3B) indicates *c-fos* expressing neuromasts. Although occasional light staining for some of these clusters were seen in controls, the staining observed in the ginger treated embryos was much stronger.

C-fos expressing nuclei in ginger stimulated embryos do not express Tyrosine Hydroxylase (TH)

Previously identified diencephalic neurons that send efferent connections to the neuromasts have been shown to be immunoreactive for anti-tyrosine hydroxylase (Bricaud et al. 2001). We therefore tested if the clusters that expressed *c-fos* in response to stimulation by ginger oil were also tyrosine hydroxylase-positive. Fish were stimulated and double labeled by mRNA hybridization for *c-fos* and immunostaining for tyrosine hydroxylase. We failed to detect any cells in the brain that co-expressed *C-fos* and tyrosine hydroxylase (Figure 2.4), though tyrosine hydroxylase immunoreactivity was observed in cells adjacent to some of the *C-fos* expressing clusters (arrowhead in Figure 2.4). We therefore conclude that the pathways directly activated by ginger are not the previously identified TH positive efferent pathways.

Discussion

C-fos expression is not due to motion induced by addition of chemicals

C-fos is an early gene that is rapidly induced within neurons, including sensory neurons, upon stimulation (Herdegen and Leah 1998). However its suitability for reporting activation of neuromast sensory hair cells had not been tested. Since neuromasts are established mechanosensors, we mechanically stimulated neuromasts and tested *c-fos* expression and our results show that *c-fos* expression can be used as a marker for activation of neuromasts. *c-fos* expression in mechanically stimulated neuromasts however raises the possibility that the initial swimming movement often seen after addition of chemical stimulants causes *c-fos* expression in the neuromasts. However, we observed that addition of mustard oil induces much more movement in the embryos than is seen with ginger oil. Ginger oil induced less motion, but was a very strong inducer of *c-fos* expression. Mustard oil on the other hand did not induce *c-fos* expression. This demonstrates that the *c-fos* expression we see upon chemical stimulation is principally induced by the chemicals and not by motion. The DMSO treatment, where embryos are handled similarly to stimulation experiments, controls for possible stimulation due to pipetting of solutions.

Differential response to chemicals points to specific receptor channels

All compounds we tested are known agonists of one or more of 3 TRP channels, TRPA1, TRPV1 and TRPM8. There is strong evidence for the presence of TRPA1 in neuromast hair cells. In mammals, TRPA1 is often co-expressed in a subset of TRPV1 expressing nociceptive sensory neurons. These co-expressing cells do not express TRPM8 (Story et al. 2003). We tested

the compounds ginger oil, acetic acid, allyl isothiocyanate, peppermint oil, clove oil and wintergreen oil.

Gingerol, the active component in ginger oil, is a known agonist of both TRPA1 and TRPV1. We exposed zebrafish to different concentrations of ginger oil and all three concentrations led to *c-fos* induction in significantly higher numbers of neuromasts than with DMSO. Exposure to different strengths of ginger show a gradient in the average number of neuromasts stimulated (Chart 2) suggesting that the effect is physiological.

We tested acetic acid since TRPV1 can be activated by protons (Leffler et al. 2006). At 0.5% acetic acid *c-fos* expression was induced at levels close to that seen for the highest concentration (2%) of ginger oil. This suggests that TRPV1 or TRPV1 like receptors may be present in the neuromasts. Peppermint, whose major active component is menthol, an activator of TRPM8, activated at similar levels. Thus we observe strong activation by compounds that are known agonists of either the TRPV1 channels or TRPM8 channels in mammals. This suggests that these channels or their zebrafish equivalents may be mediating the observed response. The effect of allyl isothiocyanate, the active component of mustard oil, is thought to be mediated exclusively through TRPA1. In our experiments, allyl isothiocyanate at 0.075% (the highest concentration tested) did not induce *c-fos* expression in any neuromasts compared to DMSO. It needs to be noted that the molarity of the active ingredients of the various oils tested or the exact proportion of those ingredients in the oils tested were not determined. We also tested cinnamon oil, another agonist of TRPA1, and did not see activation of neuromasts. Thus we do not observe any activation by compounds that are thought to induce their effects exclusively through TRPA1 in mammalian cells. This would suggest that TRPA1 is not mediating chemosensation in the neuromasts of zebrafish. On the other hand, there is evidence that zfTRPA1 is present in

neuromast hair cells (Corey et al. 2004), where it mediates mechanoception. This calls attention to the fact that zebrafish, unlike mouse or human, has two TRPA1 genes, zfTRPA1 and zfTRPA2. Morpholino induced knock-down of zfTRPA1 led to reduced uptake of the dye FM1-43 into neuromasts. Morpholino induced loss of zfTRPA2 had no such effect (Corey, 2004 #10). A possible explanation of this fact is that the mechanosensory and chemosensory functions of mammalian TRPA1 are split between the two proteins in zebrafish, and zfTRPA1, although present, is missing the chemosensory function of TRPA1. It is also possible that both zebrafish TRPA1 and TRPA2 are not sensitive to the same pharmacological agonists as the mammalian TRPA1.

C-fos expressing nuclei in ginger stimulated embryos do not express Tyrosine Hydroxylase

Horseradish peroxidase filling and dye (DiI) filling revealed three efferent nuclei in the brain, the diencephalic efferent of the lateral line (DELL) in the ventral diencephalon, the rostral efferent nucleus (REN) and the caudal efferent nucleus (CEN) in the rhombencephalon (Metcalfe et al. 1985; Bricaud et al. 2001). All three clusters seem to innervate both the anterior and posterior lateral line system. While different neurons within each hindbrain cluster are thought to innervate the anterior and posterior lateral line system, it is not known if the same is true for the forebrain nuclei.

Neurons of the efferent nuclei in the rhombencephalon were shown to be cholinergic (Meredith et al. 1987). DELL neurons for both the anterior and posterior lateral line have been shown to be immunoreactive to anti-tyrosine hydroxylase, an enzyme required for catecholamine synthesis (Bricaud et al. 2001). These authors also suggest that the DELL neurons are possibly excitatory catecholaminergics, and are likely dopaminergics as noradrenergic neurons are

restricted to the hindbrain, while dopaminergics are found in the fore- and midbrain (Guo et al. 1999). All or most neurons of the rhombencephalic nuclei express choline acetyltransferase (ChAT), and possibly represent a cholinergic inhibitory component of the lateral line system (Flock and Russell 1973; Brantley and Bass 1988; Danielson et al. 1988).

In our co-labeling experiments we did not detect any neurons that co-expressed *c-fos* and TH in the brain. The symmetrical pattern obtained consistently and specifically in response to stimulus, suggests that it is not an artifact. This implies that ginger oil does not turn on excitatory dopaminergic efferents. It will be interesting to determine if the *c-fos* expressing neurons are immunoreactive to gamma amino butyric acid (GABA) or ChAT, implying that ginger oil stimulation may be turning on inhibitory efferent components of the lateral line system as in a classic feedback loop by which a stimulant down-regulates its own receptor. Though several forebrain nuclei for the lateral line system were previously described, components of the circuit, especially its inhibitory nuclei remain to be described. *C-fos* expression may have marked components of the circuit that do not involve TH expressing neurons.

References

Bandell, M., Story, G.M., Hwang, S.W., Viswanath, V., Eid, S.R., Petrus, M.J., Earley, T.J., and Patapoutian, A. 2004. Noxious cold ion channel TRPA1 is activated by pungent compounds and bradykinin. *Neuron* **41**(6): 849-857.

Baraban, S.C., Taylor, M.R., Castro, P.A., and Baier, H. 2005. Pentylenetetrazole induced changes in zebrafish behavior, neural activity and *c-fos* expression. *Neuroscience* **131**(3): 759-768.

Brantley, R.K. and Bass, A.H. 1988. Cholinergic neurons in the brain of a teleost fish (Porichthys notatus) located with a monoclonal antibody to choline acetyltransferase. *J Comp Neurol* **275**(1): 87-105.

Bricaud, O., Chaar, V., Dambly-Chaudiere, C., and Ghysen, A. 2001. Early efferent innervation of the zebrafish lateral line. *J Comp Neurol* **434**(3): 253-261.

Corey, D.P., Garcia-Anoveros, J., Holt, J.R., Kwan, K.Y., Lin, S.Y., Vollrath, M.A., Amalfitano, A., Cheung, E.L., Derfler, B.H., Duggan, A., Geleoc, G.S., Gray, P.A., Hoffman, M.P., Rehm, H.L., Tamasauskas, D., and Zhang, D.S. 2004. TRPA1 is a candidate for the

mechanosensitive transduction channel of vertebrate hair cells. *Nature* **432**(7018): 723-730.

Danielson, P.D., Zottoli, S.J., Corrodi, J.G., Rhodes, K.J., and Mufson, E.J. 1988. Localization of choline acetyltransferase to somata of posterior lateral line efferents in the goldfish. *Brain Res* **448**(1): 158-161.

Flock, A. and Russell, I.J. 1973. The post-synaptic action of efferent fibres in the lateral line organ of the burbot Lota lota. *J Physiol* **235**(3): 591-605.

Guo, S., Brush, J., Teraoka, H., Goddard, A., Wilson, S.W., Mullins, M.C., and Rosenthal, A. 1999. Development of noradrenergic neurons in the zebrafish hindbrain requires BMP, FGF8, and the homeodomain protein soulless/Phox2a. *Neuron* **24**(3): 555-566.

Hargrave, M. and Koopman, P. 2000. In situ hybridization of whole-mount embryos. *Methods Mol Biol* **123**: 279-289.

Harris, J.A. 1998. Using *c-fos* as a neural marker of pain. *Brain Res Bull* **45**(1): 1-8.

Herdegen, T. and Leah, J.D. 1998. Inducible and constitutive transcription factors in the mammalian nervous system: control of gene expression by Jun, Fos and Krox, and CREB/ATF proteins. *Brain Res Brain Res Rev* **28**(3): 370-490.

Hua, F., Harrison, T., Qin, C., Reifsteck, A., Ricketts, B., Carnel, C., and Williams, C.A. 2004. *c-fos* expression in rat brain stem and spinal cord in response to activation of cardiac ischemia-sensitive afferent neurons and electrostimulatory modulation. *Am J Physiol Heart Circ Physiol* **287**(6): H2728-2738.

Hudspeth, A.J. 1982. Extracellular current flow and the site of transduction by vertebrate hair cells. *J Neurosci* **2**(1): 1-10.

Hudspeth, A.J. and Corey, D.P. 1977. Sensitivity, polarity, and conductance change in the response of vertebrate hair cells to controlled mechanical stimuli. *Proc Natl Acad Sci U S A* **74**(6): 2407-2411.

Jordt, S.E., Bautista, D.M., Chuang, H.H., McKemy, D.D., Zygmunt, P.M., Hogestatt, E.D., Meng, I.D., and Julius, D. 2004. Mustard oils and cannabinoids excite sensory nerve fibres through the TRP channel ANKTM1. *Nature* **427**(6971): 260-265.

Jowett, T. and Lettice, L. 1994. Whole-mount in situ hybridizations on zebrafish embryos using a mixture of digoxigenin- and fluorescein-labelled probes. *Trends Genet* **10**(3): 73-74.

Leffler, A., Monter, B., and Koltzenburg, M. 2006. The role of the capsaicin receptor TRPV1 and acid-sensing channels (ASICS) in proton sensitivity of subpopulations of primary nociceptive neurons in rats and mice *Neuroscience* **139**(2): 699-709.

Meredith, G.E., Roberts, B.L., and Maslam, S. 1987. Distribution of afferent fibers in the brainstem from end organs in the ear and lateral line in the European eel. *J Comp Neurol* **265**(4): 507-520.

Metcalfe, W.K., Kimmel, C.B., and Schabtach, E. 1985. Anatomy of the posterior lateral line system in young larvae of the zebrafish. *J Comp Neurol* **233**(3): 377-389.

Montgomery, J. 1997. The lateral line can mediate rheotaxis in fish. *Nature* **389**: 960-963.

Montgomery, J., Carton, G., Voigt, R., Baker, C., and Diebel, C. 2000. Sensory processing of water currents by fishes. *Philos Trans R Soc Lond B Biol Sci* **355**(1401): 1325-1327.

Montgomery, J.C., Macdonald, F., Baker, C.F., and Carton, A.G. 2002. Hydrodynamic contributions to multimodal guidance of prey capture behavior in fish. *Brain Behav Evol* **59**(4): 190-198.

Mullis, K., Faloona, F., Scharf, S., Saiki, R., Horn, G., and Erlich, H. 1986. Specific enzymatic amplification of DNA in vitro: the polymerase chain reaction. *Cold Spring Harb Symp Quant Biol* **51 Pt 1**: 263-273.

Mullis, K.B. and Faloona, F.A. 1987. Specific synthesis of DNA in vitro via a polymerase-catalyzed chain reaction. *Methods Enzymol* **155**: 335-350.

Partridge, B.L. and Pitcher, T.J. 1979. Evidence against a hydrodynamic function for fish schools. *Nature* **279**(5712): 418-419.

Pitcher, T.J., Partridge, B.L., and Wardle, C.S. 1976. A blind fish can school. *Science* **194**(4268): 963-965.

Stoflet, E.S., Koeberl, D.D., Sarkar, G., and Sommer, S.S. 1988. Genomic amplification with transcript sequencing. *Science* **239**(4839): 491-494.

Story, G.M., Peier, A.M., Reeve, A.J., Eid, S.R., Mosbacher, J., Hricik, T.R., Earley, T.J., Hergarden, A.C., Andersson, D.A., Hwang, S.W., McIntyre, P., Jegla, T., Bevan, S., and Patapoutian, A. 2003. ANKTM1, a TRP-like channel expressed in nociceptive neurons, is activated by cold temperatures. *Cell* **112**(6): 819-829.

Westerfield, M., ed. 2000. *The zebrafish book: A guide for the laboratory use of zebrafish (Danio rerio)*. University of Oregon Press.

Figures

Figure 2.1: Expression of *c-fos* in neuromasts of a mechanically stimulated zebrafish. (A) 4 day zebrafish embryo labeled with DASPEI show positions of neuromasts. A Inset. Higher magnification view of neuromasts IO4 and O2 show DASPEI in the hair cells. (B) *C-fos* mRNA expression (blue) detected by mRNA *in situ* hybridization, in a 4 day embryo stimulated mechanically. Note the expression pattern is similar to the pattern of neuromasts showed in Figure 2.1A. (C) High magnification view of a neuromast stained for *c-fos* mRNA, showing expression within the neuromast cells. Inset in A showing schematic of the lateral line system if from Tanya Whitfield.

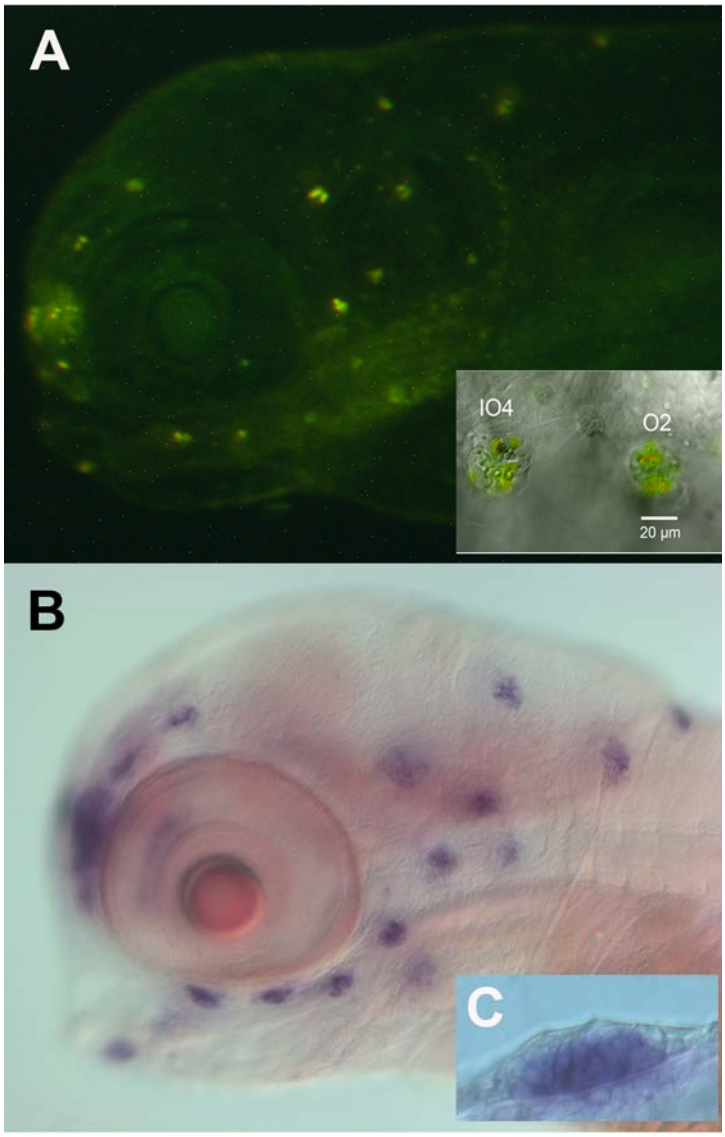
A
IO4
O2
20 µm
B
C

Figure 2.2: *C-fos* mRNA expression in chemically stimuated 4 day old zebrafish embryos. (A) DMSO 10%. (B) Ginger oil 2%. (C) Acetic acid 0.5%. (D) Allyl isothiocyanate 0.075% (active component of mustard oil).

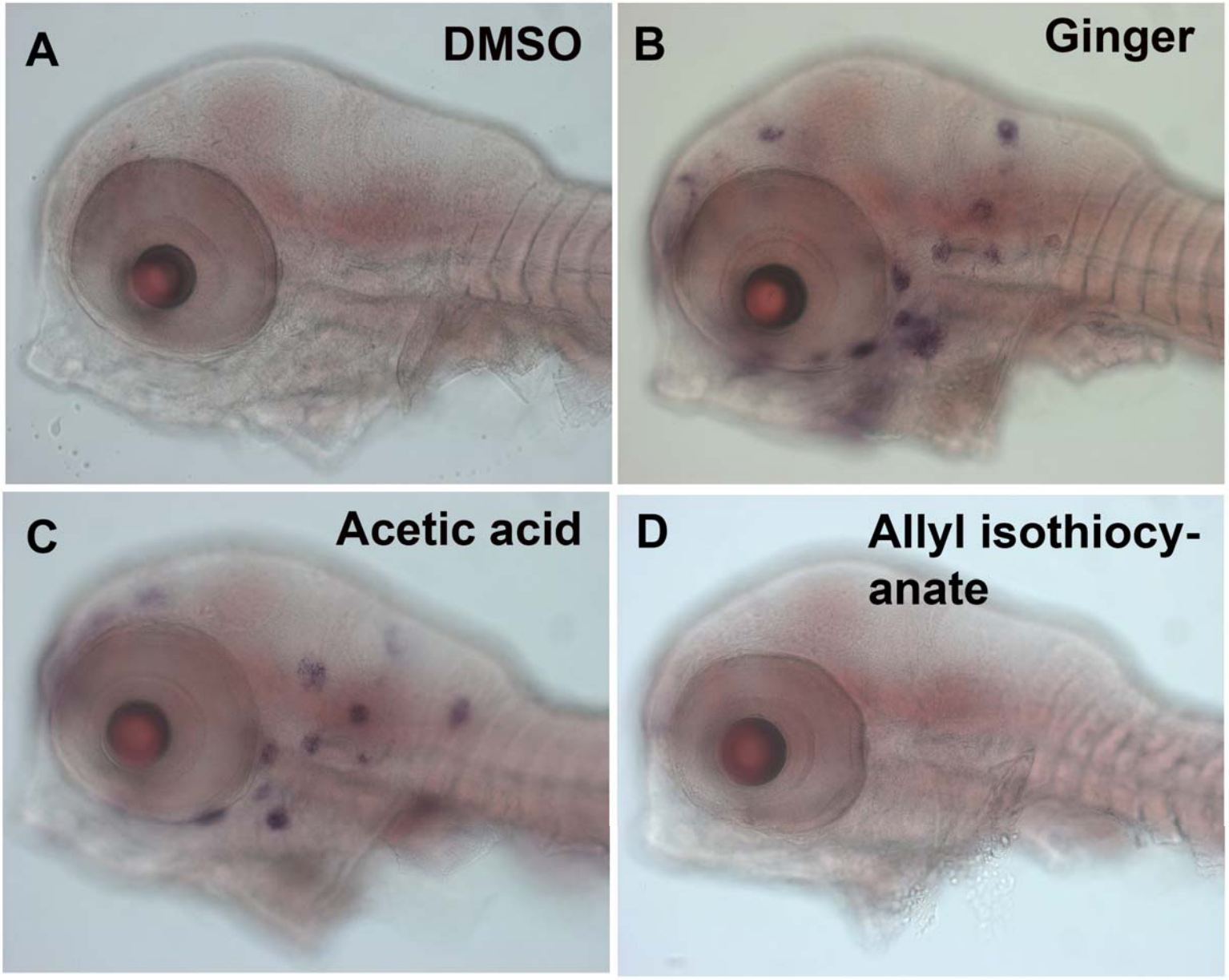
A
DMSO
B
Ginger
C
Acetic acid
D
Allyl isothiocy-
anate

Chart 1: Anterior lateral line neuromasts expressing *c-fos* in response to different chemical stimuli, expressed as percent of total number of anterior neuromasts in 4 days post fertilization embryos. Light grey bars represent activated neuromasts (X-axis) in the head region that expressed *c-fos* in response to each potential stimulant (Y-axis). Mean and standard error of the number of *c-fos* expressing neuromasts are provided in table. T-test was applied to find if the estimated mean is significantly different from mean of *c-fos* expressing neuromasts in control embryos exposed to DMSO (carrier).

In the head region, ginger oil, acetic acid and peppermint oil induced *c-fos* in an average of approximately 14 neuromasts per embryo. Number for clove oil and wintergreen oil were lower but are significantly higher than the control. Allyl isothiocyanate and cinnamon oil did not induce *c-fos* at significantly higher numbers than the control.

Chart 1: Neuromasts expressing *c-fos* in response to chemical exposure

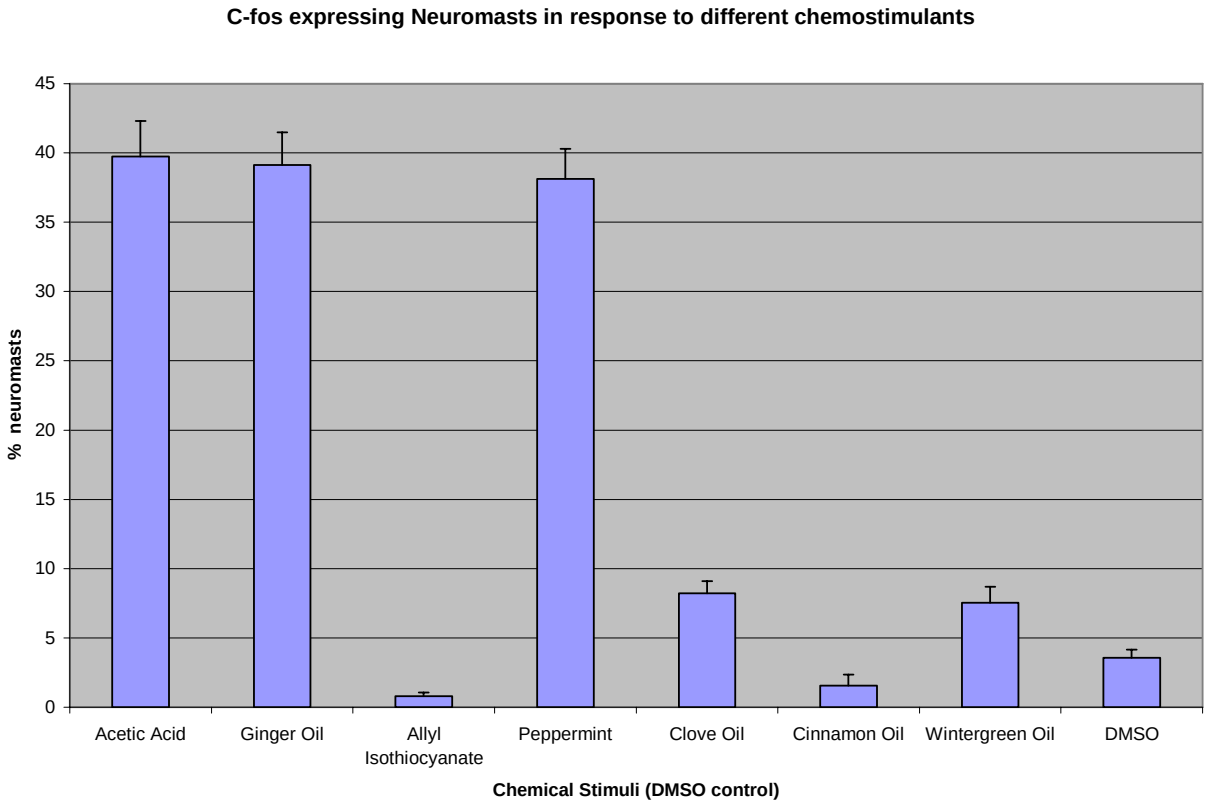

Stimulants (Conc.)	Average (Anterior)	Standard Error	T value (probability)
Acetic Acid (0.5%)	14.31	0.923991	4.36E-35
Ginger Oil (2.0%)	14.08	0.848371	2.63E-24
Allyl Isothiocyanate (0.075%)	0.27	0.098267	0.244137
Peppermint (0.25%)	13.73	0.779198	3.7E-44
Clove Oil (0.1%)	2.95	0.31352	2.05E-06
Cinnamon Oil (0.15%)	0.55	0.283809	0.477629
Wintergreen Oil (0.075%)	2.70	0.417789	0.000306
DMSO (10%) (carrier)	1.28	0.206	

Chart 2: C-fos expression in neuromasts in response to different concentration of ginger oil. 2%, 1%, 0.25% and 0% of ginger oil dissolved in DMSO (10%) were tested for their potential to induce *c-fos* in neuromasts. Each bar represents the percentage of neuromasts expressing *c-fos* per fish in the head region (X-axis) for a concentration of ginger oil (Y-axis). Average number of anterior neuromasts (expressed as % total) expressing *c-fos* in the head region per fish for each concentration tested were as follows- 2%: 39.14 ±2.36, 1%: 29.85± 1.48, 0.25%: 21.94 ± 1.92 and 3.57 ± 0.57 (DMSO control).

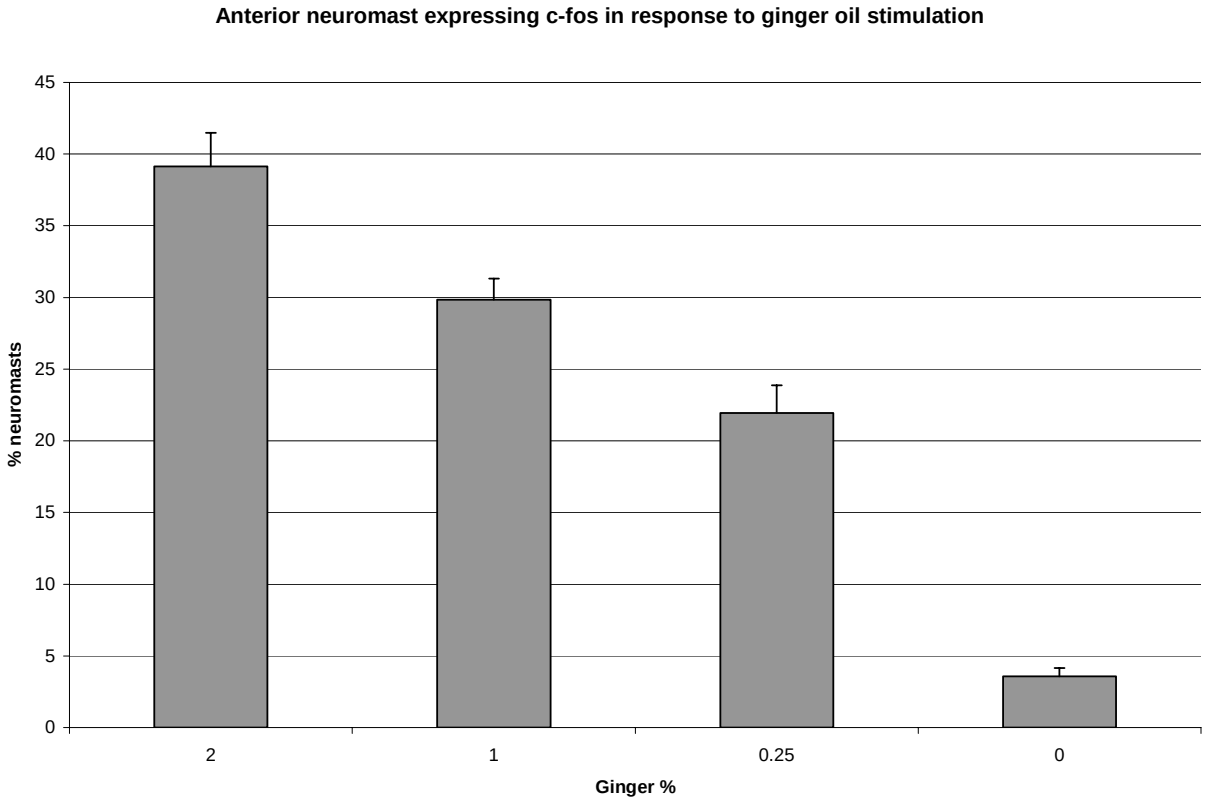
Anterior neuromast expressing c-fos in response to ginger oil stimulation
% neuromasts
45
40
35
30
25
20
15
10
5
0
2
1
0.25
0
Ginger %

Figure 2.3: Dorsal view showing expression of *c-fos* in brain. A. DMSO 10%. B. Ginger 2%. Solid arrowhead and empty arrowhead in A and B point to groups of neurons that express *c-fos* in both ginger stimulated and DMSO treated control embryos in 14% and 10 % of embryos, respectively. Note that the staining is less prominent in the DMSO treated controls. At the same time, in the DMSO treated embryos the stained cells were somewhat more prominent under the microscope than could be portrayed in the picture. In A and B, solid arrows point to stained neuromasts.

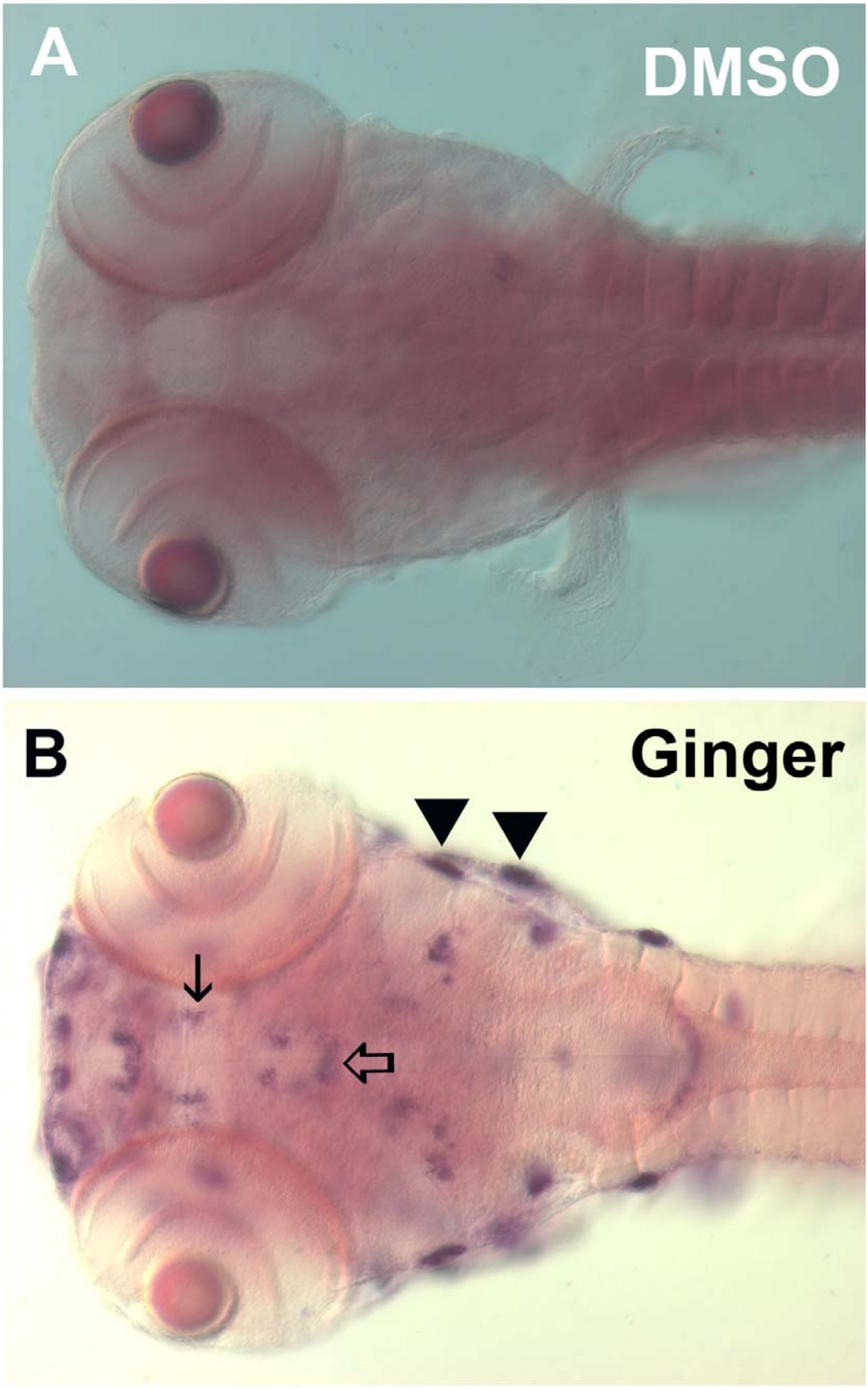
A
DMSO
B
Ginger

Figure 2.4: Tyrosine hydroxylase is not co-expressed by the *c-fos* expressing brain neurons in ginger stimulated embryos. Overlayed bright field and fluorescent images showing *c-fos* (in dark blue) mRNA expression and tyrosine hydroxilase (in red) expressing neurons show TH positive cells in close proximity to but distinct from *c-fos* positive groups of neurons in the forebrain.

Chapter 3

Estimating Weak Ratiometric Signals in Calcium Imaging

Data I: Dual-Channel Data[1]

[1]Majumder A., [1]Broder J., Porter E., Keith C., Lauderdale J, Sornborger A.
Submitted to Cell Calcium

Abstract

Ratiometric fluorescent indicators are becoming increasingly prevalent in many areas of biology. They are used for making quantitative measurements of intracellular free calcium both *in vitro* and *in vivo*, as well as measuring membrane potentials, pH and other important physiological variables of interest to researchers in many subfields. Often, functional changes in the fluorescent yield of ratiometric indicators are small and the signal-to-noise ratio (SNR) is of order unity or less. In particular, variability in the denominator of the ratio can lead to very poor ratio estimates. For this reason, some sort of averaging is necessary. A standard approach used in the calcium imaging literature is for the user to select regions of interest (ROIs), and to average over the pixels within the ROI. Such methods suffer from subjective selection of ROIs. Important, small changes in fluorescence may easily be missed by eye. An alternative to ROIs is the use of temporal averaging to get a more accurate spatial estimate of the signal. These methods sacrifice temporal information for improved spatial information. Here, we present a statistical optimization method for objectively detecting and estimating ratiometric signals in dual wavelength measurements of fluorescent, ratiometric indicators that improves on both of these methods. With the use of an appropriate statistical model for ratiometric signals and by taking the pixel-pixel covariance of an imaging dataset into account, we are able to extract user-independent spatio-temporal information that retains high-resolution in both space and time.

Keywords: Ratiometry, Calcium Imaging, Voltage Indicator, FRET, Multivariate Imaging Analysis, PC12 Cells

Introduction

Ratiometric fluorescent indicators are used extensively in biological imaging to measure changes in Ca^{++} concentrations, as voltage indicators and to measure a range of other variables of interest. They have become particularly important in biological imaging for a number of reasons: 1) Illumination variability, photobleaching and other artifacts may by eliminated by taking the ratio of signals at two different wavelengths. 2) Ratiometry results in quantitative estimates of physiological variables of interest (Truong et al. 2001). 3) A large number of extrinsic dyes such as the calcium indicators Fura-2,3,4F and Indo-1,5F (Jackson et al. 1987) and voltage indicators Di-4,8-Anepps (Molecular Probes) as well as genetically encoded calcium (Miyawaki et al. 1997) and voltage indicators (Siegel and Isacoff 1997); (Gonzalez and Tsien 1995; Gonzalez and Tsien 1997); (Zochowski et al. 2000) based on fluorescent resonant energy transfer (FRET) are ratiometric. 4) Genetically encoded FRET indicators are seeing increased application (Higashijima et al. 2003); (Li et al. 2005) since they are non-toxic and may be non-invasively introduced and accurately targeted to specific brain regions.

With ratiometric techniques, fluorescence is measured either via excitation (Grynkiewicz et al. 1985) or emission (Takahashi et al. 1999) at two different wavelengths. With these techniques, an anti-correlated signal occurs when, in one channel, fluorescence increases when the variable of interest increases and in the other channel, fluorescence decreases. Because the two measurements are made simultaneously or quasi-simultaneously, photon path length and volume factors are eliminated from the ratio (Bright et al. 1987); (Grynkiewicz et al. 1985); (Takahashi et al. 1999). This means that photobleaching and the effect of a fluctuating excitation source are removed from the signal.

Because of calcium's central role in cellular physiology, calcium imaging is used extensively to measure a wide variety of cellular processes in both prokaryotic and eukaryotic cells. Measurements of intracellular free calcium may be made by widefield fluorescence imaging or by confocal or multiphoton microscopy, which permit better optical sectioning. Particularly with confocal or multiphoton techniques, it is easiest to excite with a single laser. Therefore, emission ratiometry is preferred in this case. The majority of visible wavelength small molecule calcium indicator dyes available are either non-ratiometric (for example, fluo-2,3,4, Oregon green BAPTA, rhod-2) or are suitable for excitation ratiometry (fura-2, bis-fura-2) (Takahashi et al. 1999). Indo-1 is an emission ratiometric dye, and can be used to do emission ratiometry in confocal microscopes (Isshiki et al. 1998). However, indo-1 bleaches extremely rapidly (Takahashi et al. 1999). A solution to these problems is to mix non-ratiometric dyes to form a ratiometric one. For example, one may simultaneously load cells with fluo-3 or fluo-4 and Fura-red. Fluo-3 and fluo-4 are calcium indicators whose fluorescence increases with increasing $[Ca^{++}]$, and Fura-red's fluorescence decreases with increasing $[Ca^{++}]$ (Lipp and Niggli 1993); (Bischofberger and Schild 1995); (Gomez et al. 2001). A remaining problem with this approach is that differential bleaching, compartmentalization, or clearance of the two dyes may give rise to ratiometric signals that are partially independent of changes in $[Ca^{++}]_i$ (Lipp and Niggli 1993) these problems are all exacerbated in extended time-course experiments.

The extent of dye compartmentalization, clearance, and bleaching can all be readily evaluated by examining and quantifying the fluorescent images at the two component wavelengths before the formation of the ratiometric image. A variety of schemes have been devised to inhibit dye compartmentalization and clearance, ranging from low temperature loading (Keith et al. 1985); (Roe et al. 1990) to the use of anion transport inhibitors such as

probenecid (Merritt et al. 1990) or to the use of dextran-conjugated indicators (Schlatterer et al. 1992). In the case of differential bleaching, the options are more limited: the medium can be made hypoxic (Takahashi et al. 1999) or illumination can be minimized. Since many cells will suffer under long term hypoxia, minimizing exposure is often the only practical option. In the case of co-loaded fluo-4 and Fura-Red, minimizing exposure is made more difficult because the quantum efficiency of Fura-Red is quite low (0.013 in the Ca^{++}free form) (Kao 1994), so the red image can be quite dim unless high concentrations of dye are used (which can exacerbate compartmentalization and buffering of $[Ca^{++}]_i$). The use of dual dye ratiometric analysis for time course studies therefore constrains the investigator to work with very low light level images.

Using low light level images for ratiometry, however, presents a different set of problems. A ratio formed with low pixel intensities may be wildly inaccurate (see e.g. Figure 3.4B, below) largely due to fluctuations in the ratio when the denominator is close to zero. As a consequence, ratiometric analyses of low-intensity data have necessitated subjective thresholding and extensive data averaging. This is typically done either in space where a region of interest (ROI) is typically chosen (e.g. (Higashijima et al. 2003)) or in time where pixel timecourses are averaged (Russ, Image Processing Handbook). For analysis of slow indicators, such as calcium indicator dyes, temporal averaging is often preferred, since it does not entail a loss of spatial resolution in the resultant images.

Temporal averaging can either be applied during image acquisition or post-hoc, by the use of a low-pass filter *viz.*, use of a boxcar average. However, the amount of temporal averaging must be limited to a (small) finite number of frames, since excessive averaging can oversmooth the data and eliminate fast dynamics that may be of interest. As a consequence, signal-to-noise

considerations limit signal detection in temporally averaged ratiometric imaging data to events that have a $\Delta F/F0$ of 0.4 or more (Cheng et al. 1999). If one is willing to sacrifice spatial information, the situation may be improved by choosing ROIs within which to average time series. This method of signal detection is effectively a spatial filtering method and represents the other extreme to temporal averaging. By averaging over an ROI one sacrifices spatial information, but retains temporal information. ROI timecourses can, of course, also be temporally averaged for further smoothing.

Because the data is noisy, statistical methods, such as the averaging techniques above, are needed to detect and estimate the signal. These standard methods may be improved on by using more of the latent information in the data. In the physiological context, signals of interest are usually spatially correlated. Therefore, the best detection and estimation can often be done with multivariate, statistical optimization methods that take into account the full covariance matrix of the data (Sirovich & Kaplan, 2002;(Yokoo et al. 2001; Sornborger et al. 2005). In this paper, we present a new statistical optimization method for the analysis of ratiometric imaging data. Our method results in the detection of a subspace of the datasets from each channel that is maximally anti-correlated. After finding this subspace, the datasets are projected into it, thereby denoising the measurements in both channels. The timecourse of the datasets into the anti-correlated subspace is a filtering method based on a statistical model of ratiometric signals. Instead of filtering pixels (using an ROI) or filtering in time (using a boxcar filter) we filter in the space of anti-correlated eigenimages. We call our method SOARS, for Statistical Optimization Analysis for Ratiometric Signals.

A principle advantage of our method is that the anti-correlated subspace is determined in a user-independent (objective) way. We find weighted masks (eigenimages resulting from an

optimization problem) that indicate where anti-correlated activity is occurring in the dataset. This is preferable to user-defined ROIs since, particularly with noisy data, active regions may go undetected by eye. The eye can typically only detect contrast differences (Campbell and Robson 1968) at the 2% level or above. Furthermore, since the eigenimages are generated by linearly transforming the data, their projections in the data (i.e. timecourses) are normally distributed, by the central limit theorem. Therefore standard statistical tests may be applied to them.

For the experiments presented here, we chose to use PC12 cells, which are widely used as a model of an excitable neuron-like cell and have been extensively used in calcium imaging studies. When these cells are exposed to nerve growth factor (NGF) they differentiate into cells that, while not true neurons, morphologically and physiologically resemble sympathetic neurons: they extend long processes, and become electrically excitable (Tischler et al. 1983). During this process of differentiation into a neuron-like cell they up-regulate their expression of voltage-gated sodium channels by a factor of five (Bouron et al. 1999) and become electrically excitable (Tischler et al. 1983). Additionally, they increase their voltage-gated Ca^{++} current density by a factor of two by substantially up-regulating their expression of N-type voltage-gated calcium channels (Black et al. 2003). In part because of this up-regulation, when differentiated, these cells also exhibit repetitive calcium waves in response to appropriate neurotansmitters (Lorenzon et al. 1995). Additionally, these cells exhibit changes in calcium in response to depolarizing solutions such as potassium-containing solutions.

We note that our methods are applicable to measurements of ratiometric signals wherever they are imaged, in neuronal, cardiac or other tissues, *in vivo* or *in vitro*.

Materials and Methods

Experimental Setup

Cultured PC12 cells (see Supplementary Material) on 25 mm circular coverglasses were bulk loaded immediately before imaging with 1 μM fluo-4 (Invitrogen/Molecular Probes, Eugene, OR F14217) and 10 μM Fura-Red (Invitrogen/Molecular Probes, F3021) acetoxymethyl (AM) ester fluorescent indicator dyes in Hanks balanced salt solution (HBSS) (Hanks, 1976), 0.04% Pluronic F-127 (Invitrogen/Molecular Probes, P6867) for 20 minutes at room temperature. After loading, the cells were rinsed with HBSS and mounted in a Dvorak-Stotler chamber (Lucas-Highland, Chantilly, VA). The cells were periodically stimulated (2 minutes off/2 minutes on) for ten periods (40 minutes total) followed by 5 minutes of perfusion with a control solution of ionomycin + EGTA (low calcium clamp) to reduce calcium to base levels, followed by 5 minutes of perfusion with ionomycin + 10mM Ca^{++}. Fluorescence and optical images were acquired with a Leica SP2 confocal microscope on a DM RXE upright microscope platform (Leica Microsystems, Bannerbrook, IL) at a frame rate of 1Hz. 256 × 256 pixel images (1μmper pixel) were taken of cultured PC12 cells and their neurites. Due to computational memory limitations, images were subsequently binned to 128 × 128 pixels. Fluo-4 and Fura-Red were both excited at 488 nm. Simultaneous images were acquired in three bands: 515-535 nm for fluo-4 fluorescence emission, 620-660 nm for Fura-Red fluorescence emission and trans-illumination images were taken to detect any motion by the cells.

Statistical Imaging Analysis Techniques

In the section below, we outline the concepts behind the SOARS, the new statistical analysis method presented in this paper. In the Supplementary Material, we give a full discussion of the derivation of the method.

All analyses shown below are performed on ratiometric data from measurements of fluo-4 fluorescence and Fura-Red fluorescence.

SOARS: Statistical Optimization for the Analysis of Ratiometric Signals

SOARS analysis begins by standardizing the fluo-4 and Fura-Red datasets (subtracting means and dividing by standard deviations). After standardization, we obtain two datasets, in which, if there is an increase in calcium, pixel timecourses in the fluo-4 channel trend upwards while pixels in the Fura-Red channel trend downwards, i.e. the signal is anti-correlated. By subtracting the two datasets, pixel-by-pixel, one forms a single dataset in which any consistent trend away from zero indicates anti-correlation in the data. However, if there is no signal, the expected value at every pixel is zero. SOARS then performs a singular value decomposition (SVD) on the standardized, subtracted dataset generating a set of eigenimages that are ordered by the amount of spatial covariance in the data. The time-courses of the eigenimages in the standardized, subtracted dataset (i.e. the projections of the eigenimages in the data) will be normally distributed if no anti-correlation exists (e.g. Figure 3.5T) but non-normally distributed otherwise. The timecourses of the eigenimages in the original two channels will be anti-correlated if there is a signal. That is, the non-normal eigenimages represent weighted masks showing the spatial distribution of anti-correlation in the dataset.

SOARS is a filtering method because it throws away any eigenimages that do not correspond to anti-correlated information. Therefore, it filters the dataset in a subspace that

contains only anti-correlated information. Since SOARS provides a set of masks, one is able to visualize spatio-temporal dynamics in the imaging data. SOARS thereby avoids the loss of spatial information that comes with averaging over ROIs. In order to construct a denoised ratio, SOARS projects the eigenimages into the original datasets after standardization. This results in two denoised datasets, one for each channel. Then, the standardization is reversed by multiplying the datasets by their standard deviation and adding the mean to all frames of the dataset. One now has two channels of denoised data that have been restricted to contain only anti-correlated information from which ratios may be taken. The ratio reconstruction is, at this point, denoised to the extent possible given the statistical model and the statistical optimization framework within which SOARS works.

Further information concerning the signal may still be used to smooth the data. For example, by exploiting our repetitive stimulus paradigm, we may make additional use of frequency information to further smooth the data. Morphological information may also be used. For instance, the diffraction fringes found in Figure 3.5C might be removed from a reconstruction.

Results

Standard Analyses of Ca^{++} Imaging Data

To establish a basis for comparison, we will first show results of the analysis of our data using standard methods. PC12 cells were loaded with fluo-4 and Fura-Red (Figure 3.1). The cells were imaged with single-photon excitation at 488 nm with a confocal microscope. We measured fluorescence emission for fluo-4 and Fura-Red as well as transmitted light while continuously exposing cells to a perfusing solution (see Methods). Transmitted light was measured in a

transmission PMT and used to detect any motion in the PC12 cells. Our experimental switching paradigm was checked by replacing the stimulating solution with fluorescein and measuring changes in fluorescence in the imaging chamber (Figure 3.1C). For stimulation experiments, two solutions, a non-stimulating and stimulating solution, were periodically perfused through a closed chamber containing the PC12 cells. The non-stimulating solution was standard Hanks solution containing calcium and magnesium (see Methods). The stimulating solution was an isotonic modified Hanks solution containing calcium, magnesium but with varying levels of NaCl replaced by KCl. The fluorescence response to Ca^{++} was calibrated by exposing the cells to an ionomycin solution successively containing EGTA (low calcium clamp) or 10 mM Ca^{++}. The characteristic (anti-correlated) changes in fluo-4 and Fura-Red fluorescence from a typical experiment using 50mM KCl are shown in Figure 3.1B. Plotted are raw and superimposed averaged fluorescence traces from fluo-4 and Fura-Red channels. The superimposed traces make clear the anti-correlation of the signals in the two channels. Although the cells contain some compartmentalized dye, the dye does not respond to high-K^{+} stimulation and therefore does not contribute to the ratiometric signal. For all data shown in this paper, no periodic motion corresponding to our stimulus paradigm was observed in the transmission PMT channel.

Reconstructing Temporal Dynamics: Averaging Over Pixels

To quantitate temporal changes in imaging data, most researchers determine a region-of-interest (ROI) and average all pixel timecourses within the ROI. Ratios are then calculated by dividing the ROI time-courses resulting in a ratio as a function of time. Some ROI analysis methods also set pixels below a user defined threshold to zero (cf. RatioPlus plugin for ImageJ). This is a non-linear manipulation of the data that can severely bias estimates of low amplitude

fluorescence changes and we avoid such procedures.

Figure 3.2 shows an ROI analysis of one of our datasets. We show an optical image of a field primarily containing neurites (A) and the mean fluo-4 fluorescence image (A') with an ROI chosen from the bright pixel region shown in Figure 3.2A'. The ratio from the ROI is plotted in Figure 3.2B. While this method provides quantitative estimates of the ratio in time, it sacrifices spatial information and is adhoc from the point of view that ROIs are typically chosen subjectively by the user. Biologically relevant information can be lost if the user fails to choose an appropriate ROI. Due to the noise in the ratio estimate, it is difficult to see any real structure in the ratio with this choice of ROI. On the other hand, picking an ROI along one of the neurites gives more evidence of a response to stimulus (see Figure 3.4C, G, K, O and text).

Reconstructing the Spatial Distribution of the Signal: Temporal Averaging

In Figure 3.2, we averaged spatial regions in the data to better visualize temporal dynamics. By contrast, temporal averaging allows us to visualize the spatial structure of the neuritic response to stimulation. In Figure 3.3B-F, we show spatially resolved dynamics of the response of neurites to stimulation as made evident by temporal boxcar averaging. Frames at 20 second increments post-stimulation-onset are shown with peak response at 100 seconds. Sharp temporal features are smoothed out in the dynamics; however, the spatial distribution of the responding neurites may be seen. By comparing with the optical image (Fig.3.3A), we can see that only a subset of neurites is responding. The neurite network structure becomes most evident at peak response (e.g. Fig.3.3F). Note that a network of neurites is evident here, whereas spatial information was averaged over in the ROI analysis shown in Figure 3.2. It is important to realize that, although to the eye, the neurite network is evident, the eye is using spatial correlations across many pixels to make sense of the picture. Individual pixel timecourses, when plotted, are

still very noisy, and the quantitation of the ratio in this data is poor (see Fig.3.4A, E,I,M and text).

A Comparison of SOARS with Current Analysis Techniques

Figure 3.4 compares ROI, temporal averaging and SOARS analyses. For the sake of consistency, we use the dataset analyzed above. SOARS was designed to extract spatially correlated and temporally anti-correlated information from the dataset and provide an optimal filter that leads to improved spatiotemporal estimates of the ratio. Because this method is not user-dependent, it provides objective criteria for analyzing ratiometric data.

The figure shows analyses of three different user-defined ROIs and a SOARS analysis for three different boxcar filters (no filter, 10 and 100 frame averaging). For each of the ROI analyses, an image of the mean fluorescence in the fluo-4 channel is shown, overlaid with an ROI. For the SOARS analysis, an eigenimage whose timecourse was used in the ratio reconstruction is shown. Note that only pixel covariance information and no spatial or morphological information was used to calculate the eigenimage, therefore, the network of neurites visible in the image is confirmation of neuritic response to stimulus that was derived from the dataset.

For the ROI analyses, the timecourses were arrived at in the following way: 1) pixels were spatially averaged within the ROI for each wavelength, 2) either no temporal filtering (panels E-G), a ten-frame boxcar average (panels I-K) or a one-hundred frame boxcar average (panels M-O) was applied to the resulting timecourses, then 3) the timecourses were ratioed. For the SOARS analysis, a single eigenimage was chosen for the ratio reconstruction (a full reconstruction will be shown later). Timecourses of an individual pixel from the reconstruction

are shown in panels H, L and P. Boxcar averaging in time was performed on the timecourses, $(\psi, X1,2(t))$, before ratioing.

We designed our experiment to establish an independent criterion for evaluating the data analysis methods. Ideally, a signal analysis method will faithfully reveal the initial periodicity and the final ionomycin/EGTA low calcium clamp. Note that by these criteria, for any amount of temporal averaging, the SOARS analysis results in the best SNR. The initial periodicity and low calcium clamp are evident in the results of the SOARS analysis for any amount of temporal averaging of the signal. However, the ROI analyses, particularly the ROI of the bright fluorescent region, clearly have a much smaller SNR and require extensive temporal averaging in order to see good evidence of a response to stimulation. To illustrate this, we replot the data from Figure 3.2 in panels B and F and to compare against temporal averaging and SOARS results, we present temporally filtered ratios in J and N. In the ROI analysis along a neurite (panels C, G, K, O), the response to stimulus is more readily visible to the eye in the first few periods of stimulation, but is swamped by high-frequency noise as the response decreases in amplitude. The results of a temporal averaging analysis may be seen in panels A, E, I, M, in which a single pixel timecourse is averaged. Here, even for boxcar averaging of 100 frames, the response to stimulation is consistent with filtered noise. As we noted in the discussion of temporal averaging analysis, the reason that temporal averaging helps to visualize the spatial distribution of the signal is that the eye finds correlations between pixels and uses this information to reject noise.

Conducting a SOARS Analysis

A SOARS analysis consists of four main steps: 1) Standardization and subtraction of the fluorescence signals from two wavelengths. 2) Performance of an SVD on the standardized,

subtracted data. 3) Statistical selection of eigenimages. And 4) reconstruction of the ratio using only statistically significant eigenimages (a denoised, or optimally filtered, ratio).

In Figure 3.5, we present intermediate results from steps 2 and 3 of a SOARS analysis of the same data that was presented in Figures 3.2-4. We present five eigenimages and associated statistical information, representative of typical signal components in our experimental setup. The first column (panels A-E) depicts eigenimages (i.e. eigenimages) 1, 2, 4, 10 and 15, respectively. The eigenimages are ordered in descending amount of variance in the dataset. The first two eigenimages (panels A and B) show evidence of obvious varicosities and neuritic structures (arrows). The fourth eigenimage (panel C) shows optical diffraction fringes resulting from partial overlap of the excitation laser wavelength with the fluo-4 emission band. These diffraction fringes are seen only in the fluo-4 channel. The tenth eigenimage (panel D) shows three putative punctate regions (arrowheads). Finally, the fifteenth eigenimage (panel E) has no evident spatial structure.

Timecourses, $(\psi, X_{1,2}(t))$, of the eigenimages in the standardized, subtracted data are presented in panels F-J. Whereas the first two standardized timecourses exhibit periodicity, the other timecourses do not.

The power of SOARS to detect temporally anti-correlated information is demonstrated in the third column (panels K-O) of Figure 3.5. Here, we plot the timecourses of the eigenimages from the SVD in the standardized fluo-4 (blue) and Fura-Red (red) datasets. Note the strongly anti-correlated timecourses in panels K and L, the timecourses of the eigenimages with evident neuritic structures. By contrast, the timecourses in panels M-O exhibit little anti-correlation. The fluo-4 timecourse of eigenimage 4 shows rapid, noisy fluctuation, whereas, the Fura-Red timecourse is relatively flat reflecting the fact that the fringes only show up in the fluo-4 channel.

Panels N and O show some small anti-correlation initially corresponding to the slow fluctuations in panels I and J. These fluctuations are confined to the punctate regions indicated by arrowheads in panel D.

In the fourth column, we present information that may be used to select the statistically significant eigenimages to be used for a reconstruction of the ratio. According to the null hypothesis (see Methods), if there is no signal, these distributions should be normally distributed. To check normality, we plot a histogram estimate of the distribution of the timecourses shown in column two and compare it against the normal distribution given by the mean and standard deviation from the data. A statistically significant violation of the null hypothesis will be seen as a histogram that does not conform to the normal distribution plotted in red. As can be seen, the first two histograms are distinctly non-normal. Subsequent eigenimages become better approximations to normality.

The two standardized datasets are both assumed to be normally distributed under the null hypothesis. Therefore, another way to approach the question of statistical significance is to investigate the joint-probability of the timecourses of the eigenimage on each of the standardized datasets, $(\varphi, X1,2(t))$. Numerical experiments on simulated normally distributed data demonstrate that under the null hypothesis, these joint probabilities are normally distributed with major axis along the $X-Y$ axis (data not shown). In column five (panels U-Y), we plot the joint probabilities from the dataset. In these plots, the diagonal axis is plotted as a white line. As expected, the joint-probabilities of the first two eigenimages are distinctly non-normal. Eigenimage 4 gives a distribution that is skewed relative to the diagonal axis. Eigenimage 10 gives a distribution that is slightly skewed relative to the diagonal axis. And by the fifteenth eigenimage, the distributions are all on the diagonal axis and therefore represent noise.

Discussion

SOARS: A User-Independent Method for Reconstructing Ratio Dynamics

We have gone to some lengths to compare SOARS with standard ratiometric analysis methods used in most laboratories. Beyond the accurate ratio estimation provided by SOARS, its most important feature is independence from user subjectivity. Often biologically meaningful signal fluctuations may go unnoticed since in the absence of edges the human eye can only detect contrast differences of about 2% (Campbell and Robson 1968). Particularly when choosing ROIs in fluorescence data, the user will be drawn to regions with large background fluorescence. This can be fatal in some contexts. For instance, it is known that calcium levels vary more in neurites than in cell bodies in neuronal cultures (Borgdorff et al. 2000) and we have seen this in PC12 cells as well (data not shown). However, cell bodies often fluoresce more brightly (as may be seen in Fig.3.1). Although a calcium response may exist somewhere in the data, the user may choose the cell body for the ROI and miss important changes in neurites. These considerations become even more important in investigations of neural circuitry in slice and whole brain preparations, where the whole imaging field is occupied by a dense network of neurons and the appropriate biologically relevant features may be difficult to identify. Furthermore, in cases where dye is compartmentalized into vesicular or other structures, vesicularized dye may be brighter than free cytoplasmic dye, but will not contribute to the ratiometric signal. Because SOARS automatically reflects the anti-correlated information in the dataset, excellent estimates may be obtained, even when compartmentalization or differential localization might be a problem for other methods.

SOARS avoids the above pitfalls with the use of a statistical model of the optical characteristics of ratiometric dyes. An optimization method is used to find masks that contain as

much anti-correlated activity as possible across the entire dataset, optimizing the likelihood that, if an anti-correlated signal exists somewhere in the data, it will be found, even if it is not where the user expected.

Another problem involved with user-defined ROIs is that they sacrifice spatial information within the ROI by averaging timecourses over the pixels within the masked region. SOARS again avoids this problem by providing multiple, orthogonal, weighted masks. Therefore, in a ratio reconstruction from SOARS, wave-like activity or other spatially distributed changes may be captured via the superposition of spatial information in the various weighted masks combined with their timecourses.

An important point to make about SOARS is that it also works for the other common ratiometric technique in which only one of the fluorophores being imaged changes fluorescence due to the variable of interest. In fact, it is for this reason that the refraction fringes, which are only present in the fluo-4 data, show up as statistically significant eigenimages in Figure 3.5C, H, M and R.

When the Noise Deviates from the Model

Sometimes, the noise in the data may not be normally distributed. For instance, in the dataset that we analyzed for Figures 3.2-5, the variance in the dataset tends to decrease slightly as a function of time (i.e. is not completely stationary). This leads to small wings in the distribution of ‘noisy’ timecourses. They are not exactly normally distributed. In this case, a Kolmogorov-Smirnov test is more appropriate for testing the equivalence of the distributions of the standardized timecourses. For instance, the timecourse of the 15th eigenimage has the same distribution as all other timecourses, except those of the 1st through 8th and 10th eigenimages.

This indicates that we can accept as 'noise' all timecourses other than these eigenimages for this dataset, since they have the same distribution. The first ten timecourses are then statistically significant deviations from the null hypothesis and represent anti-correlation in the dataset.

Empirically, we have found that testing whether the joint-probability lies diagonally in the joint probability distribution is more robust to deviations from a normal distribution.

Controlling for Motion

Ratiometry is often invoked as a method for suppressing motion artifacts in fluorescent imaging data. This has been documented in imaging studies of the beating heart (Brandes et al. 1992). However, it is clear that this is not true in general. Particularly with high-resolution microscopic methods such as confocal and two-photon microscopy, motion artifacts can creep into data even when the motion is only of order a few microns. SOARS cannot eliminate these artifacts. Therefore, in order to control for these factors, we took the following steps: 1) We imaged a volume around the focal plane of interest and determined the expected signal that we would get if the focal plane happened to change during the experiment by performing a SOARS analysis as a function of Z-position (as opposed to a SOARS analysis as a function of time). 2) We imaged transmitted light in a separate channel and investigated this dataset for motion in the X, Y plane. In the datasets that we present in this study, we were able to ensure that the signals that we were seeing were due to changes in Ca^{++} concentration within the cells and not due to motion artifacts.

References

Bischofberger, J. and D. Schild. 1995. Different spatial patterns of [Ca2+] increase caused by N- and L-type Ca2+ channel activation in frog olfactory bulb neurones. *J Physiol* **487 (Pt 2)**: 305-17.

Black, M.J., Y. Woo, and S.G. Rane. 2003. Calcium channel upregulation in response to activation of neurotrophin and surrogate neurotrophin receptor tyrosine kinases. *J Neurosci Res* **74**: 23-36.

Borgdorff, A.J., G.G. Somjen, and W.J. Wadman. 2000. Two mechanisms that raise free intracellular calcium in rat hippocampal neurons during hypoosmotic and low NaCl treatment. *J Neurophysiol* **83**: 81-9.

Bouron, A., C. Becker, and H. Porzig. 1999. Functional expression of voltage-gated Na+ and Ca2+ channels during neuronal differentiation of PC12 cells with nerve growth factor or forskolin. *Naunyn Schmiedebergs Arch Pharmacol* **359**: 370-7.

Brandes, R., V.M. Figueredo, S.A. Camacho, B.M. Massie, and M.W. Weiner. 1992. Suppression of motion artifacts in fluorescence spectroscopy of perfused hearts. *Am J Physiol* **263**: H972-80.

Bright, G.R., G.W. Fisher, J. Rogowska, and D.L. Taylor. 1987. Fluorescence ratio imaging microscopy: temporal and spatial measurements of cytoplasmic pH. *J Cell Biol* **104**: 1019-33.

Campbell, F.W. and J.G. Robson. 1968. Application of Fourier analysis to the visibility of gratings. *J Physiol* **197**: 551-66.

Cheng, K.H., J. Virtanen, and P. Somerharju. 1999. Fluorescence studies of dehydroergosterol in phosphatidylethanolamine/phosphatidylcholine bilayers. *Biophys J* **77**: 3108-19.

Gomez, T.M., E. Robles, M. Poo, and N.C. Spitzer. 2001. Filopodial calcium transients promote substrate-dependent growth cone turning. *Science* **291**: 1983-7.

Gonzalez, J.E. and R.Y. Tsien. 1995. Voltage sensing by fluorescence resonance energy transfer in single cells. *Biophys J* **69**: 1272-80.

-. 1997. Improved indicators of cell membrane potential that use fluorescence resonance energy transfer. *Chem Biol* **4**: 269-77.

Grynkiewicz, G., M. Poenie, and R.Y. Tsien. 1985. A new generation of Ca2+ indicators with greatly improved fluorescence properties. *J Biol Chem* **260**: 3440-50.

Higashijima, S., M.A. Masino, G. Mandel, and J.R. Fetcho. 2003. Imaging neuronal activity during zebrafish behavior with a genetically encoded calcium indicator. *J Neurophysiol* **90**: 3986-97.

Isshiki, M., J. Ando, R. Korenaga, H. Kogo, T. Fujimoto, T. Fujita, and A. Kamiya. 1998. Endothelial Ca2+ waves preferentially originate at specific loci in caveolin-rich cell edges. *Proc Natl Acad Sci U S A* **95**: 5009-14.

Jackson, A.P., M.P. Timmerman, C.R. Bagshaw, and C.C. Ashley. 1987. The kinetics of calcium binding to fura-2 and indo-1. *FEBS Lett* **216**: 35-9.

Kao, J.P. 1994. Practical aspects of measuring [Ca2+] with fluorescent indicators. *Methods Cell Biol* **40**: 155-81.

Keith, C.H., R. Ratan, F.R. Maxfield, A. Bajer, and M.L. Shelanski. 1985. Local cytoplasmic calcium gradients in living mitotic cells. *Nature* **316**: 848-50.

Li, J., J.A. Mack, M. Souren, E. Yaksi, S. Higashijima, M. Mione, J.R. Fetcho, and R.W. Friedrich. 2005. Early development of functional spatial maps in the zebrafish olfactory

bulb. *J Neurosci* **25**: 5784-95.

Lipp, P. and E. Niggli. 1993. Ratiometric confocal Ca(2+)-measurements with visible wavelength indicators in isolated cardiac myocytes. *Cell Calcium* **14**: 359-72.

Lorenzon, P., D. Zacchetti, F. Codazzi, G. Fumagalli, J. Meldolesi, and F. Grohovaz. 1995. Ca2+ waves in PC12 neurites: a bidirectional, receptor-oriented form of Ca2+ signaling. *J Cell Biol* **129**: 797-804.

Merritt, J.E., S.A. McCarthy, M.P. Davies, and K.E. Moores. 1990. Use of fluo-3 to measure cytosolic Ca2+ in platelets and neutrophils. Loading cells with the dye, calibration of traces, measurements in the presence of plasma, and buffering of cytosolic Ca2+. *Biochem J* **269**: 513-9.

Miyawaki, A., J. Llopis, R. Heim, J.M. McCaffery, J.A. Adams, M. Ikura, and R.Y. Tsien. 1997. Fluorescent indicators for Ca2+ based on green fluorescent proteins and calmodulin. *Nature* **388**: 882-7.

Roe, M.W., J.J. Lemasters, and B. Herman. 1990. Assessment of Fura-2 for measurements of cytosolic free calcium. *Cell Calcium* **11**: 63-73.

Schlatterer, C., G. Knoll, and D. Malchow. 1992. Intracellular calcium during chemotaxis of Dictyostelium discoideum: a new fura-2 derivative avoids sequestration of the indicator and allows long-term calcium measurements. *Eur J Cell Biol* **58**: 172-81.

Siegel, M.S. and E.Y. Isacoff. 1997. A genetically encoded optical probe of membrane voltage. *Neuron* **19**: 735-41.

Sornborger, A., T. Yokoo, A. Delorme, C. Sailstad, and L. Sirovich. 2005. Extraction of the average and differential dynamical response in stimulus-locked experimental data. *J Neurosci Methods* **141**: 223-9.

Takahashi, A., P. Camacho, J.D. Lechleiter, and B. Herman. 1999. Measurement of intracellular calcium. *Physiol Rev* **79**: 1089-125.

Tischler, A.S., L.A. Greene, P.W. Kwan, and V.W. Slayton. 1983. Ultrastructural effects of nerve growth factor on PC 12 pheochromocytoma cells in spinner culture. *Cell Tissue Res* **228**: 641-8.

Truong, K., A. Sawano, H. Mizuno, H. Hama, K.I. Tong, T.K. Mal, A. Miyawaki, and M. Ikura. 2001. FRET-based in vivo Ca2+ imaging by a new calmodulin-GFP fusion molecule. *Nat Struct Biol* **8**: 1069-73.

Yokoo, T., B.W. Knight, and L. Sirovich. 2001. An optimization approach to signal extraction from noisy multivariate data. *Neuroimage* **14**: 1309-26.

Zochowski, M., M. Wachowiak, C.X. Falk, L.B. Cohen, Y.W. Lam, S. Antic, and D. Zecevic. 2000. Imaging membrane potential with voltage-sensitive dyes. *Biol Bull* **198**: 1-21.

Acknowledgments

We thank Partha Mitra, Emery Brown and David Kleinfeld of the Neuroinformatics course at the Woods Hole Marine Biological Laboratory for providing a conducive environment to think about and discuss the analysis of neural imaging data. This work was supported by a Faculty Research Grant (S), a University of Georgia Engineering Grant (SKL) from the University of Georgia Research Foundation and an NIH grant: EB005432 (SKL). Broder and Majumder were co-First Authors and Lauderdale and Sornborger were co-Senior Investigators on this project.

Figures

Figure 3.1: Analysis of the fluorescence of PC12 cells loaded with fluo-4 and Fura-Red in response to depolarization with 50 mM KCl. (A) Transmitted light image of three loaded cells. (A') Fluo-4 fluorescence of the same cells. Note that some dye is compartmentalized, but there is a significant amount of dye in the cytoplasm. (A") Fura-Red fluorescence of the same three loaded cells. Scale bar: 20 μm. (B) Timecourses of fluo-4 and Fura-Red fluorescence in response to 10 cycles of stimulation (2 minutes on, 2 minutes off) with 50 mM K^{+}solution, followed by 5 minutes with ionomycin + EGTA (low calcium clamp), followed by 5 minutes ionomycin + saturating Ca^{++}. (C) Switching profile (black trace) and concentration profile of 0.0005% fluorescein flowing through the Dvorak-Stotler chamber (blue trace).

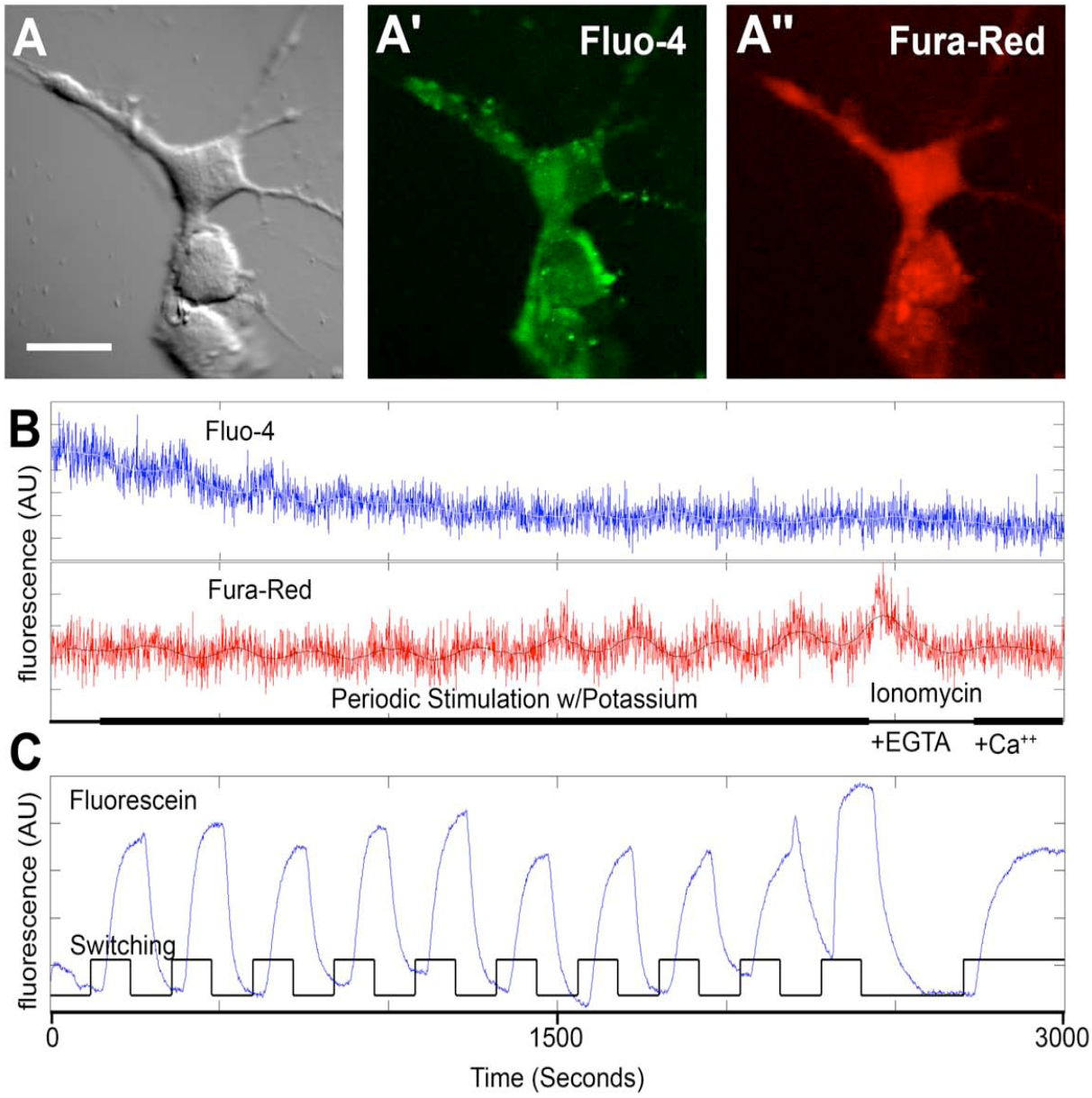
A
A'
Fluo-4
A''
Fura-Red
B
Fluo-4
Fura-Red
fluorescence (AU)
Periodic Stimulation w/Potassium
Ionomycin
+EGTA
+Ca++
C
Fluorescein
Switching
fluorescence (AU)
0
1500
3000
Time (Seconds)

Figure 3.2: Standard ROI analysis of ratiometric calcium imaging data. PC12 cells were loaded with fluo-4 and Fura-Red. Fluorescence measurements of the response to periodic stimulation with a high-potassium medium followed by a low calcium clamp (ionomycin + EGTA) were made in the fluo-4 and Fura-red emission bands. (A) Transmitted light image of a field of neurites. (A') Fluo-4 mean fluorescence with ROI indicated (red bordered region). Scale bar A, A': 40 μm. (B) Timecourse of fluorescence ratio in ROI depicted in A and A'. Although a periodic change in the ratio is visible initially, as its amplitude decreases, it becomes invisible in the noise.

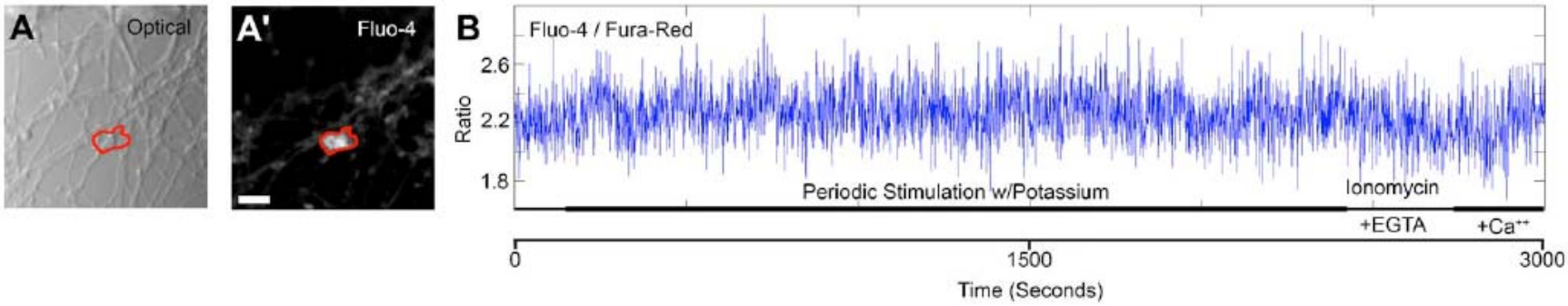
A
Optical
A'
Fluo-4
B
Fluo-4 / Fura-Red
2.6
2.2
1.8
Ratio
Periodic Stimulation w/Potassium
Ionomycin
+EGTA
+Ca++
0
1500
3000
Time (Seconds)

Figure 3.3: Standard temporal averaging analysis of ratiometric calcium imaging data (see Methods). The PC12 cells were loaded with fluo-4 and Fura-Red. Fluorescence measurements of the response to periodic stimulation with a high-potassium medium followed by a low calcium clamp (ionomycin + EGTA) were made in the fluo-4 and Fura-Red emission bands. (A) Transmitted light image of a field of neurites. (B-F) Ratio estimates at 20, 40, 60, 80 and 100 seconds post-stimulus-onset (timing of onset was based on the fluorescein timecourse shown in panel D of Figure 3.2). These frames show baseline to peak response to stimulus. Obvious neuritic structures start to become evident by 60 seconds post-stimulus-onset. For temporal averaging, a boxcar window of 100 frames was used.

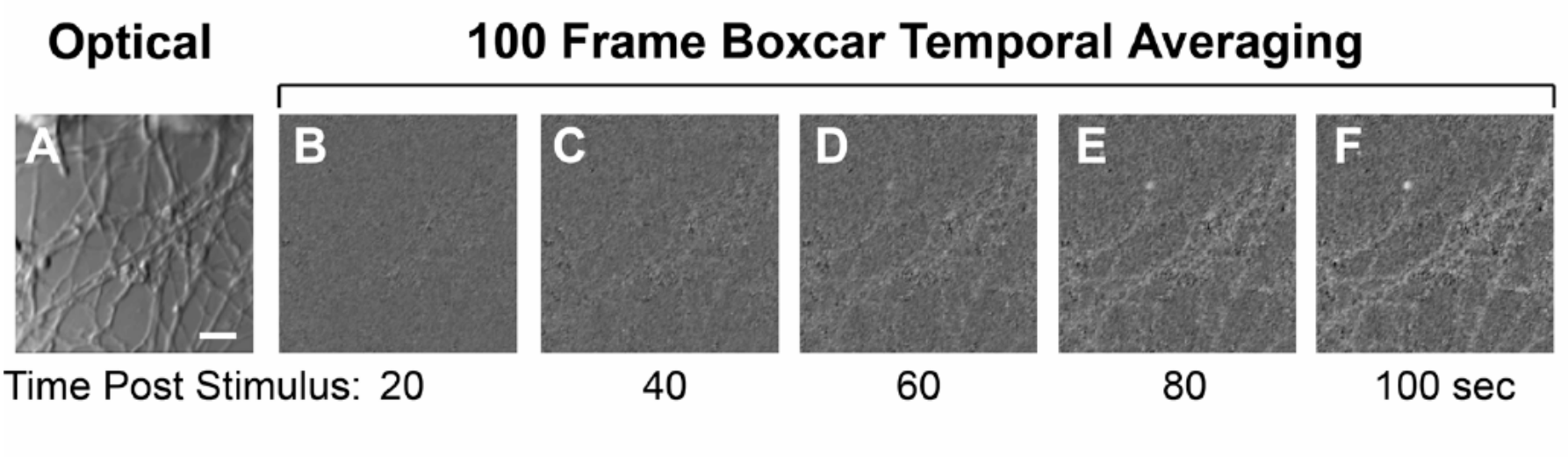
Optical
100 Frame Boxcar Temporal Averaging
A
B
C
D
E
F
Time Post Stimulus: 20
40
60
80
100 sec

Figure 3.4: Comparison of ROI, temporal averaging and SOARS analyses of ratiometric data. The first column shows spatial information: (A-C) Three different ROIs superimposed on the mean fluorescence image from the fluo-4 channel: (A) Single pixel ROI; (B) ROI around region of bright fluorescence; (C) ROI along a neurite. (D) Eigenimage arising from a SOARS analysis of the data. The next three columns show temporal information: (E-G) Timecourses of the ratio calculated with the three different ROIs. (H) Timecourse from a SOARS analysis. Because SOARS is a multivariate analysis technique, the ratio reconstruction has information from across the entire imaging region. For comparison with the ROI analyses, we plot the timecourse of the pixel depicted in D (inset). (I-L) As E-H, except temporally filtered (before ratioing) with a 10 frame boxcar average. (M-P) As E-H, except filtered with a 100 frame boxcar average.

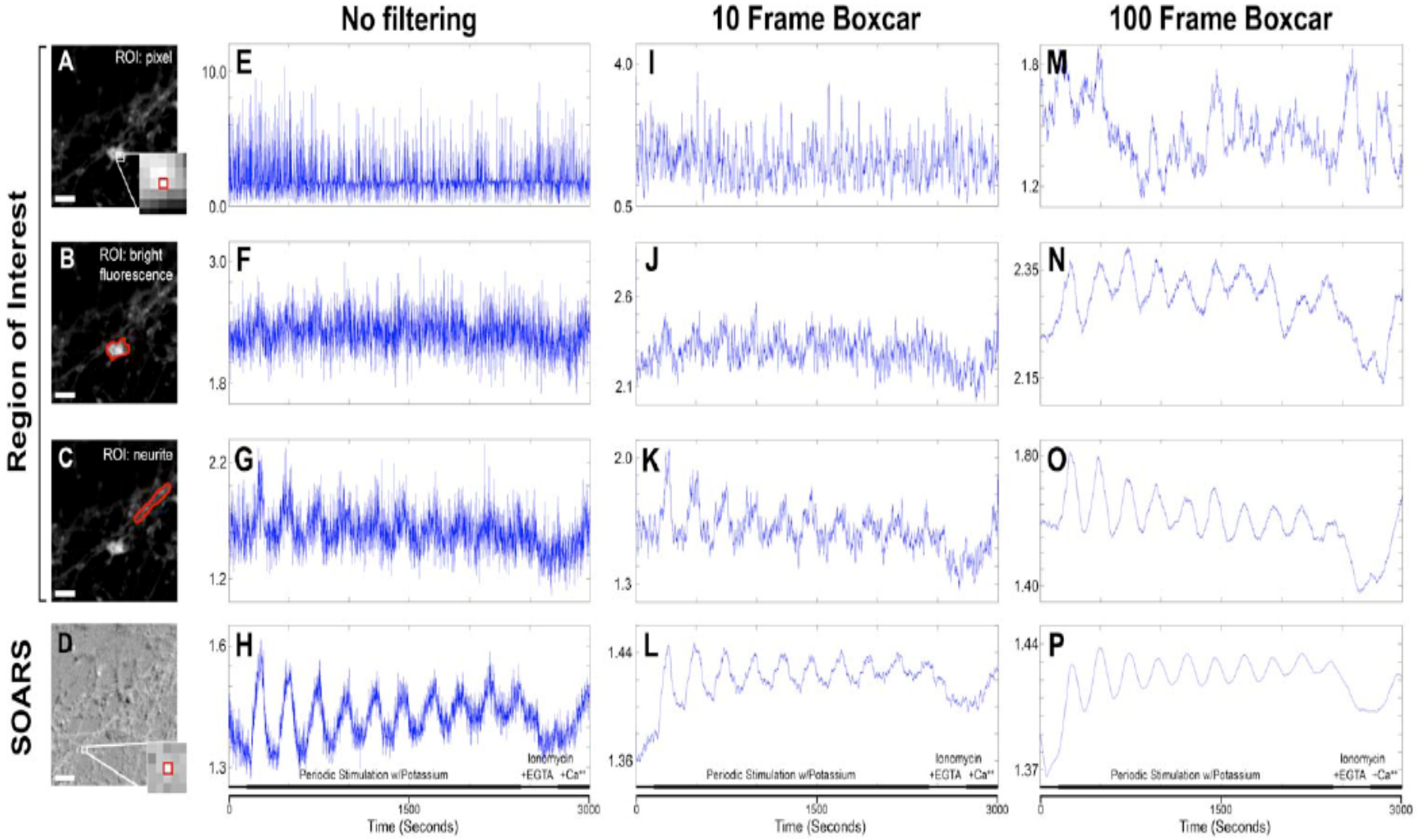
No filtering
10 Frame Boxcar
100 Frame Boxcar
Region of Interest
SOARS
A
ROI: pixel
B
ROI: bright fluorescence
C
ROI: neurite
D
E
F
G
H
I
J
K
L
M
N
O
P
10.0
0.0
3.0
1.8
2.2
1.2
1.6
1.3
4.0
0.5
2.6
2.1
2.0
1.3
1.44
1.36
1.8
1.2
2.35
2.15
1.80
1.40
1.44
1.37
Periodic Stimulation w/Potassium
Ionomycin +EGTA +Ca++
0
1500
3000
Time (Seconds)

Figure 3.5: Conducting a SOARS analysis: Shown are intermediate results from the SOARS analysis in Figure 3.4A-E Eigenimages (scale bar = 40μm). (F-J) Standardized timecourses of the eigenimages. (K-O) Timecourses of eigenimages in fluo-4 and Fura-Red bands. Note the obvious periodic anti-correlation in panels K and L, which correspond to the eigenimages with evident cellular and neuritic structures in panels A and B. (P-T) Histogram estimate of the distribution of standardized timecourses. Normal distribution based on mean and standard deviation of timecourse plotted in red. An eigenimage is taken to represent anti-correlated information in the data if its distribution is non-normal. (U-Y) Joint probability of the timecourses of the eigenimage on the standardized fluo-4 and Fura-Red datasets. An alternative measure of statistical significance is deviation of the joint-probability from the diagonal axis.

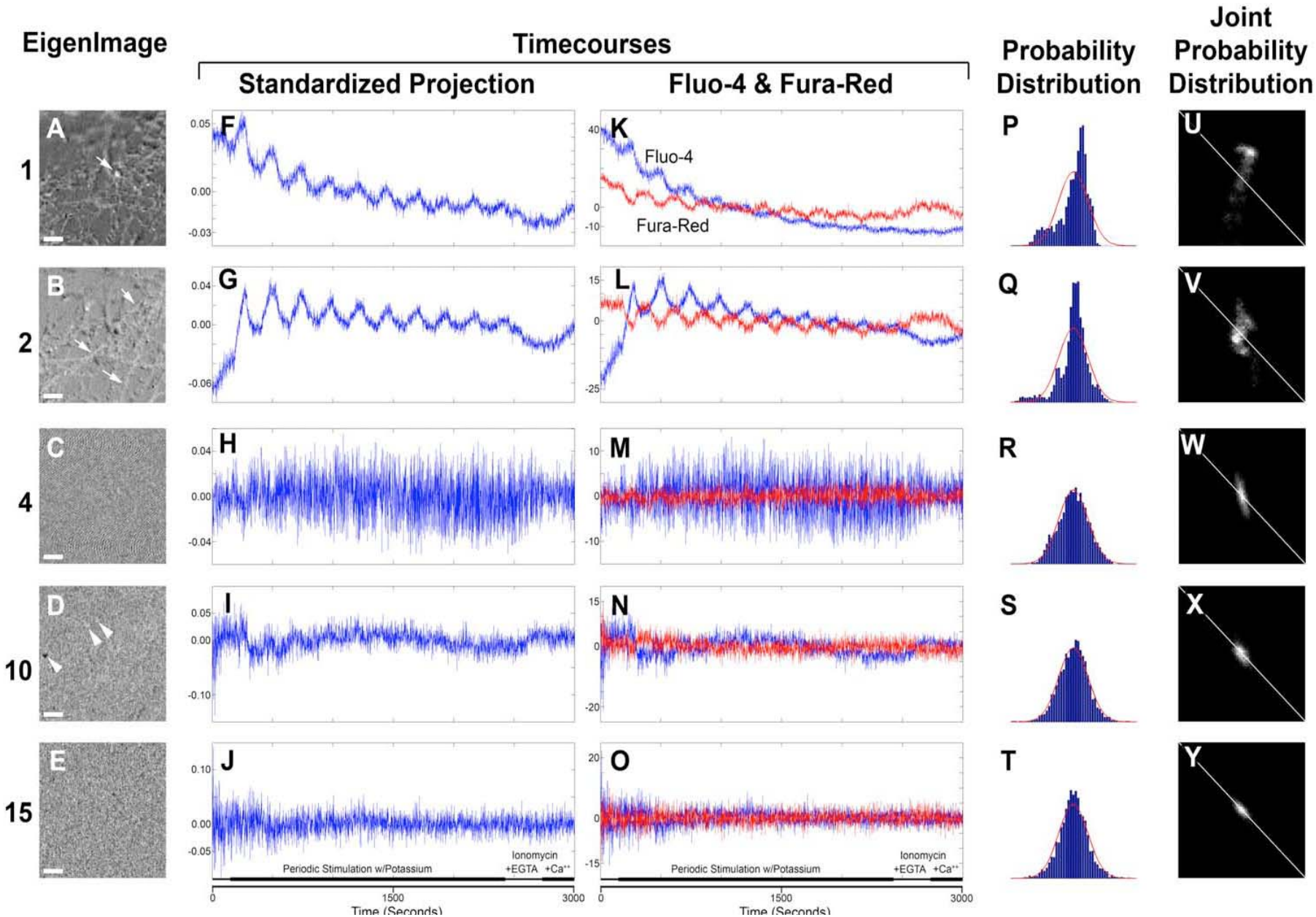
EigenImage
Timecourses
Standardized Projection
Fluo-4 & Fura-Red
Probability Distribution
Joint Probability Distribution
1
2
4
10
15
A
B
C
D
E
F
G
H
I
J
K
L
M
N
O
P
Q
R
S
T
U
V
W
X
Y
Fluo-4
Fura-Red
Periodic Stimulation w/Potassium
Ionomycin
+EGTA +Ca++
Time (Seconds)

Chapter 4

New Statistical Methods Enhance Imaging of Cameleon FRET in Cultured Zebrafish Spinal Neurons[1]

[1]Majumder A., Fan X., Reagin S., Porter E., Sornborger A., Keith C., Lauderdale J. Submitted to J Biol Optics

Abstract

Cameleons are genetically encoded FRET based Ca^{2+} indicators. Attempts to use cameleons to detect neural activity in vertebrate systems have been largely frustrated by the small FRET signal, in contradistinction to the higher signals seen in Drosophila and Caenorhabditis elegans. We have developed a statistical optimization method capable of detecting small ratiometric signals in noisy imaging data, called Statistical Optimization for the Analysis of Ratiometric Signals (SOARS). Using this method, we show that we can detect and estimate anti-correlated ratiometric signals with subcellular resolution in cultured, dissociated zebrafish spinal neurons. This method may make it possible to use yellow cameleons for measuring neural activity at high-resolution in transgenic animals.

Introduction

A fundamental problem in neurobiology is to link behavior with neural activity. A full understanding of the neural mechanisms underlying behavior requires that we be able to monitor the activity of multiple neurons at a cellular level; however, this is difficult to accomplish using traditional electrophysiological methods. Alternate approaches use proxies for the electrical activity of cells. A particularly good example of such a proxy for the electrical activity of neurons is changes in intracellular calcium levels resulting from the influx of calcium through voltage-gated calcium channels.

The measurement of intracellular calcium levels in living cells can be accomplished through the use of synthetic calcium indicator dyes, such as fura-2 or fluo-4, which can be introduced into cells by bulk loading techniques such as ester loading or cell permeabilization, or by individual cell techniques, such as microinjection (Takahashi, Camacho et al. 1999). These dyes have proved extremely valuable in measuring changes in intracellular calcium indicators in a wide variety of neuronal and non-neuronal cell types. However, most calcium indicators act as chelators, and can affect the function of the cells of interest (Takahashi, Camacho et al. 1999). Furthermore, bulk-loading techniques can damage cells and are difficult to restrict to particular types of cell in a tissue.

To circumvent these problems, genetically encoded calcium biosensors have been generated using variants of Aequorea Green Fluorescent Protein (GFP) (Zhang, Campbell et al. 2002; Miyawaki, Mizuno et al. 2003; Miesenbock 2004; Miesenbock and Kevrekidis 2005; Miyawaki 2005). Because genetically encoded biosensors can be selectively expressed, in principle they should be able to dissect the activity of neural circuits in an intact animal more efficiently than synthetic calcium indicator dyes. Furthermore, when these dyes are expressed in

an animal, animal viability and/or behavior offers an assay of whether they affect cell function (Higashijima, Masino et al. 2003).

Cameleons are genetically encoded Ca^{2+} indicators (GECI's) based on fluorescent proteins and calmodulin (CaM) (Miyawaki, Llopis et al. 1997; Tsien 1998). They are chimeric proteins built of a short-wavelength variant of GFP (a fluorescence resonance energy transfer (FRET) donor), CaM, the CaM-binding peptide of myosin light-chain kinase (M13), and a long-wavelength variant of GFP (a FRET acceptor). Binding of Ca^{2+} to the CaM moiety initiates an intramolecular interaction between the CaM and M13 domains, causing the chimeric protein to shift from an extended conformation to a more compact one, thereby bringing the modified GFP domains close enough together to allow FRET from the shorter to the longer-wavelength variant of GFP (Patterson, Piston et al. 2000; Habuchi, Cotlet et al. 2002). This technique is useful for emission ratioing, which eliminates artifacts due to bleaching, variable illumination, and is more immune to movement or changes in focus than single-wavlength monitoring. Emission ratioing is an ideal readout for fast imaging by laser-scanning confocal microscopy (Higashijima, Masino et al. 2003; Miyawaki 2005).

There are currently several different cameleons (Truong, Sawano et al. 2001; Nagai, Yamada et al. 2004; Miyawaki 2005). Yellow cameleons (YCs) have cyan and yellow fluroscent proteins (CFP and YFP) as the FRET donor and acceptor, respectively, and have been used to observe Ca^{2+} dynamics in the Drosophila neuromuscular junction (Guerrero, Reiff et al. 2005; Reiff, Ihring et al. 2005), mechanosensory neurons of Caenorhabditis elegans (Suzuki, Kerr et al. 2003), and in sensory and spinal cord neurons in zebrafish (Higashijima, Masina et al. 2003). YCs are classified into several groups based on the composition of their Ca^{2+} binding domain

(Miyawaki 2003). Of those that include the intact CaM, the YC2.1 version was used in zebrafish (Higashijima, Masino et al. 2003).

Although cameleons were expected to be superior to synthetic dyes for investigating ensemble activity of neural circuitry in living animals, this expectation has been largely unmet in vertebrates. While YCs display robust Ca^{2+} responses *in vitro* and in transiently transfected cell samples, their dynamic range is significantly reduced in the nervous systems of transgenic vertebrates (Miyawaki, Griesbeck et al. 1999; Miyawaki, Mizuno et al. 2003; Nagai, Yamada et al. 2004; Miyawaki 2005) and in primary neurons from vertebrates (Truong Sawano et al. 2001). Most YCs, including YC2.1, exhibit at most a 120% change in the ratio of YFP/CFP upon Ca^{2+} binding in solution. However, this dynamic range appears to be attenuated in neuronal cell types that have a large amount of CaM and CaM-associated proteins, perhaps through interactions with the sensing domains of YCs (Hasan, Friedrich et al. 2004; Heim and Griesbeck 2004; Palmer, Jin et al. 2004). Because of this problem, the successful use of YC in measuring stimulus-dependent responses in the Rohan-Beard neurons of transgenic zebrafish required extensive spatial averaging of fluorescence signals before ratiometric analysis (Higashijima, Masino et al. 2003).

Because of the difficulties presented by cameleons, recent work in vertebrates has focused more on other GECI's such as Inverse Pericam (Nagai, Sawano et al. 2001), G-CaMP (Nakai, Ohkura et al. 2001), and Camgaroo-2 (Griesbeck, Baird et al. 2001), which are single-wavelength indicators. While these indicators have proved workable in vertebrate neurons (Pologruto, Yasuda et al. 2004) and nervous systems (Hasan, Friedrich et al. 2004; Li, Mack et al. 2005), they forgo the benefits of ratiometric approaches. Additionally, this change, as well as the switch to improved cameleons (Truong, Sawano et al. 2001; Heim and Griesbeck 2004;

Nagai, Yamado et al. 2004; Palmer, Jin et al 2004), leaves a large number of transgenic animals that are already expressing earlier versions of YCs unusable for functional imaging studies.

We recently developed an analytical technique that we called Statistical Optimization for the Analysis of Ratiometric Signals (SOARS), which offers improved, user bias-independent detection of weak ratiometric signals at high-resolution (Broder, Majumder et al, submitted). We have found that SOARS can reliably detect small changes in noisy imaging data in the ratio of YFP/CFP in cultured yellow cameleon-expressing zebrafish spinal neurons in response to high-potassium stimulation. This suggests that these techniques may enhance our ability to use YC to detect stimulus-dependent activity in vertebrates.

Methods

Zebrafish strains and maintenance

Wild-type (WIK or TL) embryos were obtained from zebrafish (Danio rerio) lines maintained in the University of Georgia Zebrafish Facility following standard procedures (Westerfield 2000). WIK, and Tuebingen long fin (TL) were obtained from the Zebrafish International Resource Center (ZIRC). Zebrafish transgenic for the YC2.1 cameleon Ca^{2+} indicator (Higashijima, Masino et al. 2003) were originally obtained from Dr. Joe Fetcho (Cornell University, NY). Embryos were reared as previously described (Westerfield 2000) and staged by hours post fertilization (hpf) at 28°C and by standard staging criteria (Kimmel, Ballard et al. 1995). Heterozygous cameleon embryos were generated by crosses between wild-type adults and adults heterozygous for cameleon.

Preparation of dissociated spinal neuron cultures

All experiments were performed in accordance with National Institutes of Health guidelines under protocols approved by the University of Georgia Animal Care and Use Committee. Dissociated zebrafish spinal neuron cultures were prepared from either wild-type embryos or embryos heterozygous for the cameleon transgene following established procedures (Anderson 2001). Briefly, eggs collected from natural matings were bleached after collection, and transferred to embryo medium (Westerfield 2000). Embryos were allowed to develop to the 18-somite stage. Cameleon embryos were sorted by fluorescence using a stereomicroscope equipped for epifluorescence. Embryos were disinfected while still in their chorions with a 30 second rinse in a 70% ethanol solution, then transferred into MMR medium (Andersen 2001). The embryos were manually dechorionated, and the yolk sac and head were removed by mechanical dissection using sterilized forceps. The trunks from 10-14 embryos were transferred to 15 ml conical centrifuge tubes containing 5 ml Custom ATV solution (Andersen 2001), and incubated at room temperature for 9 minutes. The cells were collected by low-speed centrifugation (3 minutes at 720 rpm) in a clinical centrifuge. The supernatant was carefully removed, and the cell pellet resuspended in 0.5 ml culture medium (Andersen 2001). The cells were plated on either acid-washed or laminin-coated 25 mm round coverslips, and cultured at room temperature in the dark. The neurons in these cultures remained viable for up to seven days. We typically imaged neurons cultured for 3 days.

For calcium measurements in wild-type neurons, the cultured neurons were bulk loaded immediately before imaging with 1 μM fluo-4 (Invitrogen/Molecular Probes, Eugene, OR F14217) and 10 μM Fura-Red (Invitrogen/Molecular Probes, F3021) acetoxymethyl (AM) ester fluorescent indicator dyes in a 60% dilution of Hanks' balanced salt solution (HBSS) (Hanks

1976), 0.04% Pluronic acid F-127 (Invitrogen/Molecular Probes, P6867) for 20 minutes at room temperature. After loading, the cells were rinsed with 60% HBSS and mounted in a Dvorak-Stottler chamber (Lucas-Highland, Chantilly, VA). For calcium measurements in cameleon-expressing neurons, coverslips were rinsed in 60% HBSS and mounted in a Dvorak-Stottler chamber.

Confocal microscopy

Confocal microscopy was performed on a Leica SP2 confocal microscope on a Leica DM RXE upright microscope (Leica Microsystems, Bannerbrook, IL). Excitation of cameleon-expressing cells was with the 458 nm line of a 50 mW argon laser, with emission bands of 40 and 30 nm, centered around 485 (cyan) and 535 (yellow) nm, respectively. Cells were maintained in a Dvorak-Stottler chamber and perfused at a rate of 8.3 μl/second with 60% HBSS, alternating with a 60% dilution of a modified HBSS, with 30mM KCl substituting for 30 mM of the normal NaCl (High-K^+ HBSS). Images were taken with the acoustic optical beam splitter set to deliver 5-7% of the laser intensity. This excitation level was generally sufficient to excite approximately 10% of the pixels in the cyan image, and a few pixels in the yellow image, to saturation (grey level 255 in an 8-bit image). The photomultiplier gain in each channel was then adjusted downward to eliminate saturated pixels. Images for ratiometric analyses were collected at a rate of 1/second, at a scale of 256X256 pixels. Cells were perfused alternately with HBSS and High-K^+ HBSS, switching at 2 minutes intervals, for a total of 10 cycles. Subsequently, they were perfused for 5 minutes with HBSS containing 10 μM ionomycin (Invitrogen/Molecular Probes, Eugene, OR) and 10 mM EGTA (low calcium clamp), and then for 5 minutes with HBSS containing 10 μM ionomycin and saturated Ca^{2+}. In some cases, a

separate data series was taken in which cells were perfuesd with 2 minute pulses of HBSS alternating with HBSS + 0.0005% fluorescein, so that the perfusion profile of the chamber could be established.

Wild-type neurons loaded with fluo-4 and Fura-Red were imaged in the same fashion as cameleon-expressing neurons, except that the excitation was at 488nm, and emission was at 516 and 655 nm from fluo-4 and Fura-Red respectively.

Before each series of wild type neurons loaded with fluo-4 and Fura-Red, high resolution images were collected in HBSS (non-stim) and High-K HBSS (stim) conditions (Figure 4.2). these images were taken at a scale of 1024X1024 pixels, at a 10% laser intensity, with 8-fold image averaging. With cameleon-expressing neurons, only a single high-resolution image was taken because of concerns that we might engender rapid bleaching of the YC (Higashimija et al. 2003).

Data Analysis

Due to the low signal-to-noise ratio (SNR) of approximately 1/10 in the data, ratiometric imaging data was analyzed with the multivariate SOARS method [Broder et al. submitted]. This method makes use of the anti-correlated nature of ratiometric signals. SOARS finds orthogonal weighted masks (eigenimages) that are statistically significant estimators of anti-correlated activity in the two-channel ratiometric data. These eigenimages are used to denoise the two-channel data. Finally, the ratio is taken to give an estimate of Ca^{2+} activity.

Results

Dissociated sipinal neurons express cameleon in culture

Cameleon is expressed in all neurons in the line of transgenic fish used for these experiments (Higashijima, Masinao et al. 2003). At the time that the dissections are performed (18-20 hpf), the spinal cord contains at least five classes of neurons, ventral longitudinal descending (VeLD), dorsal longitudinal ascending (DoLA), and primary motor neurons (Benrhardt, Chitnis et al. 1990). RB neurons have large somata (~9 μm diameter; ~64 μm^2), which are located in the dorsal-most neurl tube, and extend two thin axons from the ventral side of the cell body; one of these axons forms a sidebranch, which is usually located near the soma (Benrhardt, Chitnis et al. 1990). There are several types of commissural neurons, all of which project axons to the ventral midline of the neural tube. Of there, the CoPA commissural neurons have a distinctive morphology, which aids in the identification of these neurons. CoPA commissural neurons tend to have spherical soma of ~89 μm^2 with three unbranched processes, giving the neuron a characteristic T-shape (Benrhardt, Chitnis et al. 1990).

We tested if dissociated spinal neurons continued to express cameleon in culture. Dissociated zebrafish spinal neuron cultures (Andersen 2001) were prepared from embryos heterozygous for the cameleon transgene. This procedure produces a heterogeneous population of cells, which includes epithelial or fibroblast cells, myocytes, and neurons (data not shown) [see also, (Andersen 2001)]. Because of the way the dissection was performed, the culture likely also contained trunk neural crest cells, which are migrating from the dorsal neural tube at this time (Raible, Wood et al. 1992). Of these only neurons expressed cameleon (Figure 4.1B). We observed cameleon-expressing neurons with different morphologies, including unipolar and bipolar neurons and putative RBs (Figure 4.1B and data not shown).

Imaging dissociated zebrafish spinal neurons loaded with fluo-4 and Fura-Red

We next measured the response of cameleon expressing neurons to stimulation (Figure 4.3). In these experiments, the cultured neurons were periodically stimulated with a 60% dilution of HBSS containing 30 mM KCl (2 minutes off/2 minutes on) for ten periods (40 minutes total). At the end of each experiment, response to Ca^{2+} was calibrated by exposure to an ionomycin solution containing EGTA followed by ionomycin + saturating Ca^{2+} (Figure 4.3D). Transmitted light was measured in a transmission PMT and used to detect any motion in the cells (data not shown).

The FRET fluorescence data was analyzed using the SOARS method (Broder et al.). This is a statistical optimization method for denosing ratiometric data by detecting spatially correlated, temporally anti-correlated information in the two channels being imaged. The method results in a set of statistically significant eigenimages whose projection in the data is maximally anti-correlated. Typically, the first few eigenimages capture the response to stimulation. We show one such eigenimage (Figure 4.3B)along with the anti-correlated timecourses of the CFP and YFP channels (Figure 4.3C). The eigenimage in Figure 4.3B shows that even though the mean fluorescence is largest in the cell bodies part of the FRET response captured in this eigenimage is fairly even throughout the cell, although some subcellular structure (lighter and darker regions) is visible.

Our experimental paradigm makes it particularly simple to identify the response to stimulus (Figure 4.3C) since it results in a characteristic periodic epoch, followed by large changes due to the ionomycin + EGTA ‘low calcium clamp’. As well as these obvious features, there is an apparent slow increase in Ca^{2+} over time. No FRET response is seen in a negative control (alternate exposure to non-potassium containing solutions, data not shown).

Reconstruction of a denoised ratio with SOARS

Ratiometric signals may be used to obtain quantitative information on Ca^{2+} concentrations. Ratioing also eliminates fluorescence excitation fluctuations due to the illumination source, eliminates the effects of bleaching, and ameliorates motion artifacts. However, quantitative information can be wildly inaccurate in noisy data, particularly due to noise in the denominator and consequent spikes in the ratio, SOARS is an effective method for denoising the data, which leads to a more accurate estimate of the ratio.

Only one of the statistically significant eigenimages was presented in Fiugre 4.3. In Figure 4.4, we show a complete reconstruction of the ratio using all of the statistically significant eigenimages from the SOARS analysis. Whereas one eigenimage (e.g. Figure 4.3B) often captures the dominant response, subtle statistically significant information concerning the FRET response is captured by a few other eigenimages. This additional information can provide insight into physiological changes in the preparation that might well go unseen in the absence of a SOARS analysis.

Discussion

SOARS is a method that we have developed to detect and estimate weak signals in ratiometric imaging data. It is based on a statistical optimization procedure that identifies maximally spatially correlated and temporally anti-correlated information in two-channel ratiometric imaging data. Standard methos rely on user-defined datamasks (regions-of-interest or ROIs) to reduce the signal-to-noise ratio by averaging over pixels. Although ROI methods are easy to use, there can be significant disadvantages to using this approach (see Broder et al.). A major advantage of using SOARS is that user defined maskes (ROIs), which are determined

subjectively by the analyst, are replaced by eigenimages (weighted masks) that are objectively calculated using optimization methods from the data. SOARS results in a set of eigenimages along with their timcourses that may be used to reconstruct (then ratio) two denoised datasets. Since multiple eigenimages are used in the reconstruction, high-resolution spatial and temporal information is retained in the estimated ratio.

The ability to use genetically encoded indicators of neural activity at cellular and subcellular scales is necessary for the analysis of the activity of entire neuronal circuits, and provides both more local and global information in comparison to standard electrophysiological measurements of neuronal activity. A useful model for imaging a complete vertebrate neural system is the YC2.1 transgenic zebrafish. However, it is known that the cameleon signal in zebrafish is weak. We have applied SOARS to the analysis of cameleon FRET data in order to highlight the method's usefulness for detecting weak ratiometric signals and to help rescue zebrafish and other vertebrate models for neural studies. As a first step, in this *in-vitro* study, we corroborate the *in-vivo* results of Higashijima and colleagues (Higashijima, Masino et al. 2003) that indicate that panneurally-expressed YC2.1 can be used to indicate neural activity in zebrafish neurons. Because these investigators had to average spatially in order to be able to detect a signal, they sacrificed spatial resolution in their data. Because of our analytical techniques and experimental design, we are able to extend the spatio-temporal characterization of the cameleon response to the subcellular scale of resolution ($\leq$ 1 micron in Figure 4.3). Although this study was performed using dissociated zebrafish spinal neurons in culture, we have applied the SOARS method to detect neural activation in intact zebrafish with similar results (Majumder, Keith, Sornborger, and Lauderdale, *unpublished*).

Despite their low signal-to-noise in transgenic vertebrates, yellow cameleons are valuable tools for measuring neural activity:

- Cameleons are inherently ratiometric, and thus give measurements that are relatively insensitive to variations in tissue thickness and focus (Miyawaki 2005).
- Cameleons (and other GECI's) are built around calmodulin, or other calcium-binding proteins, rather than BAPTA. They therefore have K_ds for the binding of calcium in the 0.1-1 μM range, and will buffer intracellular calcium less than will many synthetic calcium indicators (Takahashi, Camacho et al. 1999). In one experiment, Fura-Red loading into cameleon expressing neurons completely damped the periodic Ca2+ response, but left the EGTA 'low calcium clamp' intact (data not shown), suggesting that Fura-Red was buffering calcium in the cell.
- GECI's can be introduced into cells or organisms in ways that do not injure the neurons of interest. Any deleterious effects they may have on cellular or organismal function can be readily assessed (Higashijima, Masino et al. 2003). Furthermore, by using tissue-specific promoters, GECI's can be selectively expressed in tissues or cell types of interest.
- Existing organisms transgenic for cameleons are currently available (Higashijima, Masino et al. 2003; Suzuki, Kerr et al. 2003; Reiff Ihring et al. 2005), and can be used immediately, without investing the time to generate new transgenic lines.

Our results demonstrate the ability of SOARS to detect weak ratiometric signals in YC2.1 imaging data. This method is equally applicable to any ratiometric imaging data, including those obtained with the synthetic ratiometric dyes Di-4,8-Anepps, Indo-1,5F and Fura-2,3,4F, as well as intrinsic ratiometric signals such as NADH/Flavoprotein fluorescence and other genetically

encoded ratiometric indicators. The newer generation of GECIs (Hasan, Friedrich et al. 2004; Heim and Griesbeck 2004; Li, Mack et al. 2005; Miyawaki 2005; Miyawaki, Nagai et al. 2005) should prove to be particularly powerfulfor imaging neural activity due to the improved quantum yields of the indicators. In combination with SOARS, these indicators may become even more useful for detecting the subtleties of neural activity in noisy measurements.

Efforts to generate mice transgenic for cameleons have, to our knowledge, been unsuccessful to date, and in cases where mosaic expression of YC's is seen, existing analytical techniques have yielded only small functional signals (Tsai, Friedman et al. 2003; Hasan, Friedrich et al. 2004). Our experience in other systems (Broder et al, submitted) suggests that SOARS particularly when used in a repetitive-stimulus paradigm, may allow us to use YC, even in these challenging systems.

References

Andersen, S. S. (2001). "Preparation of dissociated zebrafish spinal neuron cultures." Methods Cell Sci **23**(4): 205-9.

Bernhardt, R. R., A. B. Chitnis, et al. (1990). "Identification of spinal neurons in the embryonic and larval zebrafish." J. Comp. Neurol. **302**(3): 603-616.

Bischofberger, J. and D. Schild (1995). "Different spatial patterns of [Ca2+] increase caused by N- and L-type Ca2+ channel activation in frog olfactory bulb neurones." J Physiol **487 (Pt 2)**: 305-17.

Gomez, T. M., E. Robles, et al. (2001). "Filopodial calcium transients promote substrate-dependent growth cone turning." Science **291**(5510): 1983-7.

Griesbeck, O., G. S. Baird, et al. (2001). "Reducing the environmental sensitivity of yellow fluorescent protein. Mechanism and applications." J Biol Chem **276**(31): 29188-94.

Guerrero, G., D. F. Reiff, et al. (2005). "Heterogeneity in synaptic transmission along a Drosophila larval motor axon." Nat Neurosci **8**(9): 1188-96.

Habuchi, S., M. Cotlet, et al. (2002). "Resonance energy transfer in a calcium concentration-dependent cameleon protein." Biophys J **83**(6): 3499-506.

Hanks, J. (1976). "Hanks' balanced salt solution and pH control." Tissue Culture Association Manual **3**: 3.

Hasan, M. T., R. W. Friedrich, et al. (2004). "Functional fluorescent Ca2+ indicator proteins in transgenic mice under TET control." PLoS Biol **2**(6): e163.

Heim, N. and O. Griesbeck (2004). "Genetically encoded indicators of cellular calcium dynamics based on troponin C and green fluorescent protein." J Biol Chem **279**(14): 14280-6.

Higashijima, S., M. A. Masino, et al. (2003). "Imaging neuronal activity during zebrafish behavior with a genetically encoded calcium indicator." J Neurophysiol **90**(6): 3986-97.

Kimmel, C. B., W. W. Ballard, et al. (1995). "Stages of embryonic development of the zebrafish." Dev. Dyn. **203**(3): 253-310.

Li, J., J. A. Mack, et al. (2005). "Early development of functional spatial maps in the zebrafish olfactory bulb." J Neurosci **25**(24): 5784-95.

Lipp, P. and E. Niggli (1993). "Ratiometric confocal Ca(2+)-measurements with visible wavelength indicators in isolated cardiac myocytes." Cell Calcium **14**(5): 359-72.

Miesenböck, G. (2004). "Genetic methods for illuminating the function of neural circuits." Curr Opin Neurobiol **14**(3): 395-402.

Miesenböck, G. and I. G. Kevrekidis (2005). "Optical imaging and control of genetically designated neurons in functioning circuits." Annu Rev Neurosci **28**: 533-63.

Miller, R. J. (1987). "Multiple calcium channels and neuronal function." Science **235**(4784): 46-52.

Miller, R. J. (1988). "Calcium signalling in neurons." Trends Neurosci **11**(10): 415-9.

Miyawaki, A. (2003). "Visualization of the spatial and temporal dynamics of intracellular signaling." Dev Cell **4**(3): 295-305.

Miyawaki, A. (2005). "Innovations in the imaging of brain functions using fluorescent proteins." Neuron **48**(2): 189-99.

Miyawaki, A., O. Griesbeck, et al. (1999). "Dynamic and quantitative Ca2+ measurements using improved cameleons." Proc Natl Acad Sci U S A **96**(5): 2135-40.

Miyawaki, A., J. Llopis, et al. (1997). "Fluorescent indicators for Ca2+ based on green fluorescent proteins and calmodulin." Nature **388**(6645): 882-7.

Miyawaki, A., H. Mizuno, et al. (2003). "Development of genetically encoded fluorescent indicators for calcium." Methods Enzymol **360**: 202-25.

Miyawaki, A., T. Nagai, et al. (2005). "Engineering fluorescent proteins." Adv Biochem Eng Biotechnol **95**: 1-15.

Nagai, T., A. Sawano, et al. (2001). "Circularly permuted green fluorescent proteins engineered to sense Ca2+." Proc Natl Acad Sci U S A **98**(6): 3197-202.

Nagai, T., S. Yamada, et al. (2004). "Expanded dynamic range of fluorescent indicators for Ca(2+) by circularly permuted yellow fluorescent proteins." Proc Natl Acad Sci U S A **101**(29): 10554-9.

Nakai, J., M. Ohkura, et al. (2001). "A high signal-to-noise Ca(2+) probe composed of a single green fluorescent protein." Nat Biotechnol **19**(2): 137-41.

Palmer, A. E., C. Jin, et al. (2004). "Bcl-2-mediated alterations in endoplasmic reticulum Ca2+ analyzed with an improved genetically encoded fluorescent sensor." Proc Natl Acad Sci U S A **101**(50): 17404-9.

Patterson, G. H., D. W. Piston, et al. (2000). "Forster distances between green fluorescent protein pairs." Anal Biochem **284**(2): 438-40.

Pologruto, T. A., R. Yasuda, et al. (2004). "Monitoring neural activity and [Ca2+] with genetically encoded Ca2+ indicators." J Neurosci **24**(43): 9572-9.

Raible, D. W., A. Wood, et al. (1992). "Segregation and early dispersal of neural crest cells in the embryonic zebrafish." Dev Dyn **195**(1): 29-42.

Reiff, D. F., A. Ihring, et al. (2005). "In vivo performance of genetically encoded indicators of neural activity in flies." J Neurosci **25**(19): 4766-78.

Suzuki, H., R. Kerr, et al. (2003). "In vivo imaging of C. elegans mechanosensory neurons demonstrates a specific role for the MEC-4 channel in the process of gentle touch sensation." Neuron **39**(6): 1005-17.

Takahashi, A., P. Camacho, et al. (1999). "Measurement of intracellular calcium." Physiol Rev **79**(4): 1089-125.

Truong, K., A. Sawano, et al. (2001). "FRET-based in vivo Ca2+ imaging by a new calmodulin-GFP fusion molecule." Nat Struct Biol **8**(12): 1069-73.

Tsai, P. S., B. Friedman, et al. (2003). "All-optical histology using ultrashort laser pulses." Neuron **39**(1): 27-41.

Tsien, R. W., D. Lipscombe, et al. (1988). "Multiple types of neuronal calcium channels and their selective modulation." Trends Neurosci **11**(10): 431-8.

Tsien, R. Y. (1998). "The green fluorescent protein." Annu Rev Biochem **67**: 509-44.

Westerfield, M., Ed. (2000). The zebrafish book: A guide for the laboratory use of zebrafish (Danio rerio), University of Oregon Press.

Zhang, J., R. E. Campbell, et al. (2002). "Creating new fluorescent probes for cell biology." Nat Rev Mol Cell Biol **3**(12): 906-18.

Figures

Figure 4.1: Dissociated spinal neurons express cameleon in culture. (A) Side view of the posterior hindbrain and anterior spinal cord of a heterozygous *cameleon* embryo at 18 somites (18s). Anterior is to the left and dorsal is up. Arrows denote putative Rohon-Beard sensory neurons and arrowheads denote commissural neurons. (B) Dissociated spinal neurons express cameleon after 3 days in culture. The neuron denoted with an arrow has a large soma and has extended two thin axons fro mside of the cell body (arrowheads); one of those axons has formed a sidebranch (asterisk). This morphology is characteristic of Rohon-Beard neurons (Bernhardt, Chitnis et al. 1990). Scale bars: 10 μm.

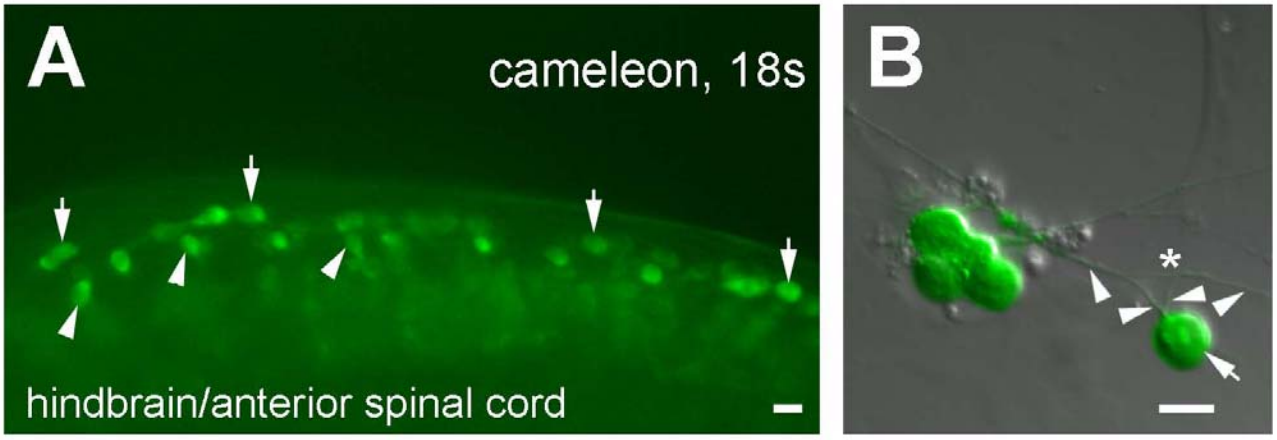
A
cameleon, 18s
hindbrain/anterior spinal cord
B
*

Figure 4.2: Fluorescence images of dye-loaded zebrafish neurons and neuritis in culture. The AM esters of fluo-4 and Fura-Red were used to bulk load dissociated spinal neurons. Fluo-4 fluorescence increased and Fura-Red fluorescence decreased in response to exposure to KCl, which causes depolarization of the neurons and an increase in $[Ca^{2+}]_i$. Sacle bar in transmitted light image applies to all panels.

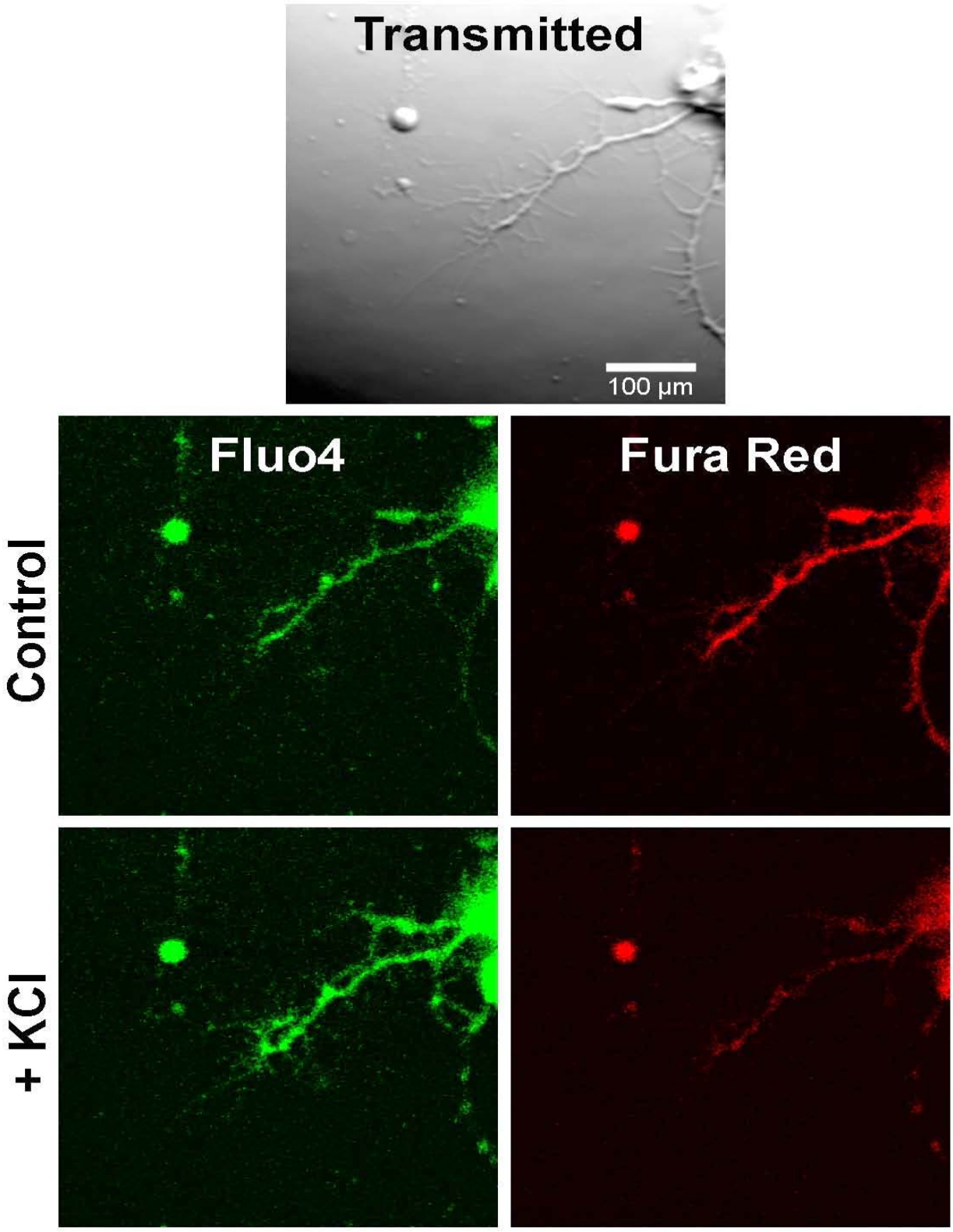
Transmitted
100 µm
Fluo4
Fura Red
Control
+ KCl

Figure 4.3: SOARS analysis of the FRET response of cameleon-expressing neurons to stimulation. (A) Optical (transmitted light) image overlaid with fluorescence image of zebrafish neurons and a fibroblast in culture. Note that only neurons express cameleon. Mean YFP fuorescence is shown in green. An axon extending along the fibroblast is denoted with arrows and the fibroblast is denoted with arrowheads. (B-C) Results of a SOARS analysis on FRET imaging data of the response of cameleon expressing neurons to our stimulation paradigm (see panel D). (B) Weighted mask (eigenimage) resulting from SOARS analysis of the FRET data. This eigenimage represents spatially correlated, temporally anti-correlated information in the dataset. No morphological information was used to generate this image (see Broder et al.). (C) The projections (time-courses) of the weighted mask in the CFP and YFP datasets. The anti-correlated emission fluorescence of CFP and YFP is evident. (D) Sitmulation paradigm: solutions were changed every two minutes for ten periods, followed by five minute exposure to ionomycin + EGTA, followed by exposure to ionomycin + Ca^{2+} (Switching, black trace). Stimulus concentration timecourse was visualized by flowing fluorescein through the Dvorak-Stottler chamber (blue trace). Note the timelag between on- and off-switches and the corresponding change in fluorescein concentration. Scale bar: 40 μm.

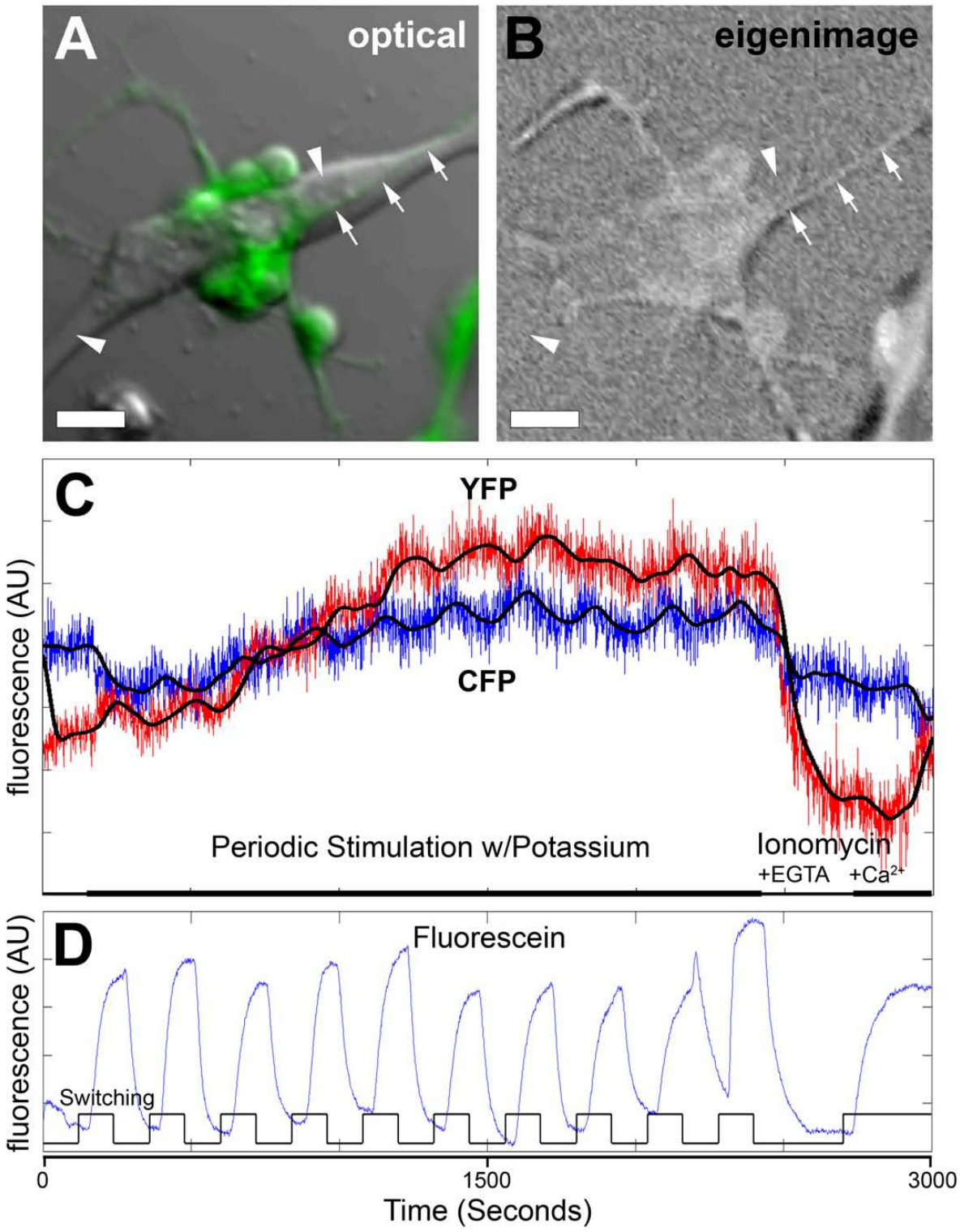
A
optical
B
eigenimage
C
YFP
CFP
fluorescence (AU)
Periodic Stimulation w/Potassium
Ionomycin
+EGTA +Ca2+
D
Fluorescein
Switching
fluorescence (AU)
0
1500
3000
Time (Seconds)

Figure 4.4: A SOARS estimate of the dynamics of the Ca^{2+} response in zebrafish neurons. (A) Optical (transmitted light) image overlaid with fluorescence image of zebrafish neurons and a fibroblast in culture. (B) The SOARS denoised, spatio-temporal reconstruction of the ratio shown over slightly less than one stimulus interval (approximately from baseline to maximal response). Depicted is the deviation of the ratio from the baseline ratio (i.e. the initial frame is subtracted from subsequent frames). Plotting this differential response as a function of time allows us to better see the dynamics of the ratio as the neurons respond to a depolarizing solution. Whereas the intensity of the cameleon fluorescence is higher in the soma relative to the neuritis (A), the ratiometric FRET response to calcium is more uniform throughout the neuron, indicating a uniform Ca2+ increase throughout the cell. Scale bar 40 μm; applies to all panels.

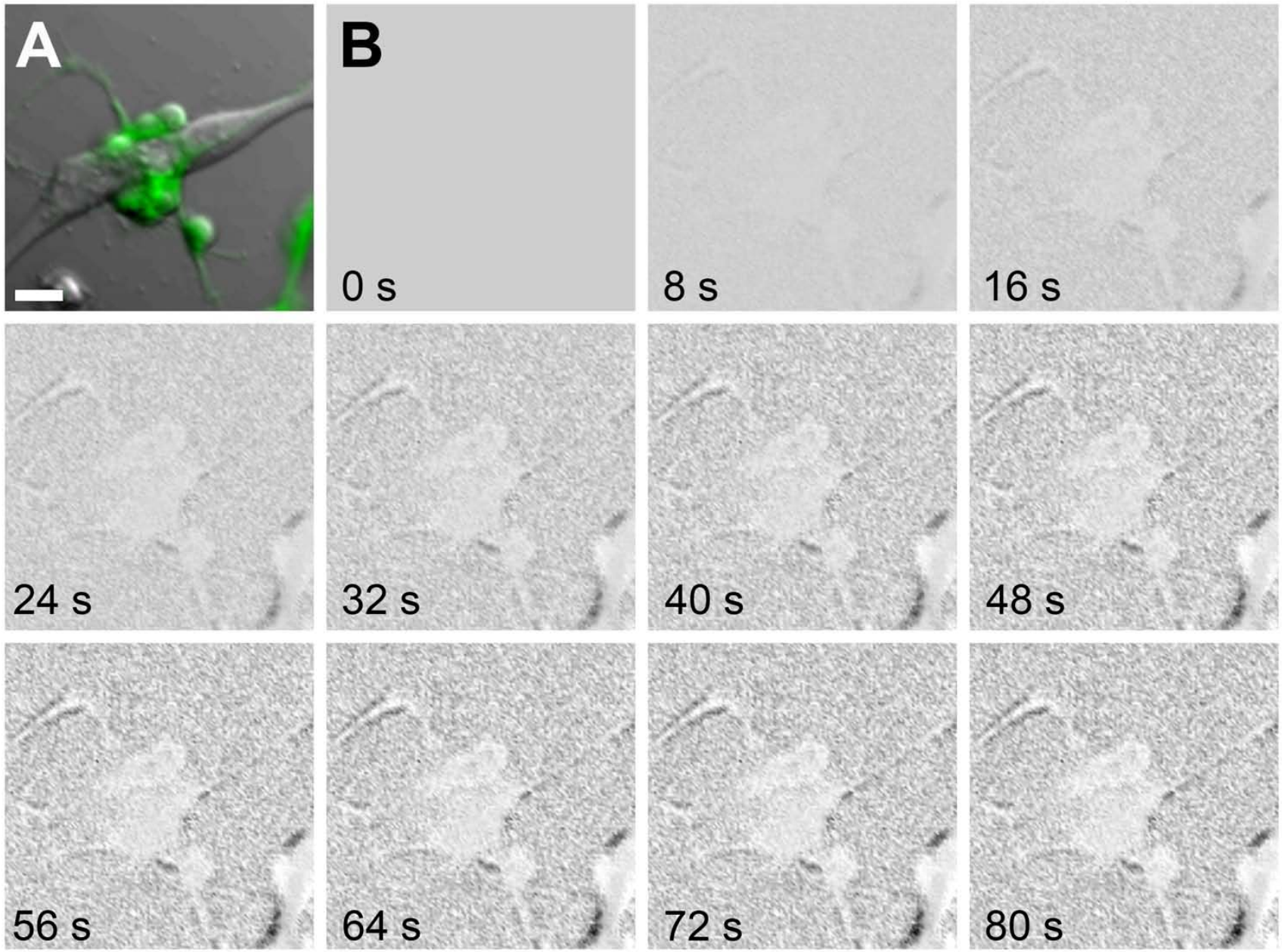
A
B
0 s
8 s
16 s
24 s
32 s
40 s
48 s
56 s
64 s
72 s
80 s

Chapter 5

Optical imaging of neural response in the lateral line system of live zebrafish embryo[1]

[1]Majumder A., Porter E., Keith C. H., Sornborger A. T., Lauderdale J. D.
To be submitted to BMC Neuroscience

Abstract

Detecting responses to stimuli in complete neural circuits in live vertebrates is crucial to many investigations in neurobiology. One approach that has recently gained popularity is the use of FRET based genetically encoded calcium indicators (GECIs) to detect changes in intracellular calcium as a marker for neural activity. Unlike extrinsic calcium indicators that need to be injected into the animal, GECI expression can be targeted to specific neural tissue, thus preventing damage to the tissue. However FRET signals from GECIs are often very small in the physiological context, limiting their utility. We have developed a statistical optimization method, SOARS, that permits detection of weak ratiometric signals without the loss of spatial information usually associated with processing of weak signals. Here we use SOARS to detect chemosensory responses of the zebrafish lateral line system. We show that using SOARS we can identify higher order components of the lateral line circuit that are activated when sensory structures of the system, called neuromasts, are stimulated. Thus, our results open up the possibility of using this non-invasive method to detect neural activity in GECI transgenic animals with minimal manipulation.

Introduction

Linking an organism's behavior to neural activity is of fundamental importance to neurobiology. Crucial to this is the ability to simultaneously detect a stimulus induced response in complete neural circuits. One approach to detecting neural activity at the systems scale is to perform non-invasive high resolution optical imaging that measures physiological changes occurring within activated neurons. A change in intracellular calcium is a robust physiological proxy for neural activity and can be measured by ratiometric calcium indicators such as synthetic calcium indicator dyes or genetically encoded calcium indicator proteins (GECI) (Zhang et al. 2002; Miyawaki et al. 2003; Miesenböck 2004; Miesenböck and Kevrekidis 2005; Miyawaki 2005). Genetically encoded calcium indicators, based on fluorescence resonant energy transfer (FRET), are becoming increasingly important in the measurement of functional changes in neuronal tissues. The expression of GECIs can be directed to specific tissues by use of appropriate regulatory sequences, getting rid of tissue damage associated with extrinsic dyes that usually require invasive loading techniques. However, the FRET signals from GECIs are often small in real physiological contexts. Functional changes in the fluorescent yield of these ratiometric indicators are small and the signal-to-noise ratio (SNR) is of order unity or less. In particular, variability in the denominator of the ratio can lead to very poor ratio estimates. Because the data are noisy, statistical methods are needed to detect and estimate the signal. In the physiological context, signals of interest are usually spatially correlated; therefore, the best detection and estimation can often be done with statistical, multivariate methods that take into account the full covariance matrix of the data. We previously reported a statistical optimization technique, called SOARS (Chapter 3), that does this. It is a simple yet powerful method for detecting and estimating ratiometric signals in dual wavelength measurements of fluorescent,

ratiometric indicators. SOARS takes advantage of the fact that biological signals are often spatially correlated.

The lateral line system is comprised of superficial sensory structures called neuromasts that occur in a stereotypic pattern in fish and amphibians (Metcalfe et al. 1985). We previously reported that the zebrafish neuromasts are activated by specific pungent compounds (Chapter 2). Neuromasts receive afferent connections from the anterior lateral line ganglion, and efferent projections from nuclei in the brain. The anterior lateral line ganglion in turn sends projections to a neuropil in the hindbrain (Metcalfe et al. 1985; Bricaud et al. 2001). Here we image the activity of higher order components of the lateral line system, namely the anterior lateral line ganglion and its associated structures, in a live zebrafish responding to chemical stimulation. This extends the application of SOARS from imaging cultured neurons to systems level imaging in a live organism. It also allows us to analyze the participation of these lateral line components in the chemosensory context.

Materials and methods

All experimental procedures were approved and performed in accordance with University of Georgia Institutional Animal Care and Use Committee regulations. A 4-days-post-fertilization (dpf) zebrafish larva was anaesthetized with tricaine, immobilized and laterally mounted in agar in a Dvorak-Stottler perfusion chamber. The agar was removed about the head allowing the zebrafish to be exposed to sensory stimulation by solutions perfused through the chamber.

In the stimulus experiment, ten second pulses from a reservoir of 0.5% acetic acid were periodically alternated with 110 second pulses from a reservoir of fish water. The pulses were delivered in this way every two minutes for twenty minutes. The control experiment consisted of

ten second pulses of fish water from one reservoir alternated with fishwater from the second reservoir. A femtosecond-pulsed Ti-Sapphire laser (Coherent) tuned to 820nm was used to induce two-photon excitation of the genetically encoded cameleon Ca^{2+} indicator. Two wavelength bands were measured at 460 ± 25nm (Chroma HQ460/50) and 550 ± 25nm (Chroma HQ550/50) with a beam splitter at 500nm (Chroma 500dclp) at a frame rate of 2Hz. 256 × 256 pixel images (1 μm per pixel). Images were taken from the region of the head between the eye and otocyst at a depth of approximately 50 μm. The images were later binned to 64 × 64 pixels for the data analysis due to computer memory constraints. Data was analyzed using SOARS (Broder, Majumder et al, submitted).

Results

We stimulated 4-dpf zebrafish larvae transgenic for cameleon (Higashijima et al. 2000) with a periodic paradigm. In these experiments, we detect changes in neural activity in response to periodic stimulation with dilute acetic acid. The eigenimage resulting from SOARS (Figure 5.1C) revealed that only a subset of neurons and their axons exhibited a response to stimulation. Statistically significant, anti-correlated periodic responses (Figure 5.1D) were observed in the timecourse associated with this eigenimage and the periodicity matched that of stimulus presentation. Such changes were not observed in the water control (not shown). Activity was observed in regions that anatomically correlated with a neuromast (Figure 5.1 A,C), a region in the neuropil in the hindbrain (* in Figure 5.1 C) and neurons in the anterior lateral line ganglion (arrowheads in Figure 5.1 A,B,C).

Discussion

The objective of this study was to extend the applicability of SOARS imaging neural activity in a live vertebrate. Earlier we showed that the technique can be used to study activation of PC12 cells and also dissociated zebrafish neurons. The results presented above show that the method can detect neural activity in a whole zebrafish embryo at the systems level. We have previously demonstrated that the zebrafish lateral line system is activated by dilute acetic acid express the neural activation marker *C-fos* in the neuromasts. Here, using periodic stimulation with acetic acid, and applying SOARS analysis, we detected activation of higher order components of the lateral line system in addition to the neuromasts, in a live embryo. The observation support our results obtained using *C-fos* whole mount mRNA *in situ* hybridization. We stimulated 4-day old larvae transgenic for cameleon. In these experiments, changes in neural activity in response to periodic stimulation with dilute acetic acid would be expected to release Ca^{2+} from intracellular stores, which would be reflected as a change in the cameleon FRET signal. The resulting data were analyzed using SOARS with the addition of harmonic analysis to detect periodic responses in the resulting timecourses. Although all neurons in the CNS expressed cameleon (Figure 5.1B; Higashijima et al., 2003), the eigenimage resulting from SOARS (Figure 5.1C), which shows maximally variant data, revealed that only a subset of neurons and their axons exhibited a response to stimulation. The time-course associated with this eigenimage show that these changes occurred in response to pulses of acetic acid and not in the embryo presented with water alone. Regions exhibiting activity were determined without using any anatomical information, and could be anatomically correlated with components of the lateral line system. Thus SOARS allows us to identify components of the lateral line system that respond to chemical stimulation.

The ability of SOARS to analyze weak ratiometric signals allows us to utilize FRET based GECIs in the zebrafish and should encourage the development of new GECI transgenic zebrafish lines. Due to the small size of the zebrafish embryo, large areas of CNS can be imaged simultaneously, thus allowing detection of activity in entire neural circuits. It is currently not possible to achieve the same in mammals. Thus our imaging approach in the zebrafish will greatly enhance our ability to functionally address many neurobiologocal problems in vertebrates.

References

Bricaud, O., V. Chaar, C. Dambly-Chaudiere, and A. Ghysen. 2001. Early efferent innervation of the zebrafish lateral line. *J Comp Neurol* **434**: 253-61.

Higashijima, S., Y. Hotta, and H. Okamoto. 2000. Visualization of cranial motor neurons in live transgenic zebrafish expressing green fluorescent protein under the control of the islet-1 promoter/enhancer. *J Neurosci* **20**: 206-18.

Metcalfe, W.K., C.B. Kimmel, and E. Schabtach. 1985. Anatomy of the posterior lateral line system in young larvae of the zebrafish. *J Comp Neurol* **233**: 377-89.

Miesenböck, G. 2004. Genetic methods for illuminating the function of neural circuits. *Curr Opin Neurobiol* **14**: 395-402.

Miesenböck, G. and I.G. Kevrekidis. 2005. Optical imaging and control of genetically designated neurons in functioning circuits. *Annu Rev Neurosci* **28**: 533-63.

Miyawaki, A. 2005. Innovations in the imaging of brain functions using fluorescent proteins. *Neuron* **48**: 189-99.

Miyawaki, A., H. Mizuno, T. Nagai, and A. Sawano. 2003. Development of genetically encoded fluorescent indicators for calcium. *Methods Enzymol* **360**: 202-25.

Zhang, J., R.E. Campbell, A.Y. Ting, and R.Y. Tsien. 2002. Creating new fluorescent probes for cell biology. *Nat Rev Mol Cell Biol* **3**: 906-18.

Figure

Figure 5.1: Optical imaging of lateral line response to acetic acid stimulation. Box in A marks the region being imaged and includes neurons of the anterior lateral line ganglion (arrowheads), between the eye and ear (oto), part of midbrain (mb) and hindbrain (hb). A. neuromast in the plane of focus is circled. B. shows cameleon expression in the plane of focus. Inset in C. shows regions of activity. * denotes activity in the neuropil which contains projections of the lateral line system. The regions exhibiting activity correlate anatomically to components of the lateral line system shown in A. D is a time course showing modulations in CFP (blue) and YFP (red) channels. The frequency correlates with the frequency of stimulation

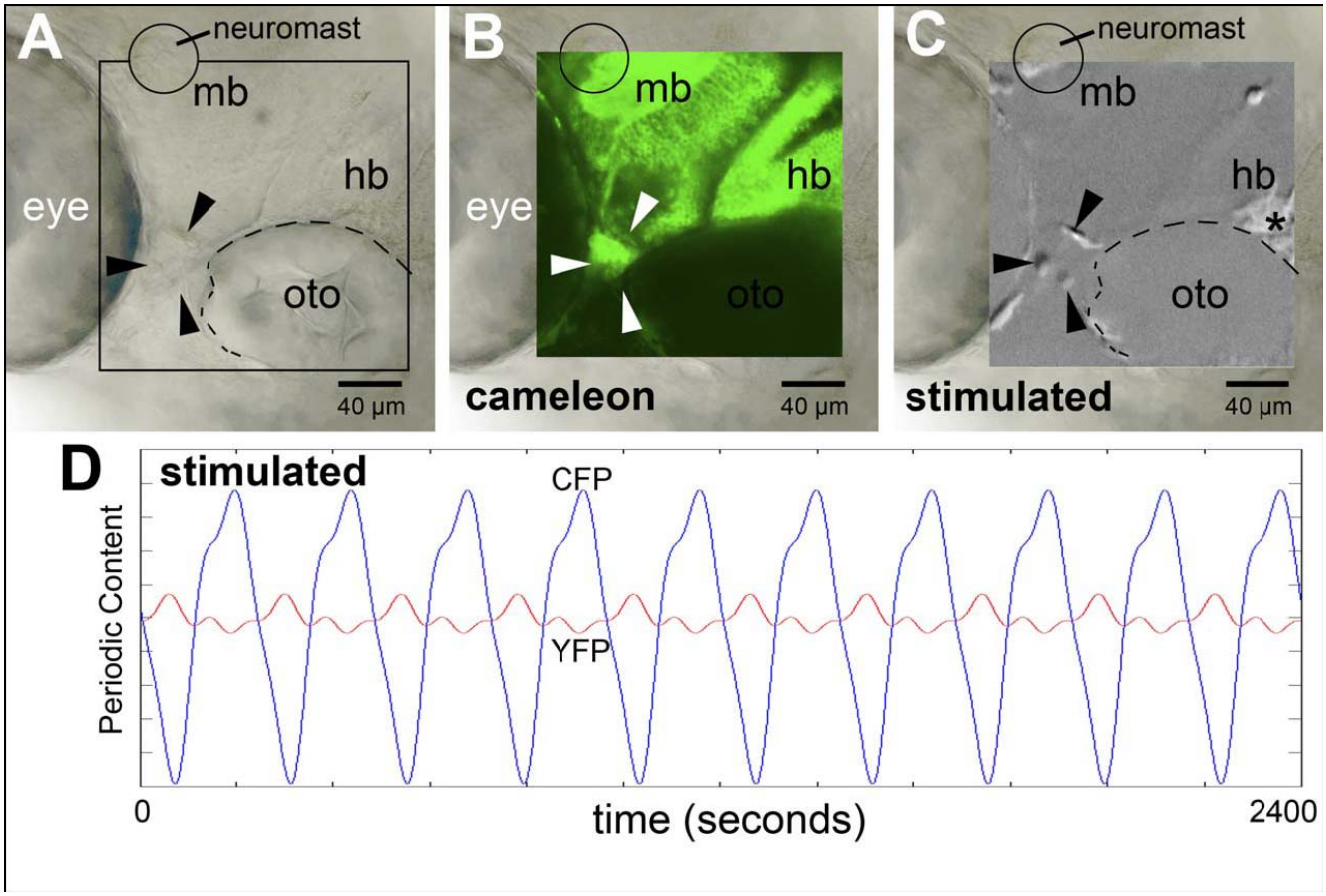
A
neuromast
mb
hb
eye
oto
40 µm
B
mb
hb
eye
oto
cameleon
40 µm
C
neuromast
mb
hb
*
oto
stimulated
40 µm
D
stimulated
CFP
YFP
Periodic Content
0
time (seconds)
2400

Chapter 6

Conclusion

My work addresses two aspects of neurobiology: 1) It demonstrates the potential of the lateral line system of zebrafish to act as a chemosensor. The lateral line has previously been studied almost exclusively as a mechanosensory organ and our findings assign a new role to the system. 2) It describes a novel non-invasive method for simultaneously detecting neural activity at high resolution in multiple neurons within a live organism. We demonstrate its application to detection of chemical induced lateral line responses in a live zebrafish embryo. Together they provide a completely novel approach to analyze mechanisms of chemosensation in vertebrates. This approach will allow us to address chemosensory neural mechanisms in vertebrates both at the level of stimulus detection and higher order processing in the CNS.

Chemosensory role for the zebrafish lateral line system

In this study we show that neuromasts of the lateral line system are activated by pungent compounds such as ginger oil, menthol, peppermint oil, and acetic acid (Chapter 2). This proves for the first time that the lateral line has the potential to act as a chemosensory system. Traditionally the lateral line of various fish and amphibians has been studied extensively as a hydrodynamic sensor (Pitcher et al. 1976; Partridge and Pitcher 1979; Montgomery 1997; Montgomery et al. 2000; Montgomery et al. 2002). In sharks and several teleosts, the lateral line was also shown to respond to salts (Katsuki et al. 1969; Katsuki et al. 1971; Katsuki 1982). The anatomical diversity of the lateral line amongst different fish and amphibians, attributed to the

diverse evolutionary requirements of each species, has been used to understand their behavioral differences in context of the mechanosensory role of the lateral line system. Results presented in this study add a chemosensory function to the lateral line and can significantly enhance our understanding of the role of this organ in influencing behavior of aquatic vertebrates.

Zebrafish as a model for vertebrate chemosensation

The involvement of the lateral line in chemosensation, by itself, is an important find in the field of zebrafish neurobiology. Its significance however stretches well beyond that. The optical transparency of the zebrafish embryo, a high degree of conservation with higher vertebrates in terms of major biological processes, and a well documented nervous system have made the zebrafish increasingly popular as a model for vertebrate neurobiology. While widely used for studying various senses like vision, hearing and olfaction, the utility of zebrafish as a model for pain sensation remains to be explored. Our results show that the zebrafish lateral line system responds to natural pungent compounds that, in mammals, are usually associated with gustation, and nociception or the sense of pain (Story et al. 2003; Bandell et al. 2004; Jordt et al. 2004; Kwan et al. 2006). This opens the door to exploring the zebrafish as a model for nociception. The compounds used in these experiments serve as noxious stimuli in mammals and are known agonists of several different members of the TRP superfamily of ion channel receptors in mammals (Voets et al. 2005). TRP channels, their natural agonists and antagonists and their synthetic variants are the subject of intense study because of their therapeutic potential, especially in the area of pain management (Wissenbach et al. 2004; Nilius et al. 2005). However the exact molecular mechanisms responsible for pain mediated by such channels are not well

understood. Moreover, although functional imaging studies in mammals correlate sense of pain to activation of different brain regions, the identities of neural circuits specifically involved in pain sensation have not been studied at the cellular level.

Studies of TRP channel mediated nociception in mammals are limited in scope due to ethical and cost issues and their dependence on complex behavioral assays. The problems are compounded by the inability to detect participation of complex neural circuits, which is essential to understand the processing of such signals. The ability to use zebrafish as an *in vivo* model will add many crucial advantages over existing model systems used for pain research. TRP channels belong to a large extremely diverse family and any one receptor studied in isolation may not provide the true biological picture. Different TRP channels are known to co-express and work cooperatively to modulate each other's behavior. It is also known that several TRP channels behave differently in different membrane environments (Clapham et al. 2001; Voets et al. 2005). Most studies on TRP channels are however performed using cloned human and mouse TRP receptors expressed in cultured cells or oocytes and it is difficult to replicate the complex endogenous environment in these cell based studies. Our results suggest that the zebrafish lateral line will provide a way to study these receptors in their native membrane environment, and serve as an excellent *in vivo* model to study nociception in vertebrates.

The zebrafish is increasingly being used for high throughput screening of potential drug candidates, and being an *in vivo* system, is more powerful than many cell based assays (Langheinrich 2003; Zon and Peterson 2005). At the same time it is much cheaper and faster than using other *in vivo* vertebrate models, making it an ideal pre-screen system. Effects of test compounds are easier to assay, and assays can be based on behavior, expression, or functional imaging. Zebrafish are already being used to screen compounds for their tumorigenic, anti-

tumor, angiogenic, apoptotic and regenerative potential, at a scale unprecedented in any other *in vivo* model and efforts at automation to handle even larger numbers are being made. Our results suggest that the zebrafish can be also be used to screen potential pain therapeutics or other drug candidates for their potential to induce pain.

Application of SOARS in the zebrafish embryo allow imaging of neural activity at the systems level

The ability to analyze neural responses to specific stimuli in vertebrates is severely limited by our inability to detect such responses in complete neural circuits at cellular resolution. Available optical techniques are limited to imaging small areas of the CNS, as exposing the whole CNS is impractical in most vertebrate models, and even with two-photon laser illumination, which has the maximum tissue penetration capability, the maximum depth achieved is about 500 µM into the cortex in mice. The zebrafish embryo is a vertebrate model that is optically transparent and application of our analysis technique SOARS (Statistical Optimization for the Analysis of Ratiometric Signals), allows us to potentially image large areas of the CNS simultaneously. Application of SOARS on transgenic zebrafish embryos expressing the FRET based calcium indicator protein cameleon in neurons allows imaging of neural activity in complete circuits at a resolution high enough to identify activity in individual neurons. This significantly enhances our ability to analyze stimulus induced CNS responses in a vertebrate.

Optical imaging techniques for detecting neural activity often take advantage of ratiometric indicator dyes to measure physiological changes associated with neural activation. A change in intracellular calcium is one such robust proxy for neural activity. Popular ratiometric calcium indicators broadly fall under two categories, synthetic dyes that need to be injected into

the tissue of interest, and genetically encoded FRET based calcium indicators (GECI) expressed by transgenic animals (Miyawaki et al. 1997; Tsien 1998; Miyawaki et al. 1999). FRET (fluorescence resonance energy transfer) based GECIs are advantageous over extrinsic synthetic indicators, because GECI expression can be directed to specific neural tissues by the use of appropriate regulatory sequences. This obviates the need for dye loading and gets rid of artifacts introduced by uneven dye spread and tissue damage.

FRET signals from available GECIs however are often weak in zebrafish, complicating their analysis. Due to their poor signal to noise ratio extensive averaging is required, resulting in loss of temporal resolution or spatial information or both depending on the analysis method used. Our method allows the use of weak FRET signals without the loss of spatial information associated with currently available techniques for analyzing low intensity ratiometric signals. Thus, it enables the use of available FRET based GECIs for system scale imaging. Using SOARS to optimize ratiometric signals from transgenic zebrafish expressing the FRET GECI cameleon (Higashijima et al. 2003) we are able to detect neural activity in higher order components of the lateral line system in response to specific chemical stimulation.

We have shown that the zebrafish lateral line responds to compounds associated with nociception in mammals. While nociception is an area of active research, the processing of nociceptive signals at the neuronal level in vertebrates is not well understood. Our method gives us an opportunity to dissect such responses in terms of neural activity. It will help identify specific brain circuits that participate in the process. Most sensory systems employ feedback mechanisms and modulate sensitivity through a combination of inhibitory and excitatory circuits. In the lateral line system, inhibitory mechanisms are also thought to play a role in distinguishing external mechanical signals from those generated by voluntary motion. However, the exact

relation between these excitatory and inhibitory components and the contribution of each to modulating sensation are difficult to study in mammalian models. The ability of our imaging approach to utilize GECIs in the zebrafish makes it a potentially powerful tool to investigate this problem. It will be possible to employ two spectrally separated GECIs, one expressed in inhibitory and the other in excitatory circuits in the same animal, to investigate the role of each type of circuit under different stimulation intensities. Such analysis is not possible in mammalian models.

The ability of our technique to analyze weak ratiometric signals also opens the door to use of another potential proxy for neural activity. Anti-correlated fluorescence changes from NADH and flavoproteins occur when a neuron is active and has increased metabolic demand. NADH and flavoprotein fluorescence will provide a truly intrinsic signal and enable the use of wildtype fish for imaging neural activity.

References

Bandell, M., G.M. Story, S.W. Hwang, V. Viswanath, S.R. Eid, M.J. Petrus, T.J. Earley, and A. Patapoutian. 2004. Noxious cold ion channel TRPA1 is activated by pungent compounds and bradykinin. *Neuron* **41**: 849-57.

Clapham, D.E., L.W. Runnels, and C. Strubing. 2001. The TRP ion channel family. *Nat Rev Neurosci* **2**: 387-96.

Higashijima, S., M.A. Masino, G. Mandel, and J.R. Fetcho. 2003. Imaging neuronal activity during zebrafish behavior with a genetically encoded calcium indicator. *J Neurophysiol* **90**: 3986-97.

Jordt, S.E., D.M. Bautista, H.H. Chuang, D.D. McKemy, P.M. Zygmunt, E.D. Hogestatt, I.D. Meng, and D. Julius. 2004. Mustard oils and cannabinoids excite sensory nerve fibres through the TRP channel ANKTM1. *Nature* **427**: 260-5.

Katsuki, Y., T. Hashimoto, and J.I. Kendall. 1971. The chemoreception in the lateral-line organs of teleosts. *Jpn J Physiol* **21**: 99-118.

Katsuki, Y., K. Yanagisawa, A.L. Tester, and J.I. Kendall. 1969. Shark pit organs: response to chemicals. *Science* **163**: 405-7.

Katsuki, Y., Yanagisawa, K. 1982. Chemoreception in the lateral line organ. In *Chemoreception in fishes* (ed. T.J. Hara), pp. 227-257. Elsevier Scientific publishing Company.

Kwan, K.Y., A.J. Allchorne, M.A. Vollrath, A.P. Christensen, D.S. Zhang, C.J. Woolf, and D.P. Corey. 2006. TRPA1 contributes to cold, mechanical, and chemical nociception but is not essential for hair-cell transduction. *Neuron* **50**: 277-89.

Langheinrich, U. 2003. Zebrafish: a new model on the pharmaceutical catwalk. *Bioessays* **25**: 904-12.

Miyawaki, A., O. Griesbeck, R. Heim, and R.Y. Tsien. 1999. Dynamic and quantitative Ca2+ measurements using improved cameleons. *Proc Natl Acad Sci U S A* **96**: 2135-40.

Miyawaki, A., J. Llopis, R. Heim, J.M. McCaffery, J.A. Adams, M. Ikura, and R.Y. Tsien. 1997. Fluorescent indicators for Ca2+ based on green fluorescent proteins and calmodulin. *Nature* **388**: 882-7.

Montgomery, J. 1997. The lateral line can mediate rheotaxis in fish. *Nature* **389**: 960-963.

Montgomery, J., G. Carton, R. Voigt, C. Baker, and C. Diebel. 2000. Sensory processing of water currents by fishes. *Philos Trans R Soc Lond B Biol Sci* **355**: 1325-7.

Montgomery, J.C., F. Macdonald, C.F. Baker, and A.G. Carton. 2002. Hydrodynamic contributions to multimodal guidance of prey capture behavior in fish. *Brain Behav Evol* **59**: 190-8.

Nilius, B., T. Voets, and J. Peters. 2005. TRP channels in disease. *Sci STKE* **2005**: re8.

Partridge, B.L. and T.J. Pitcher. 1979. Evidence against a hydrodynamic function for fish schools. *Nature* **279**: 418-9.

Pitcher, T.J., B.L. Partridge, and C.S. Wardle. 1976. A blind fish can school. *Science* **194**: 963-5.

Story, G.M., A.M. Peier, A.J. Reeve, S.R. Eid, J. Mosbacher, T.R. Hricik, T.J. Earley, A.C. Hergarden, D.A. Andersson, S.W. Hwang, P. McIntyre, T. Jegla, S. Bevan, and A. Patapoutian. 2003. ANKTM1, a TRP-like channel expressed in nociceptive neurons, is activated by cold temperatures. *Cell* **112**: 819-29.

Tsien, R.Y. 1998. The green fluorescent protein. *Annu Rev Biochem* **67**: 509-44.

Voets, T., K. Talavera, G. Owsianik, and B. Nilius. 2005. Sensing with TRP channels. *Nat Chem Biol* **1**: 85-92.

Wissenbach, U., B.A. Niemeyer, and V. Flockerzi. 2004. TRP channels as potential drug targets. *Biol Cell* **96**: 47-54.

Zon, L.I. and R.T. Peterson. 2005. In vivo drug discovery in the zebrafish. *Nat Rev Drug Discov* **4**: 35-44.